Effects of Multiple Drying Cycles on High-Burnup PWR Cladding Alloys

Fuel Cycle Research & Development

Prepared for
U.S. Department of Energy
Used Fuel Disposition Campaign

M.C. Billone, T.A. Burtseva, Z. Han
and Y.Y. Liu

Argonne National Laboratory
September 26, 2014
FCRD-UFD-2014-000052
ANL-14/11

Reviewed by:

Signature on file

Hanchung Tsai (Argonne National Laboratory)
Technical Reviewer

Submitted by:

Yung Y. Liu (Argonne National Laboratory)
Work Package Manager

Page intentionally blank

SUMMARY

The purpose of this research effort is to determine the effects of canister/cask vacuum drying and storage on radial hydride precipitation in high-burnup (HBU) pressurized water reactor (PWR) cladding alloys during cooling for a range of peak drying-storage temperatures, internal gas pressures, and hoop stresses. The HBU PWR cladding alloys have a wide range of hydrogen contents and varying hydride morphology after in-reactor service. Radial hydrides are a potential embrittlement mechanism for HBU cladding subjected to hoop-stress loading, which may be significant during normal cask transport. Ring compression tests (RCTs), which simulate pinch-type loading at grid spacers, are used to determine cladding ductility as a function of RCT temperature and the ductile-to-brittle transition temperature (DBTT). Previous tests were conducted with pressurized and sealed cladding rodlets heated to 400°C (the NRC ISG-11, Rev. 3, limit for all fuel burnups under normal conditions of storage and short-term loading operations) and cooled slowly at 5°C/h. Following this drying-storage simulation, the DBTT for HBU M5® decreased from 80°C to 70°C to <20°C as the peak hoop stress decreased from 140 MPa to 110 MPa to 90 MPa. Under similar drying-storage conditions, the DBTT for HBU ZIRLO™ decreased from 185°C to 125°C to 20°C to <20°C as the peak cladding hoop stress decreased from 140 MP to 110 MPa to 90 MPa to 80 MPa. These tests were conducted with a single heating-cooling cycle as simulation of the vacuum drying process with one drying cycle. (ISG-11, Rev. 3 allows <10 drying cycles, with cladding temperature variations that are less than 65°C each.)

To examine the effects of multiple drying cycles at peak cladding temperature of 400°C, the HBU ZIRLO™ test at 90 MPa was repeated with three heating-cooling cycles and with a 100°C temperature drop at 5°C/h for the first two cycles. Temperature cycling was found to have no apparent effect on the extent of radial hydride precipitation and the resulting DBTT, even though dissolution and re-precipitation of hydrides occurred during each of the drying cycles. Metallographic examinations of cross sections from the 3-cycle rodlet showed essentially the same hydride orientation and morphology as were observed for the 1-cycle rodlet. These temperature-cycling results are very significant in that they clearly indicate the important role of the peak cladding hoop stress, as well as the end-of-life pressure inside of fuel rods that determines the peak hoop stress, in hydride reorientation. The Argonne results are also in direct contrast to reported results for non-irradiated, pre-hydrided Zircaloy-4, which showed increased radial hydride precipitation with temperature cycling at high constant stress (e.g., 160 MPa).

On the basis of current best estimates from thermal calculations, it appears that cladding temperatures may not exceed 350°C during vacuum drying and storage. For cladding alloys with high hydrogen content (350 to 650 wppm), the dissolved hydrogen available to precipitate as radial hydrides decreases by 80 wppm with a peak temperature decrease from 400°C to 350°C. Also, for the same amount of gas inside a fuel rod, there would be a decrease in the temperature, internal pressure, and hoop stress at which radial-hydride precipitation would initiate. A 3-cycle drying test has been conducted at 350°C peak temperature with HBU ZIRLO™ at a peak hoop stress of 92 MPa, which is slightly higher than the 90 MPa used in the 3-cycle test at 400°C. The expectation was that the lower peak temperature would result in precipitation of shorter radial hydrides than observed for samples cooled from 400°C. Metallographic examination conducted to date for the 3-cycle rodlet subjected to intermediate cooling from 350°C to 250°C revealed significant radial hydride precipitation [a radial hydride continuity factor (RHCF) of 32±12%], which corresponds to a DBTT of ≈120°C. On the basis of these results, the potential benefits of the decrease in peak drying temperature appear to be negated by the small increase in the peak hoop stress. As dissolved hydrogen does not precipitate during the temperature decrease from 400°C to 350°C, hoop stresses

may be compared at 350°C: values were extrapolated to be 82 MPa for the 3-cycle test with 20°C DBTT and 92 MPa for the 3-cycle test with ≈120°C DBTT. It appears that multiple drying cycles from 250°C to 350°C might result in more radial hydride precipitation than what was observed with multiple drying cycles from 300°C to 400°C.

CONTENTS

Summary v

Acronyms, Units and Symbols xi

1. Introduction 1

2. HBU Cladding Materials and Test Methods 5
   - 2.1 HBU Cladding Materials 5
   - 2.2 Test Protocol 5

3. Results From Single-Cycle Drying Tests 11
   - 3.1 Radial Hydride Metrics 11
   - 3.2 Re-evaluation of Cladding RCT Ductility 20

4. Results From Multiple-Cycle Drying Tests 23
   - 4.1 Three-Cycle Drying Test at 400°C Peak RHT Temperature 23
   - 4.2 Three-Cycle Drying Test at 350°C Peak RHT Temperature 25

5. Discussion and Summary 31

References 33

Appendix A: Metallographic Images of ZIRLO™ Cross Section From Three-Cycle 350°C Test of Sample 105E6 35

FIGURES

1 Steady-state curves for hydrogen dissolution and precipitation in Zr alloys. 3

2 RCT measured load and controlled displacement. 7

3 Load-displacement curve for non-irradiated M5® ring tested at RT and 5 mm/s to 1.7 mm displacement. 7

4 RCT benchmark results for determining the ratio of unloading/loading stiffness as a function of the traditional offset strain. 8

5 Sectioning diagram for HBU ZIRLO™ rodlet 648C subjected to 1-cycle 400°C RHT at target peak hoop stress of 110 MPa. 11

6 100X image of HBU ZIRLO™ sample 648C7 at 4:30 o'clock orientation from 1-cycle 400°C RHT rodlet with 110-MPa peak hoop stress 12

7 Images of HBU ZIRLO™ sample 648C7 at 4:30 o'clock orientation from 1-cycle 400°C RHT rodlet with 110-MPa peak hoop stress: 200X and 500X. 13

8 Sectioning diagram for HBU M5® rodlet subjected to 1-cycle 400°C RHT at 90-MPa peak stress. 14

9 100X image of HBU M5® sample 651E3D1 at 10:00 o'clock orientation from 1-cycle 400°C RHT rodlet with 90-MPa peak hoop stress 14

10 Images of HBU M5® sample 651E3D1 at 10:00 o'clock orientation from 1-cycle 400°C RHT rodlet with 90-MPa peak hoop stress: 200X and 500X 15

11 RCT offset strain vs. RCT temperature for HBU M5® following irradiation and following RHT at peak 400°C hoop stresses of 90 MPa, 110 MPa, and 140 MPa. 21

12 RCT offset strain vs. RCT temperature for HBU ZIRLO™ following irradiation and following RHT at peak 400°C hoop stresses of 80 MPa, 90 MPa, and 110 MPa. 22

13 Sectioning diagram for HBU ZIRLO™ rodlet 105D subjected to 3-cycle 400°C RHT at peak hoop stress of 90 MPa. 23

14 Peak RHCF value (36%) for HBU ZIRLO™ rodlet 105D subjected to 3-cycle 400°C RHT at peak hoop stress of 90 MPa. 24

15 Load-displacement curve for RCT conducted at 60°C with sample from the HBU ZIRLO™ rodlet subjected to 3-cycle 400°C RHT at peak hoop stress of 90 MPa. 24

16 Ductility data and DBTT for HBU ZIRLO™ subjected to 1-cycle and 3-cycle 400°C RHT at peak hoop stress of 90 MPa. 25

17 Sectioning diagram for HBU ZIRLO™ rodlet 105E subjected to 350°C RHT at peak hoop stress of 92 MPa with two intermediate cooling-heating cycles. 26

18 Metallographic images for HBU ZIRLO™ sample 105E6 at the 7:30 o'clock orientation from the 3-cycle 350°C rodlet: 100X and 200X. 27

A.1 Image of ZIRLO™ sample 105E6 at 12:00 o'clock orientation from 3-cycle 350°C rodlet. RHCF = 36%. 36

A.2 Image of ZIRLO™ sample 105E6 at 12:30 o'clock orientation from 3-cycle 350°C rodlet. RHCF = 46%. 37

A.3 Image of ZIRLO™ sample 105E6 at 1:00 o'clock orientation from 3-cycle 350°C rodlet. RHCF = 42%. 38

A.5 Image of ZIRLO™ sample 105E6 at 2:00 o'clock orientation from 3-cycle 350°C rodlet. RHCF = 16%. 40

A.6 Image of ZIRLO™ sample 105E6 at 2:15 o'clock orientation from 3-cycle 350°C rodlet. RHCF = 38%. 41

A.7 Image of ZIRLO™ sample 105E6 at 2:30 o'clock orientation from 3-cycle 350°C rodlet. RHCF = 19%. 42

A.8 Image of ZIRLO™ sample 105E6 at 2:45 o'clock orientation from 3-cycle 350°C rodlet. RHCF = 28%. 43

A.9 Image of ZIRLO™ sample 105E6 at 3:00 o'clock orientation from 3-cycle 350°C rodlet. RHCF = 22%. 44

A.10 Image of ZIRLO™ sample 105E6 at 3:15 o'clock orientation from 3-cycle 350°C rodlet. RHCF = 20%. 45

A.11 Image of ZIRLO™ sample 105E6 at 3:30 o'clock orientation from 3-cycle 350°C rodlet. RHCF = 15%. 46

A.12 Image of ZIRLO™ sample 105E6 at 3:45 o'clock orientation from 3-cycle 350°C rodlet. RHCF = 39%. 47

A.13 Image of ZIRLO™ sample 105E6 at 4:00 o'clock orientation from 3-cycle 350°C rodlet. RHCF = 34%. 48

A.14 Image of ZIRLO™ sample 105E6 at 4:30 o'clock orientation from 3-cycle 350°C rodlet. RHCF = 53%. 49

A.15 Image of ZIRLO™ sample 105E6 at 5:00 o'clock orientation from 3-cycle 350°C rodlet. RHCF = 55%. 50

A.16 Image of ZIRLO™ sample 105E6 at 5:30 o'clock orientation from 3-cycle 350°C rodlet. RHCF = 30%. 51

A.17 Image of ZIRLO™ sample 105E6 at 6:00 o'clock orientation from 3-cycle 350°C rodlet. RHCF = 23%. 52

A.18 Image of ZIRLO™ sample 105E6 at 6:30 o'clock orientation from 3-cycle 350°C rodlet. RHCF = 36%. 53

A.19 Image of ZIRLO™ sample 105E6 at 7:00 o'clock orientation from 3-cycle 350°C rodlet. RHCF = 53%. 54

A.20 Image of ZIRLO™ sample 105E6 at 7:30 o'clock orientation from 3-cycle 350°C rodlet. RHCF = 50%. 55

A.21 Image of ZIRLO™ sample 105E6 at 7:45 o'clock orientation from 3-cycle 350°C rodlet. RHCF = 51%. 56

A.22 Image of ZIRLO™ sample 105E6 at 8:00 o'clock orientation from 3-cycle 350°C rodlet. RHCF = 45%. 57

A.23 Image of ZIRLO™ sample 105E6 at 8:15 o'clock orientation from 3-cycle 350°C rodlet. RHCF = 32%. 58

A.24 Image of ZIRLO™ sample 105E6 at 8:30 o'clock orientation from 3-cycle 350°C rodlet. RHCF = 26%. 59

A.25 Image of ZIRLO™ sample 105E6 at 8:45 o'clock orientation from 3-cycle 350°C rodlet. RHCF = 25%. 60

A.26 Image of ZIRLO™ sample 105E6 at 9:00 o'clock orientation from 3-cycle 350°C rodlet. RHCF = 31%. 61

A.27 Image of ZIRLO™ sample 105E6 at 9:15 o'clock orientation from 3-cycle 350°C rodlet. RHCF = 17%. 62

A.28 Image of ZIRLO™ sample 105E6 at 9:30 o'clock orientation from 3-cycle 350°C rodlet. RHCF = 21%. 63

A.29 Image of ZIRLO™ sample 105E6 at 9:45 o'clock orientation from 3-cycle 350°C rodlet. RHCF = 27%. 64

A.30 Image of ZIRLO™ sample 105E6 at 10:00 o'clock orientation from 3-cycle 350°C rodlet. RHCF = 16%. 65

A.31 Image of ZIRLO™ sample 105E6 at 10:30 o'clock orientation from 3-cycle 350°C rodlet. RHCF = 18%. 66

A.32 Image of ZIRLO™ sample 105E6 at 11:00 o'clock orientation from 3-cycle 350°C rodlet. RHCF = 18%. 67

A.33 Image of ZIRLO™ sample 105E6 at 11:30 o'clock orientation from 3-cycle 350°C rodlet. RHCF = 34%. 68

A.34 Image of ZIRLO™ sample 105E6 at 11:45 o'clock orientation from 3-cycle 350°C rodlet. RHCF = 38%. 69

TABLES

1 Summary of HBU M5® and ZIRLO™ cladding materials used in studies of cladding ductility following simulated drying storage at peak RHT temperature 5

2 Detailed analysis of local RHCF values and locations for HBU ZIRLO™ sample 648C7..... 18

3 Detailed analysis of local RHCF values and locations for HBU M5® sample 651E3D1 19

4 Hoop stresses for HBU ZIRLO™ samples subjected to 1-cycle 400°C RHT. 20

5 Hoop stresses for HBU M5® samples subjected to 1-cycle 400°C RHT. 20

6 Post-RHT characterization results for HBU ZIRLO™: 3-cycle 350°C rodlet (105E) subjected to 92 MPa and 3-cycle 400°C rodlet (105D) subjected to 90 MPa prior to cooling at 5°C/h. 28

ACRONYMS, UNITS AND SYMBOLS

ACRONYMS

CWSRA	cold-worked, stress-relief annealed
DBTT	ductile-to-brittle transition temperature
DOE	Department of Energy
HBU	high burnup
ID	inner diameter surface
ISG	Interim Staff Guidance
NRC	Nuclear Regulatory Commission
OD	outer diameter surface
PWR	pressurized water reactor
RCT	ring compression test
RHCF	radial hydride continuity factor (in %)
RHF	radial hydride fraction (length of radial hydrides normalized to length of all hydrides)
RHLD	total length of radial hydrides normalized to cladding cross-sectional surface area (1/mm)
RHT	radial-hydride treatment
RT	room temperature
RXA	recrystallized-annealed
TMT	thermo-mechanical treatment
Zry-2	Zircaloy-2
Zry-4	Zircaloy-4

UNITS

°C	degree Celsius
GWd/MTU	giga-watt-days per metric tonne of uranium
h	hour
kN	kilo-Newton
m	meter
mm	millimeter
µm	micron
MPa	mega-Pascal
N	Newton
s	second
wppm	weight parts per million

SYMBOLS

C_H	hydrogen content in weight parts per million (wppm)
C_{HD}	dissolved hydrogen in wppm
C_{HP}	amount of dissolved hydrogen needed to initiate hydride precipitation (in wppm)
D_{mi}	inner diameter of cladding alloy
D_{mo}	outer diameter of cladding alloy
D_o	cladding outer diameter (includes outer-surface corrosion layer if present)
d_p	permanent displacement (pre-test diameter minus post-test diameter in loading direction)
d_p/D_{mo}	RCT permanent strain (%)
δ	controlled and measured RCT displacement at the 12 o'clock sample position
δ_{max}	maximum RCT displacement at the 12 o'clock sample position
Δp	pressure difference across cladding wall ($p_i - p_o$)
δ_p	RCT offset displacement at 12 o'clock position relative to static support at 6 o'clock
δ_p/D_{mo}	RCT offset strain (%)
ΔT	temperature drop per drying cycle
ΔT_{PD}	difference between hydride precipitation (T_P) and dissolution (T_D) temperatures
$(\varepsilon_\theta)_{max}$	maximum hoop strain
fn(40)	ratio of number of hydrides within ±40° of radius and total number of hydrides
fn(45)	ratio of length of hydrides within ±45° of radius and total length of hydrides
h_m	cladding metal wall thickness
h_{ox}	thickness of outer surface corrosion (oxide) layer
K_{LC}	calculated linearized loading slope (also known as loading stiffness) for RCT samples
K_{LM}	measured linearized loading slope
K_U	calculated linearized unloading slope
K_{UM}	measured linearized unloading slope
L	length of RCT samples
M_{max}	maximum RCT bending moment
P	measured RCT load at the 12 o'clock sample orientation
p_i	internal gas pressure
P_{max}	maximum RCT load
p_o	external gas pressure
R_{mi}	inner radius of cladding alloy
σ_θ	hoop stress
T	temperature
T_{max}	maximum hold temperature for RHT
T_D	hydrogen dissolution temperature
T_h	hold temperature for RHT
T_P	hydrogen precipitation temperature

1. INTRODUCTION

Structural analyses of high-burnup (HBU) fuel rods require cladding mechanical properties and failure limits to assess fuel behavior during long-term dry-cask storage, post-storage retrieval and transportation, and post-transport retrieval. License applications for transport casks containing HBU fuel assemblies have used properties and failure limits for as-irradiated cladding [1]. The Zircaloy-4 (Zry-4) properties and limits in Ref. 1 were based primarily on axial-tensile and pressurized tube tests. Isotropic correlations were developed for stress vs. strain and failure limits. However, pre-storage drying-transfer operations and early stage storage subject cladding to higher tensile hoop stresses induced by higher temperatures and pressure relative to in-reactor operation and pool storage. Under these conditions, radial hydrides may precipitate during slow cooling and may introduce an embrittlement mechanism if the cladding temperature decreases below the ductile-to-brittle transition temperature (DBTT). If embrittlement is predicted to occur in response to hoop-stress loading, then cladding failure criteria would have to be revised to account for this effect.

In Interim Staff Guidance-11, Revision 3 (ISG-11, Rev. 3), the Nuclear Regulatory Commission (NRC) recommends a peak cladding temperature limit of 400°C for all fuel burnups under normal conditions of storage and short-term loading operations (e.g., drying, backfilling with inert gas, and transfer of the cask to the storage pad) [2]. During loading operations, repeated thermal cycling (repeated heatup/cool-down cycles) may occur but should be limited to fewer than 10 cycles, with cladding temperature variations that are less than 65°C (117°F) each, according to ISG-11, Rev. 3 (see Fig. 1 at the end of this section for justification of <65°C per cycle). One concern for HBU fuel cladding is the possible precipitation of radial hydrides, which could embrittle cladding in response to tensile hoop stresses caused by internal pressure loading and “pinch-type” loading during transport. Limits established in ISG-11, Rev. 3, relied on data available before 2002, which were primarily for low-burnup and non-irradiated/pre-hydrided Zry-4. At the time ISG-11, Rev. 3, was issued (2003), NRC recognized that data for HBU fuel cladding alloys were needed to determine the extent of radial-hydride embrittlement under conditions relevant to drying-transfer operations and storage. The NRC licensing issues are summarized in “Compatibility of Requirements for Storage and Transportation of Spent Nuclear Fuel (Retrievability, Cladding Integrity, and Safe Handling),” a summary paper presented at the NRC Public Meeting to obtain stakeholder feedback on enhancements to the licensing and inspection programs for spent fuel storage and transportation under 10 CFR Parts 71 and 72 [3]. A major concern is whether or not HBU fuel will maintain cladding integrity and be readily retrievable after more than 20 years of storage. License approvals for the transport of HBU fuel assemblies have been delayed because of the lack of data for HBU fuel cladding after more than 20 years of storage, which corresponds to peak cladding temperatures of ≈200°C or less.

Argonne has developed a test protocol for studying HBU cladding embrittlement that has been used to generate data for NRC. Experimentally, the protocol involves two steps: (a) radial-hydride treatment (RHT), during which HBU cladding is exposed to simulated drying-storage temperature and hoop stress conditions, including slow cooling with decreasing stress, followed by (b) ring compression testing, in which rings sectioned from RHT HBU cladding are compressed to determine strength and ductility as a function of test temperature. The ring compression test (RCT) is used as a ductility screening test, and the RCT loading simulates the pinch-type loading on HBU cladding that occurs during normal cask transport and drop accidents. The protocol was used to generate DBTT data for HBU ZIRLO™ and Zry-4 [4, 5] (both efforts sponsored by NRC) and HBU M5® [sponsored by the Department of Energy (DOE)] [6]. Under DOE-sponsored research, Argonne has also generated baseline characterization data and data for the strength and ductility of as-irradiated Zry-4, ZIRLO™,

and M5®. These data are important not only for determining the degrading effects of drying and early stage storage, but also for serving as reference properties for future evaluations of the effects of drying storage on these cladding alloys [7–9]. Reference 10 includes all Argonne data generated through September 2013, including additional DOE-sponsored test results for HBU ZIRLO™ and M5® following cooling from 400°C and lower hoop stress levels (80 to 90 MPa). In addition to the Argonne datasets for PWR cladding alloys, Aomi et al. [11] have generated data for Zircaloy-2 (Zry-2) and Zry-4 using test methods similar to the ones used by Argonne. However, RHT samples were cooled under constant stress (vs. decreasing stress, as used by Argonne), and RCTs were conducted only at room temperature (RT) and a low displacement rate (0.033 mm/s vs. 5 mm/s used by Argonne). Their results are both revealing and relevant in evaluating the effects of hydrogen content (C_H) and thermo-mechanical treatment (TMT) on the susceptibility of cladding alloys to radial-hydride formation. Argonne and Aomi et al. test results indicate that susceptibility to radial-hydride precipitation during cooling is dependent on cladding alloy, TMT, total C_H, C_H below the hydride rim, and peak RHT temperature and hoop stress. The combination of recrystallized-annealed (RXA) microstructure and low C_H (above the inner liner for Zry-2) makes Zry-2 and M5® highly susceptible to precipitation of long radial hydrides during cooling. For cold-worked, stress-relief-annealed (CWSRA) alloys, ZIRLO™ was found by Argonne to be more susceptible to radial-hydride precipitation than Zry-4. The differences in the distribution of hydrides across the cladding wall (lower for ZIRLO™ below the hydride rim) may be partly responsible for this behavior [5].

Argonne has generated data for as-irradiated, HBU cladding, and HBU cladding subjected to single drying cycles with peak temperature of 400°C (hereafter referred to as “1-cycle 400°C test”) and peak hoop stresses in the range of 80 to 140 MPa (i.e., RHT). Data for 1-cycle 400°C tests of HBU ZIRLO™ and M5® are summarized in Section 3, along with additional determination and assessment of metrics for the extent of radial hydride precipitation and cladding ductility.

Data for multiple drying cycle tests are presented in Section 4: one test with RHT at 400°C peak temperature consisting of three heating-cooling cycles, with 100°C temperature drop and 5°C/h cooling rate for the first two cycles (“3-cycle 400°C test”) and another test with RHT at 350°C peak temperature consisting of three heating-cooling cycles, with 100°C temperature drop and 5°C/h cooling rate for the first two cycles (“3-cycle 350°C test”). The 3-cycle 400°C test was conducted at 90 MPa peak cladding stress. The results are compared to the results from the 1-cycle 400°C test conducted at the same peak hoop stress. The 3-cycle 350°C test was conducted with a rodlet having a higher fill-gas pressure than the rodlet from the 3-cycle 400°C test to determine the combined effects of lower peak temperature and higher peak stress. Results of current best-estimate thermal analyses indicate that peak cladding temperatures may not exceed 350°C during vacuum drying and storage for canisters/casks containing HBU fuel assemblies.

The 100°C temperature drop per cycle was chosen for multiple drying cycle tests because of its relevance to drying procedures, which vary depending on the drying methods and the limiting conditions of operation in the technical specifications. Conducting multiple drying cycle tests with 100°C temperature drop should bound the ΔT values specified in the drying procedures. In addition, conducting multiple cycle tests with ΔT <65°C would not yield useful results for high-C_H cladding alloys because no hydrogen is predicted to precipitate during the cooling phase.

To appreciate the influence of peak RHT temperature (i.e., decrease from 400°C to 350°C), stress, temperature cycling, and hydrogen content on radial hydride precipitation and embrittlement, it is important to review literature results for hydrogen dissolution and hydride precipitation. Unlike most, if not all, studies of radial hydride precipitation and subsequent ductility, the Argonne RHT

process includes decreasing internal gas pressure and hoop stress with decreasing temperature during cooling. Other researchers have used an open, actively pressurized cladding tube for which the pressure is kept constant during cooling. As such, it is important to understand the dependence of hydrogen solubility (C_{HD}) on temperature (T_D) during the heating phase and the initiation of hydrogen precipitation (C_{HP} at T_P) during the cooling phase. Figure 1 summarizes the data of Kearns [12], Kammenzind et al. [13], and McMinn et al. [14] for these parameters, as well as the temperature gap (ΔT_{PD}) between precipitation and dissolution. The results in Fig. 1 are used in Sections 3 and 4 to determine the cladding temperature and stress at which precipitation, especially radial hydride precipitation, can be initiated.

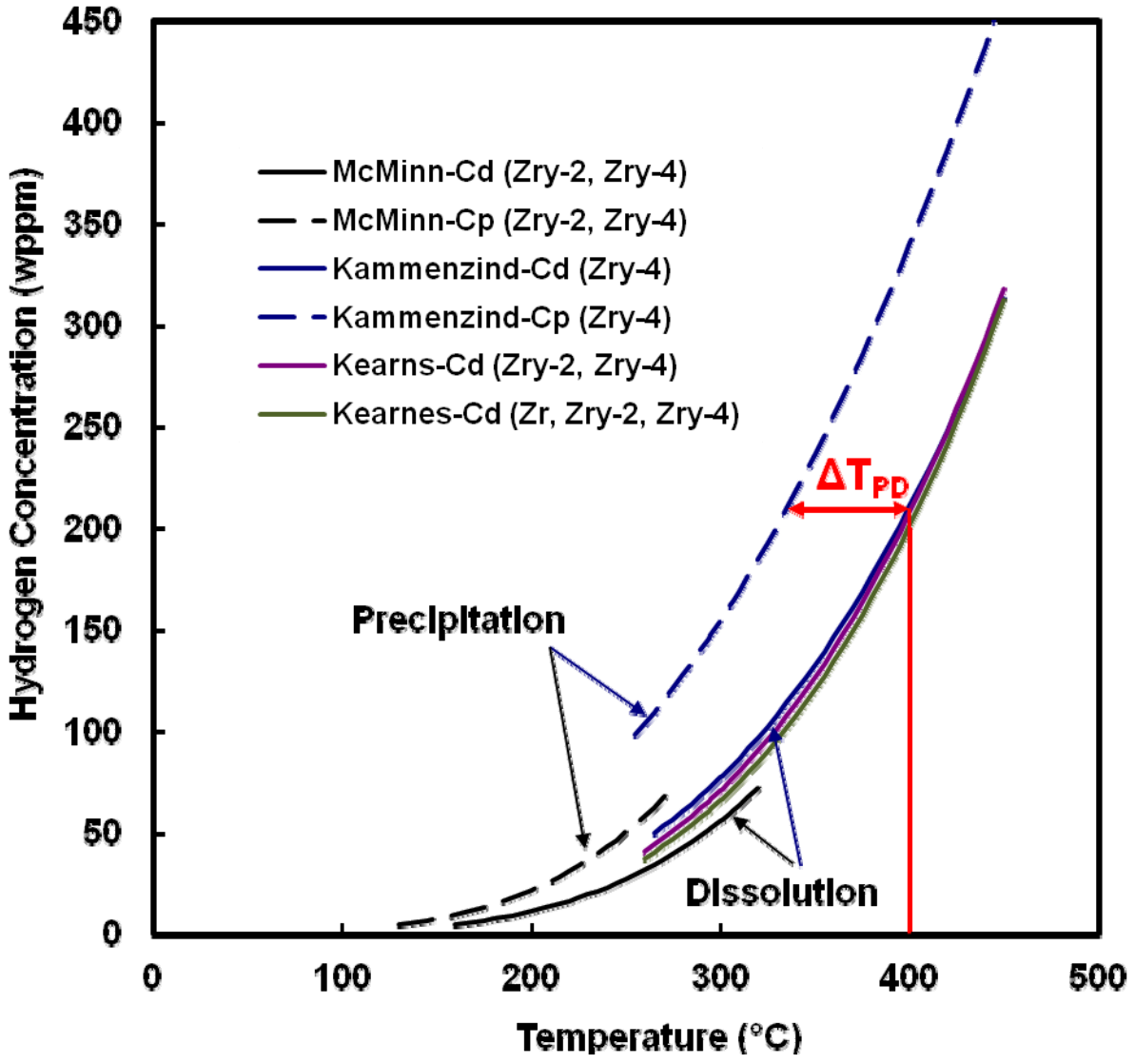

Figure 1: Steady-state curves for hydrogen dissolution and precipitation in Zr alloys.

Page intentionally blank

2. HBU CLADDING MATERIALS AND TEST METHODS

2.1 HBU Cladding Materials

Reference 10 contains a detailed list of defueled cladding materials used in previous testing. Relevant materials for the current work are listed in Table 1. The materials came from fuel rods irradiated to HBU in commercial light water reactors. The M5® cladding segment listed at 63 GWd/MTU was irradiated in one of the Ringhals reactors. M5® cladding segments listed at 68 GWd/MTU came from fuel rods irradiated in the same assembly in the North Anna reactors. ZIRLO™ cladding segments came from two fuel rods irradiated in the same assembly in the North Anna Reactors. The $\pm C_H$ values represent one-sigma variations in data collected from multiple axial locations along each segment and quarter-ring samples at each axial location. In general, the large one-sigma values were due to circumferential variation in C_H, especially for average C_H values ≥350 wppm. Additional characterization results are presented in subsequent sections.

Table 1 Summary of HBU M5® and ZIRLO™ cladding materials used in studies of cladding ductility following simulated drying storage (RHT) at peak RHT temperature (T_{max})

Cladding Alloy	TMT	Burnup, GWd/MTU	Hydrogen Content, wppm	Target Peak RHT Stress, MPa	Peak RHT T_{max}, °C	Number of Drying Cycles
M5®	RXA	63	94±4	140	400	1
		68	72±10	110	400	1
		68	58±15	90	400	1
ZIRLO™	CWSRA	70	650±190	140	400	1
		70	425±63	110	400	1
		70	350±80	110	400	1
		68	530±100	90	400	1
		68	480±131	90	400	3
		68	560±198	92	350	3
		68	535±50	80	400	1

2.2 Test Protocol

The protocol for single-cycle heating-cooling tests consisted of two steps: (a) simulated drying and storage testing (called "RHT") during which a sealed, pressurized rodlet is heated to and stabilized at 400°C within one hour, held at 400°C for one hour, cooled slowly at 5°C/h to 200°C (135°C for low-C_H M5®), and cooled at a higher rate to RT and (b) ring-compression testing at three to four temperatures from RT to 200°C and at 5 mm/s (reference value) displacement rate to a maximum displacement of 1.7 mm. For three-cycle heating-cooling RHTs, rodlets were heated to peak temperatures of 400°C or 350°C, held at T_{max} for one hour, cooled at 5°C/h to 100°C below T_{max}, reheated to T_{max}, held at T_{max} for one hour, cooled at 5°C/h to 100°C below T_{max}, reheated to T_{max}, held at T_{max} for one hour, and then cooled at the same rates used for the single-cycle tests.

HBU cladding segments were used to fabricate sealed and pressurized (with argon) rodlets. Details of rodlet fabrication are given in Ref. 10.

Prior to rodlet pressurization, the outer diameter was measured for each corroded segment at two orientations (90° apart) and at three axial locations. These values were averaged to give the cladding outer diameter (D_o). The thickness of the corrosion (oxide) layer (h_{ox}) was estimated from sibling rod data or from interpolation and extrapolation of data from the same rod at different axial locations. The same approach was used to estimate the cladding metal wall thickness (h_m). The outer diameter of the cladding alloy (D_{mo}) was calculated from $D_o - 2\ h_{ox}$, and the metal inner diameter (D_{mi}) was calculated from $D_{mo} - 2\ h_m$. The ratio R_{mi}/h_m, where R_{mi} is the metal inner radius, was used in Eq. 1 to calculate the average hoop stress (σ_θ) from the pressure difference ($\Delta p = p_i - p_o$) across the cladding wall, where p_o was 0.1 MPa during RT (23°C) fabrication and 0.17 MPa in the RHT furnace.

$$\sigma_\theta = (R_{mi}/h_m)\ \Delta p \quad (1)$$

The ideal gas law was used to relate the absolute pressure at the RHT hold temperature (T_h) to the RT pressure according to $p_i(T_h) = ([T_h + 273\ K]/296\ K)\ p_i(23°C)$. Given the target σ_θ value at T_h, the fabricated RT pressure can be calculated using Eq. 1 and the information given above.

Following RHT, the rodlet was depressurized and sectioned for C_H samples, RCT samples, and metallographic imaging samples, which allowed precise determination of the geometrical factors in Eq. 1. Using this procedure, the calculated peak rodlet stress was within 3 MPa of the target value.

The second phase of the test protocol consisted of RCTs. Figure 2 shows a schematic of RCT loading. The RCT load induces maximum hoop bending stresses (σ_θ) at the inner surfaces of the 12 (under load) and 6 (above support) o'clock positions. Tensile hoop stresses also occur at the 3 and 9 o'clock outer surfaces. Associated with these maximum tensile stresses are maximum tensile strains (ε_θ). Within the elastic range, these hoop stresses at 3 and 9 o'clock are ≈60% of the maximum stresses at 12 and 6 o'clock. Also, because the length (L ≈ 8 mm) of the rings is much greater than the cladding wall thickness (h_m = 0.54 to 0.56 mm for HBU ZIRLO™ and M5®), an axial stress is induced that is 0.37 times the hoop stress within the elastic deformation regime. The maximum displacement (1.7 mm) was chosen to give ≈10% offset strain at RT. The reference displacement rate was 5 mm/s.

Load-displacement curves and post-test examinations were used to determine offset displacements (δ_p) and permanent displacements (d_p), respectively. These were normalized to D_{mo} to give relative plastic displacement (i.e., plastic strain) for the ring structure. Permanent displacement is defined as the difference between pre- and post-test diameter measurements along the loading direction. Figure 3 shows how traditional and corrected offset displacements were determined from a benchmark load-displacement curve for a non-irradiated M5® ring. For the benchmark sample, D_{mo} = 9.50 mm, h_m = 0.61 mm, and L = 8.00 mm. The traditional offset methodology calls for unloading the sample at the same slope as the measured loading slope (K_{LM}). It should be noted that this slope is less than the calculated sample stiffness (K_{LC}) due to the influence of machine compliance. This approach gave a traditional δ_p = 0.94 mm, which is greater than the more accurate d_p = 0.83 mm. Thus, there is an inherent error in the traditional approach as the measured unloading slope (K_{UM} = 0.81 kN/mm) is always less than the measured loading slope. K_{UM} was determined from the slope of the line connecting the maximum displacement to the displacement axis value based on the measured value of d_p at zero load. Normalizing these displacements to D_{mo} gives 9.9% traditional offset strain and 8.7% permanent strain, which is also called the "corrected offset strain."

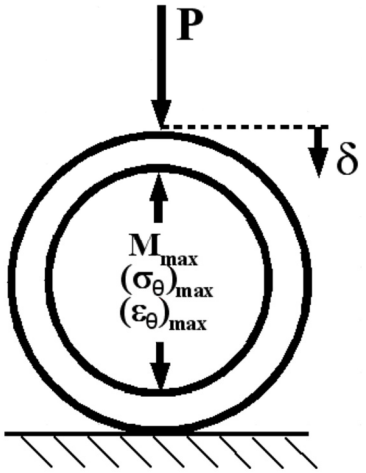

Figure 2: RCT measured load (P) and controlled displacement (δ).

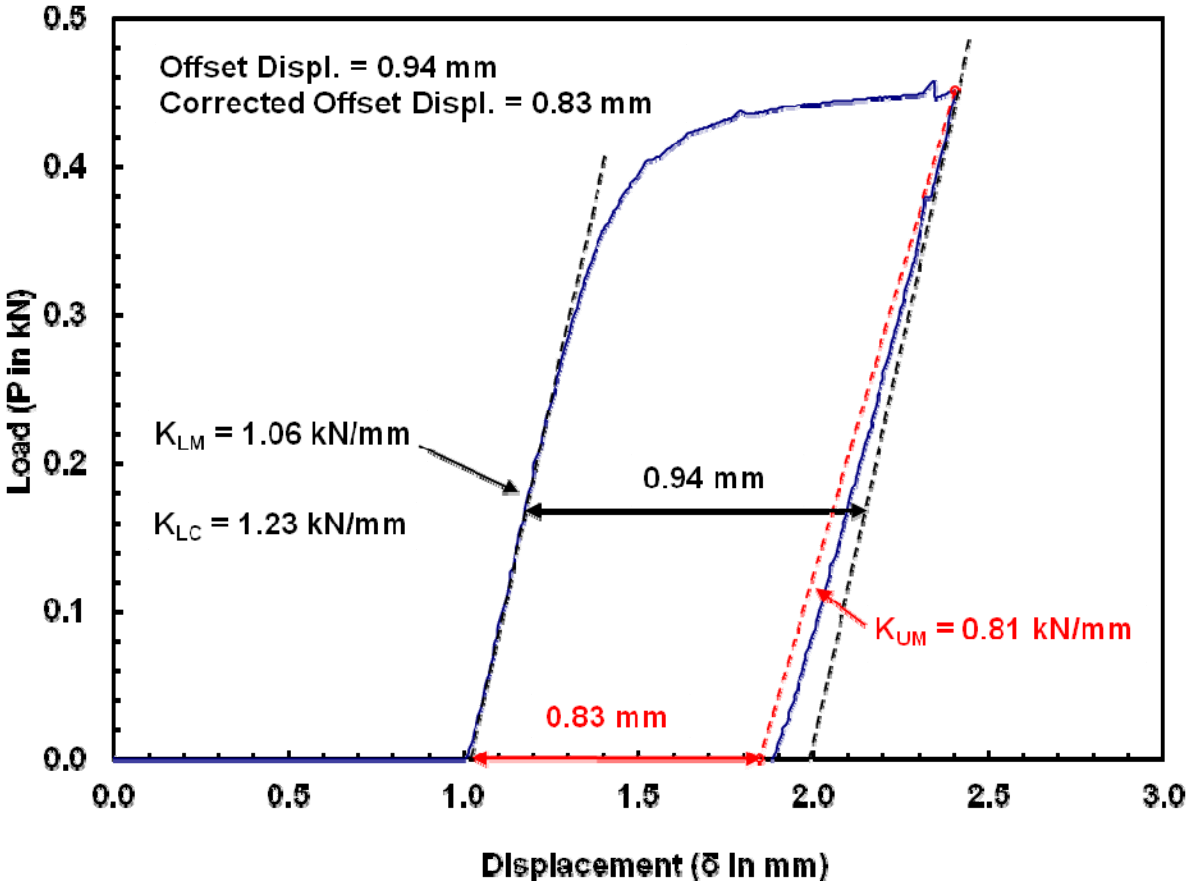

Figure 3: Load-displacement curve for non-irradiated M5® ring tested at RT and 5 mm/s to 1.7 mm displacement.

For HBU cladding rings that crack during the 1.7-mm displacement, d_p cannot be determined accurately. Thus, one must rely on a correlation for the unloading slope to determine the corrected offset displacement prior to the first significant crack, from which the ductility can be determined. The correlation developed for this application is based on the results from a large number of benchmark tests with permanent displacements ranging from 0.14 mm to 1.2 mm. Results of these benchmark tests are shown in Fig. 4 in terms of the ratio of measured unloading/loading (K_{UM}/K_{LM}) slopes vs. traditional offset strain (δ_p/D_{mo}). Also shown in Fig. 4 are results from HBU cladding samples that exhibited no cracking after 1.7 mm of total displacement. Although these data points were not used in the development of the current correlation, the agreement between the bi-linear correlation and the HBU data points is quite good.

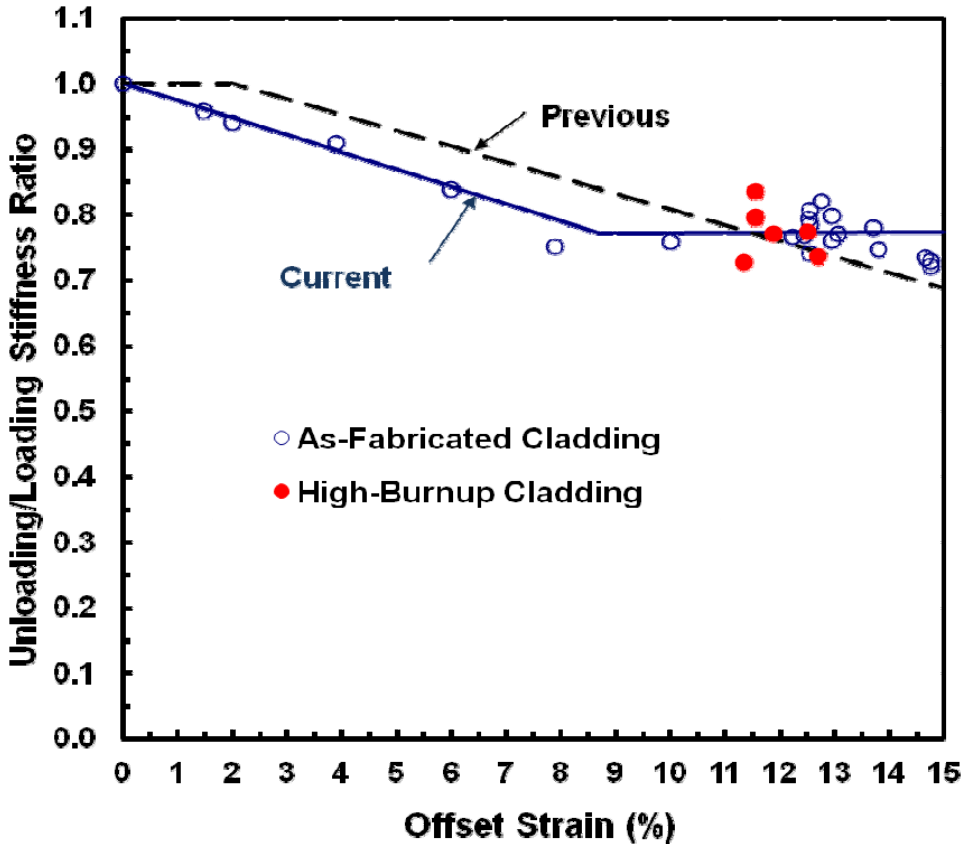

Figure 4: RCT benchmark results for determining the ratio of unloading/loading stiffness as a function of the traditional offset strain. The new correlation is labeled "Current" and the old correlation is labeled "Previous".

The new correlation for calculating the unloading slope (K_U in kN/mm) as a function of the measured loading slope (in kN/mm) and the measured traditional offset strain (in %) is given by:

$$K_U/K_{LM} = 1 - 0.02612\ \delta_p/D_{mo} \text{ for } \delta_p/D_{mo} \le 8.7\% \quad (2a)$$

$$K_U/K_{LM} = 0.773 \text{ for } \delta_p/D_{mo} > 8.7\% \quad (2b)$$

All RCT ductility results were reevaluated using Eqs. (2a) and (2b) for the corrected unloading slope. These results are presented in Sections 3 and 4.

The criteria for determining embrittlement remain the same: corrected δ_p/D_{mo} <2% prior to >25% load drop or >50% decrease in loading slope. In previous work [4-7], it was established that >25% load drop and >50% decrease in loading slope correspond to a crack or cracks extending through >50% of the wall thickness. The 2% offset strain limit is based on the uncertainty in measurement of the permanent strain (≤1%) for as-fabricated cladding and the added uncertainty (≤1%) in the permanent displacement for HBU cladding due to flaking off of the corrosion (i.e., oxide) layer under the applied load and above the support plate.

Page intentionally blank

3. RESULTS FROM SINGLE-CYCLE DRYING TESTS

In Section 3.1, several metrics for radial hydrides are determined, compared, and assessed. A meaningful metric or combination of metrics is one that can be used to assess the likelihood of crack initiation and the extent of crack propagation, particularly for offset strains approaching 2%, which is used to determine the DBTT. A useful metric or set of metrics should decrease in a consistent manner with the observed decrease in DBTT for all HBU PWR cladding alloys tested. Previously, the radial hydride continuity factor (RHCF) has been used for this purpose. It worked quite well for the high-C_H alloys ZIRLO™ and Zry-4 [4-10]. However, for comparable RHCF values, the DBTT for low-C_H M5® was considerably lower than that for ZIRLO™ and Zry-4. Qualitatively, these results make sense because the amount of dissolved hydrogen available for precipitation in M5® is much lower (58 to 94 wppm) than it is for ZIRLO™ and Zry-4 (≈200 wppm) heated to 400°C. Lower dissolved hydrogen at the peak RHT temperature would tend to lead to hydride platelets with poor connectivity in the axial direction. The RHCF metric, along with other metrics reported in the literature, is based on examination of cross sections. It does not directly give quantitative information regarding platelet connectivity in the axial direction.

In Section 3.2, ductility results are presented for ZIRLO™ and M5® based on re-analysis of all load-displacement curves. The re-analysis used the consistent methodology presented in Section 2.2 for determination of the unloading slope (see Eqs. 2a and 2b).

3.1 Radial Hydride Metrics

Two samples with about the same RHCF were chosen for evaluation of radial hydride metrics. On the basis of previously reported results [10], the ZIRLO™ and M5® rodlets had 30 to 35% RHCF, but they differed in DBTT values by >105°C. Figure 5 shows the sectioning diagram for ZIRLO™ rodlet 648C following cooling from 400°C and a target hoop stress of 110 MPa (actual hoop stress was 112 MPa).

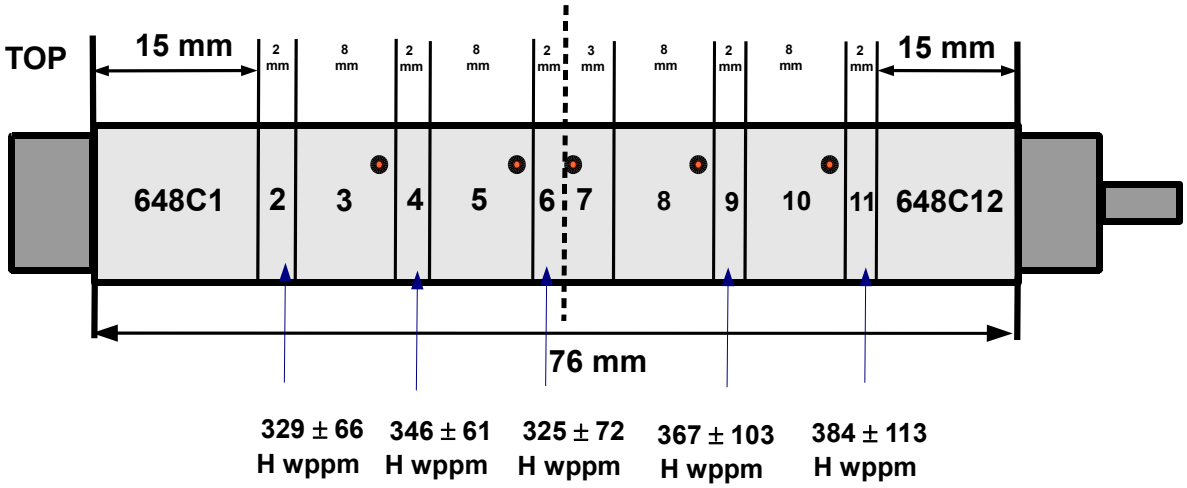

Figure 5: Sectioning diagram for HBU ZIRLO™ rodlet 648C subjected to 1-cycle 400°C RHT at target peak hoop stress of 110 MPa (112 MPa actual hoop stress).

Sample 648C7 was retrieved from storage, re-ground, re-polished, and carefully re-etched. Previous metallographic results [5, 10] appeared to be based on samples that were somewhat over-etched based on the observed thickness of the hydrides. For the re-examination of the 648C7 cross section, a significant amount of material (0.1 to 0.2 mm) had to be removed by the grinding process because the etched hydrides were relatively deep. This qualitative observation suggests relatively good axial connectivity of hydride platelets. Images were taken at 36 orientations and 100X magnification to ensure that the whole cross section could be characterized. Interesting regions of radial hydrides were also imaged at 200X and 500X to assess radial hydride continuity.

Figure 6 shows an interesting region (100X magnification at 4:30 o'clock) with a number of radial hydrides emanating from the inner surface to about 50% of the cladding wall.

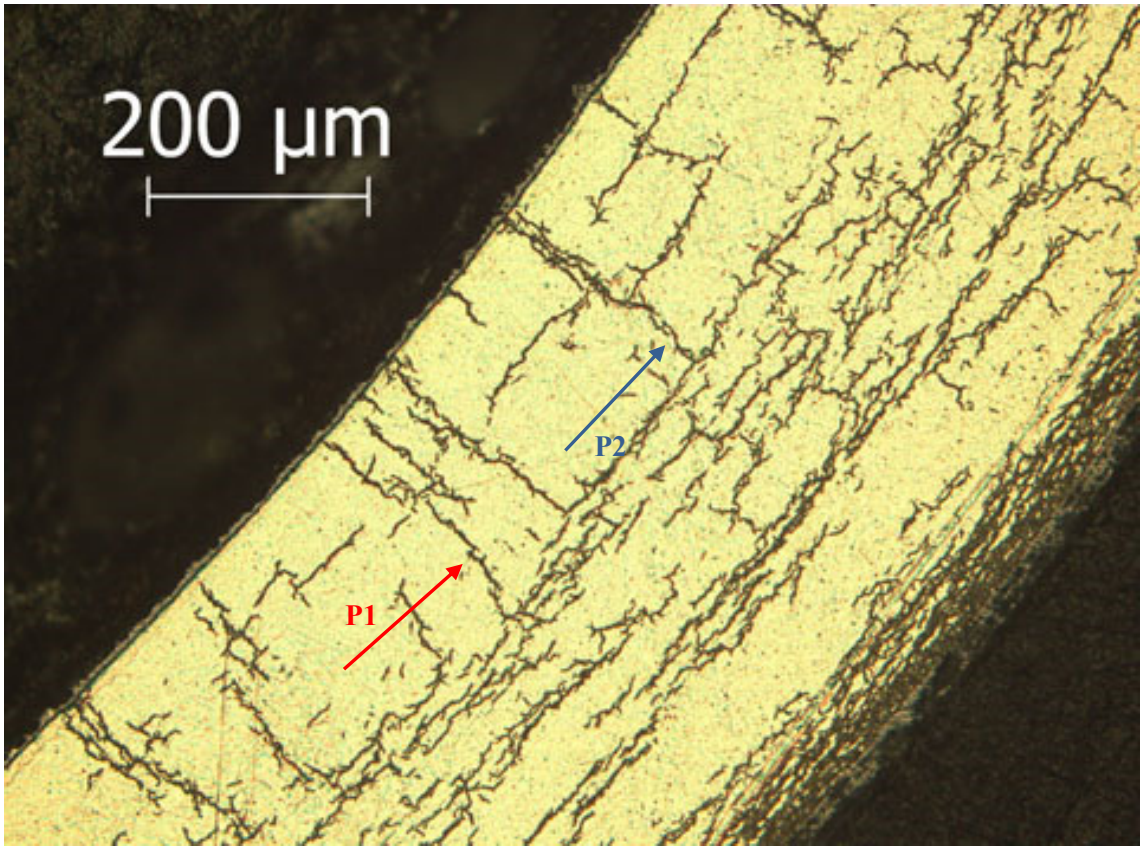

Figure 6: 100X image of HBU ZIRLO™ sample 648C7 at 4:30 o'clock orientation from 1-cycle 400°C RHT rodlet with 110-MPa peak hoop stress.

The red arrow corresponds to one assessment of the pathway (P1) of the longest continuous radial-circumferential hydride (about 50% RHCF) along which a crack could easily initiate and propagate through half the wall thickness. The blue arrow indicates another assessment of the pathway (P2) of the longest radial-circumferential hydride (about 75% RHCF). As will be discussed in the RHCF section, the differences are the result of different interpretations of the 5-µm gap that is allowed in the assessment of continuity.

Higher magnifications of the hydrides near the blue arrow in Fig. 6 are shown in Fig. 7: (a) 200X image showing P2 radial hydride pathway and (b) 500X image of the same radial hydride near the cladding inner surface.

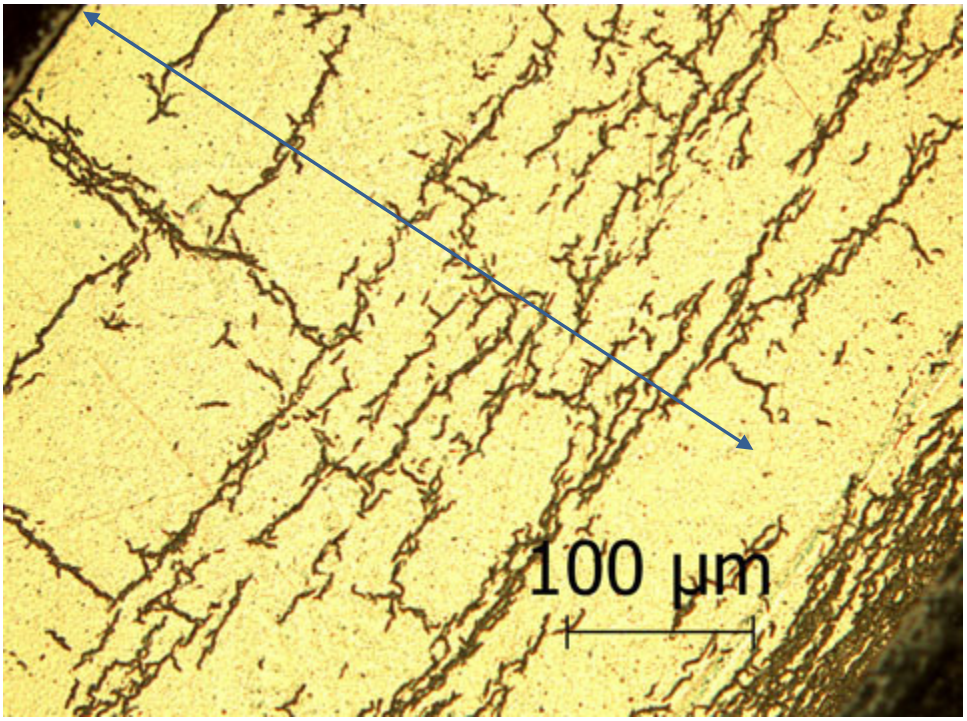

(a)

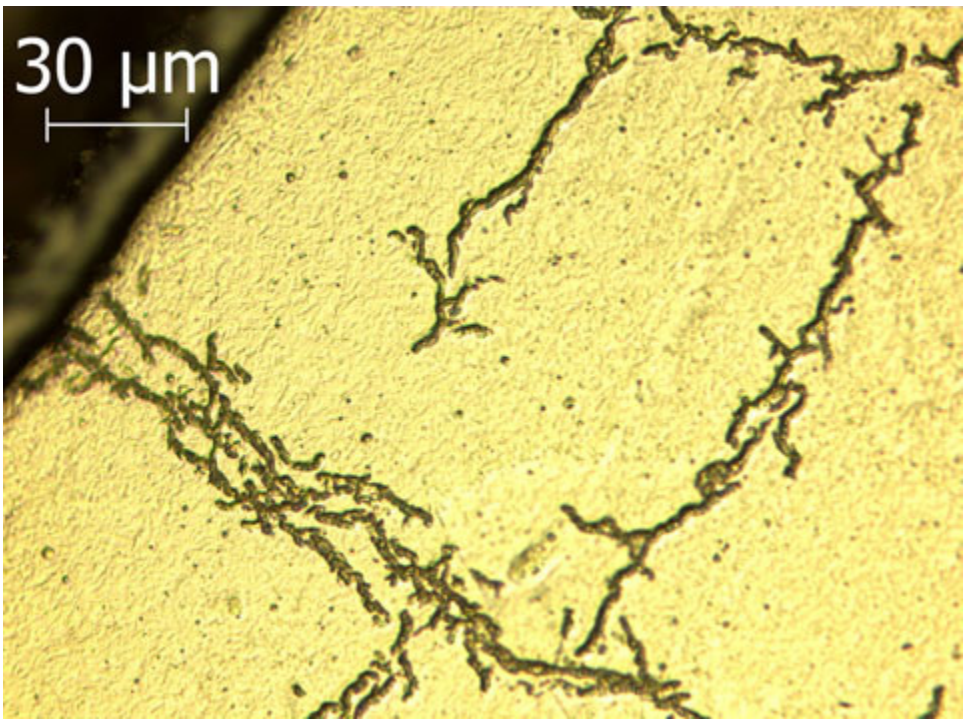

(b)

Figure 7: Images of HBU ZIRLO™ sample 648C7 at 4:30 o'clock orientation from 1-cycle 400°C RHT rodlet with 110-MPa peak hoop stress: (a) 200X and (b) 500X.

Figure 8 shows the sectioning diagram for M5® rodlet 651E3 following cooling from 400°C and target (actual) hoop stress of 90 MPa.

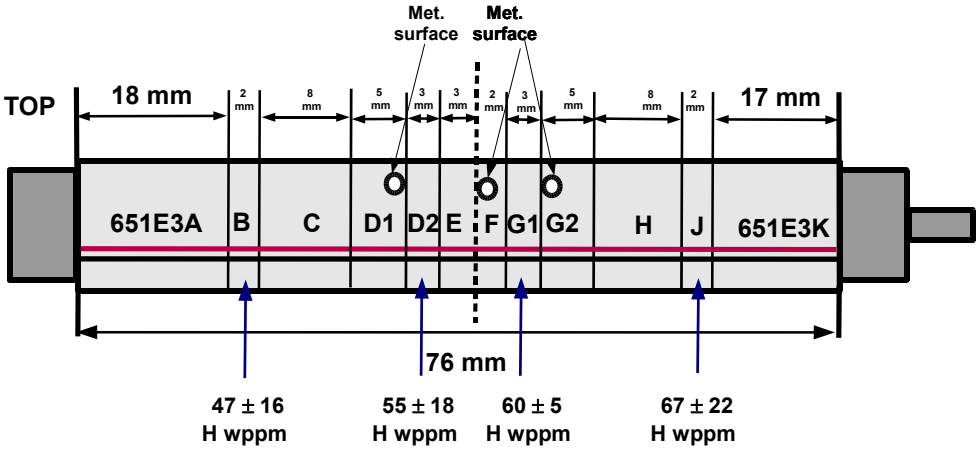

Figure 8: Sectioning diagram for HBU M5® rodlet subjected to 1-cycle 400°C RHT at 90-MPa peak stress.

Sample 651E3D1 was retrieved from storage, re-ground, re-polished, and carefully re-etched. Relative to the ZIRLO™ sample 648C7, much less material had to be ground off to reach an etch-free surface. This qualitative observation suggests relatively poor axial connectivity of hydrides for the M5® sample as compared to the ZIRLO™ sample. Images were taken at 37 orientations at 100X magnification to ensure that the whole cross section could be characterized. Interesting regions containing long radial hydrides were also imaged at 200X and 500X to assess radial hydride continuity. Figure 9 shows an interesting region (100X magnification at 10:00 o'clock orientation) with the longest radial hydrides (73% RHCF). Figure 10 shows 200X and 500X images for the same hydride.

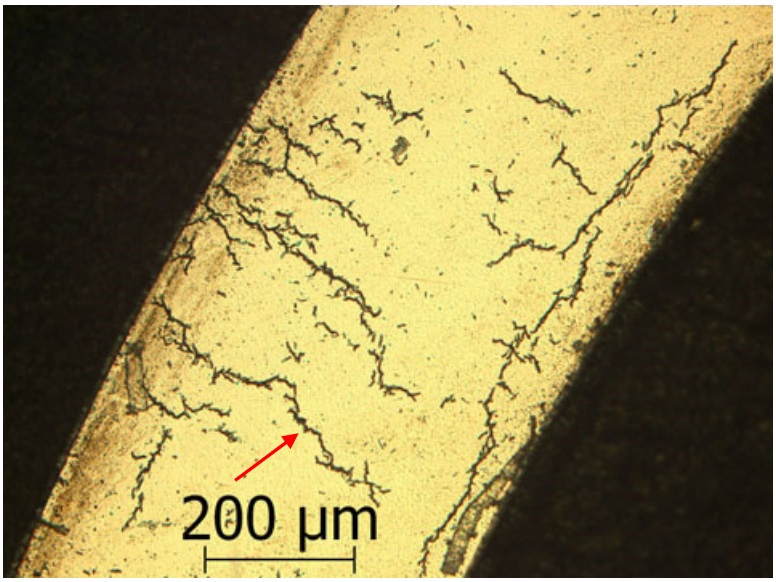

Figure 9: 100X image of HBU M5® sample 651E3D1 at 10:00 o'clock orientation from 1-cycle 400°C RHT rodlet with 90-MPa peak hoop stress.

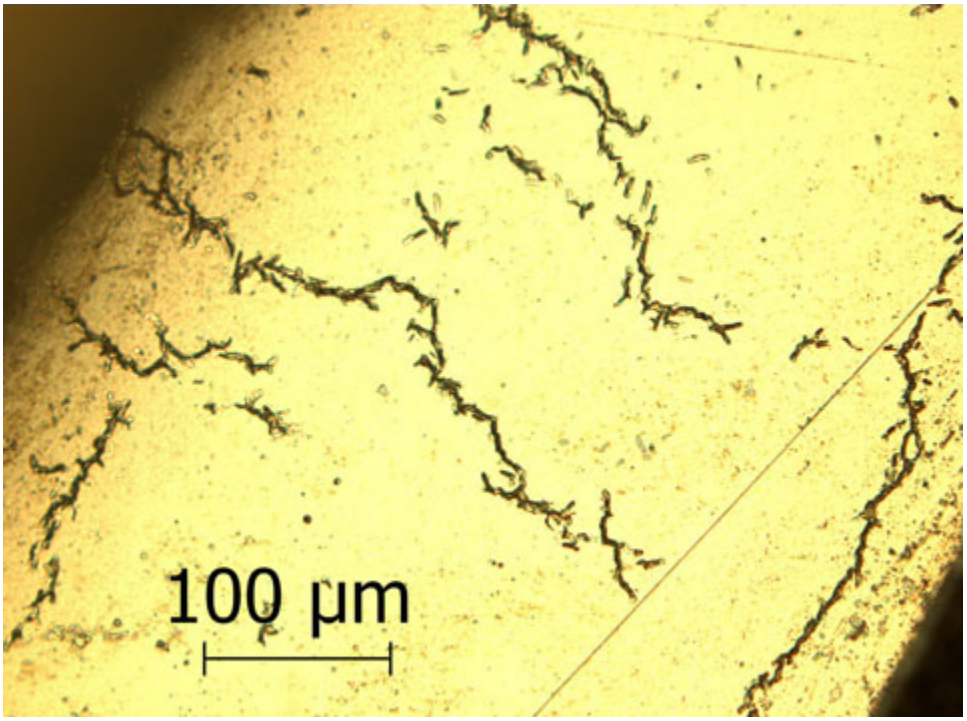

(a)

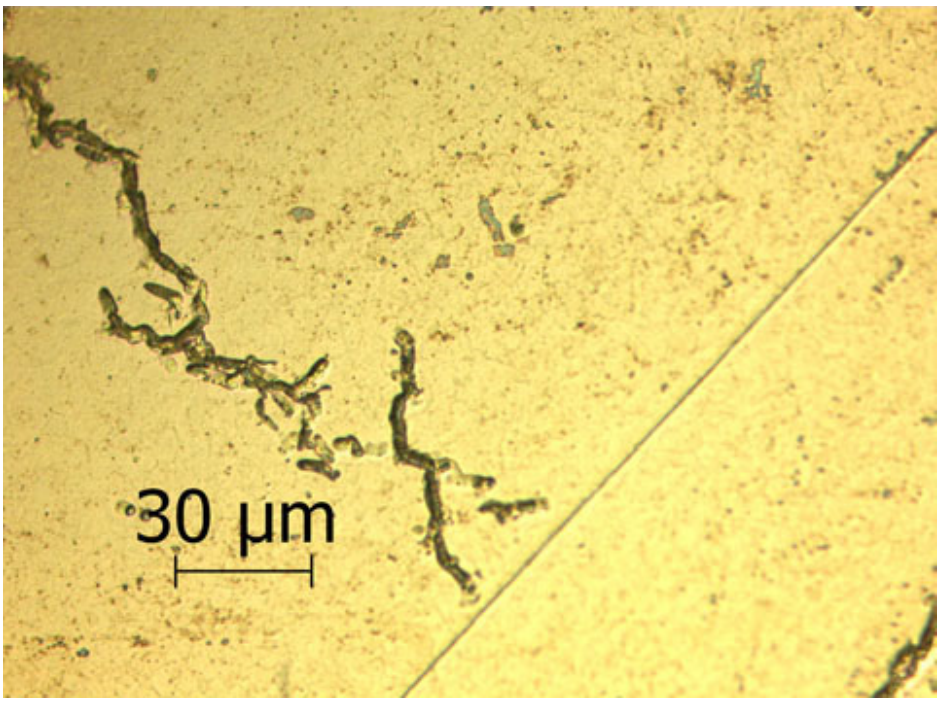

(b)

Figure 10: Images of HBU M5® sample 651E3D1 at 10:00 o'clock orientation from 1-cycle 400°C RHT rodlet with 90-MPa peak hoop stress: (a) 200X and (b) 500X.

Comparison of Figures 6-7 and 9-10 clearly indicates that the hydrides in M5® are primarily oriented in the radial direction, are long, and may be somewhat more discontinuous than the radial hydrides observed in the ZIRLO™ sample. Also, the longer hydrides observed for the ZIRLO™ cross section tend to emanate more from the cladding inner surface. From the perspective of hoop bending stress distributions in RCTs, cracks are more likely to initiate at the cladding inner surface (12:00 and 6:00 o'clock orientations) at low displacements than at the cladding outer surface (3:00 and 9:00 o'clock orientations).

Radial Hydride Fraction (RHF)

The RHF is the most common metric reported in the literature to assess the degree of hydride reorientation. Aomi et al. [11] give two definitions for RHF, fn(40) and fn(45). These differ in terms of the determination of radial hydrides: the fn(40) considers hydrides to be oriented in the radial direction if their orientation is within ±40° of the radius, and the fn(45) considers hydrides to be oriented in the radial direction if their orientations are within ±45° of the radius. Also, fn(40) is defined as ratio of the number of radial hydrides to the number of all hydrides. This definition would not result in a meaningful metric for the current work. The metric fn(45) is defined as the total length of all radial hydrides divided by the total length of all hydrides. Thus, RHF in the current work is equated to fn(45).

On the basis of the 36 images for the ZIRLO™ sample, RHF = 0.30±0.05. On the basis of 37 images for the M5® sample, RHF = 0.81±0.08. The dense circumferential hydrides in the rim region were not included in this calculation. Given that the M5® RCT samples had high ductility (<20°C DBTT) relative to the ZIRLO™ RCT samples (125°C DBTT), it is clear that RHF is not a meaningful metric for predicting radial-hydride-induced embrittlement.

Radial Hydride Length Density (RHLD)

Aomi et al. [11] also evaluated another metric, which appears to be more promising than fn(40) or fn(45). This metric, which is referred to as RHLD in this work, is defined as the total length (in mm) of radial hydrides within a given surface area normalized to the surface area (in mm^2). Because it was unlikely that this metric alone would correlate with the DBTT values, areas were identified within the inner third, the middle third, and the outer third of the cladding wall, excluding the dense hydride rim for ZIRLO™. The RHLD values for the whole cross section were 7.47±1.68 mm^{-1} for ZIRLO™ and 5.84 mm^{-1} for M5®. The RHLD is a better metric than RHF for correlation with DBTT because at least it is higher for ZIRLO™ than it is for M5®. However, an even better metric for RCT loading would take into account the locations of the radial hydrides. Radial hydrides that emanate from the inner surface of the cladding would initiate cracks at the 12:00 and 6:00 o'clock orientations at lower RCT displacements than radial hydrides that emanate from the outer surface at the 3:00 and 6:00 o'clock orientations. Radial hydrides near the mid wall would be subjected to very low bending stresses prior to crack initiation. Also, it is much more difficult to initiate a crack within the cladding wall than at the cladding surface. Thus, mid-wall radial hydrides are benign with respect to crack initiation, but they can contribute to crack propagation. The ratios of RHLD for ZIRLO™ over that for M5® were measured to be 1.77, 1.25, and 0.74. Thus, RHLD for the inner third of the cladding wall would be a better metric than the wall-averaged RHLD for correlation with DBTT.

Radial Hydride Continuity Factor (RHCF)

The RHCF has been used throughout the Argonne work for correlation with DBTT. It is defined as the path length of connected radial-circumferential hydrides within a mid-wall arc length of 150 µm projected onto the radius and normalized to the cladding wall thickness. In simpler terms, it is an assessment of how far a crack might grow across the cladding wall. Also, the assessment of "continuity" allows a 5-µm gap between radial hydrides that are aligned. This allowance was established based on the assumption that a radial crack could easily propagate 5 µm through the matrix metal from one brittle radial hydride to another. The allowance was not intended to be used for parallel radial hydrides or for junctions between radial and circumferential hydrides because it would be more difficult for a crack to propagate through the matrix metal parallel to the global stress field, which is in the hoop direction. There are also practical factors to consider in this gap allowance. The apparent gap based on 100X images is larger than the apparent gap for 200X images. Also, the 200X images are more likely to capture small, lighter-colored regions that partially fill the gap between the darker hydrides. It is unclear as to whether or not these regions represent hydrides (perhaps just below the cross-section surface) or are an artifact of the etching and imaging process. Thus, in evaluating an image to determine the RHCF, some judgment needs to be exercised to assess whether or not a growing crack can rapidly cross the small gap to continue growing along another hydride.

The RHCF for the cross section of ZIRLO™ sample 648C7 was previously evaluated to be 33±14% based on 33 images that essentially included the whole cross section. Re-examination of 36 new images at a location about 0.1 to 0.2 mm below the original surface led to essentially the same results: RHCF = 32±12%. Overall, the average of the two sets of results leads to RHCF = 32±13%. Within experimental error in determining RHCF, these results are essentially the same. It should be noted that if the 5-µm gap is treated as an absolute distance independent of hydride orientation, the RHCF increases to 39±14%. The largest difference between P1- and P2-determined RHCF values is 49% vs. 76% (see Fig. 6 for the different pathways used to determine RHCF).

The RHCF for the cross section of the M5® sample 651E3D1 was 36±14% based on 21 orientations around the cross section. New results for the re-ground, re-polished, and re-etched cross section were higher based on both P1 and P2 treatments of the 5-µm gap: RHCF = 47±15% for P1 and RHCF = 50±16% for P2. For the other location examined (at 15 orientations) based on P1, the RHCF was 33±19% (651E3G2). Overall, the average RHCF for M5® rodlet 651E3 was calculated to be 37±17%.

Although improved values of RHCF have been determined, those for low-DBTT M5® and high-DBTT ZIRLO™ are still comparable: 37±17% and 32±13%. Tables 2 (ZIRLO™) and 3 (M5®) were generated to include the location of these radial hydrides with respect to the cladding inner surface (more damaging) and outer surface (less damaging). For ZIRLO™, hydrides in the outer region of the cladding that contacted the hydride rim were treated as radial hydrides in contact with the cladding outer surface. Radial hydrides that contact neither surface are the least damaging. The results clearly indicate that the radial hydrides in ZIRLO™ would lead to a higher DBTT than the radial hydrides in M5®. In particular, many (21 out of the 36 orientations listed) of the radial hydrides in the M5® sample contact neither the inner surface (ID) nor the outer surface (OD), and only 7 of the radial hydrides contact the cladding inner surface.

The results in Tables 2 and 3 suggest that the RHCF could be modified by applying a weighted averaging technique that accounts for the locations of the radial hydrides across the cladding wall.

Also, to ensure consistency in RHCF measurement, the 5-µm gap allowed in the determination of continuity is defined as a gap within ±45° of the cladding radius.

Table 2 Detailed analysis of local RHCF values and locations for HBU ZIRLO™ sample 648C7

Orientation, o'clock	RHCF, %	ID Contact	OD Contact
12:00	42	Yes	No
12:30	58	Yes	No
1:00	20	Yes	No
1:15	13	No	No
1:30	21	Yes	No
1:45	28	Yes	No
2:00	22	No	No
2:15	24	Yes	No
2:30	18	No	Yes
2:45	52	Yes	No
3:00	16	No	Yes
3:15	19	No	No
3:30	23	No	Yes
4:00	41	Yes	No
4:30	49	Yes	No
4:45	39	Yes	No
5:00	31	Yes	No
5:30	40	Yes	No
6:00	20	Yes	No
6:15	42	No	No
6:30	37	Yes	No
7:00	20	Yes	No
7:15	49	Yes	No
7:45	22	Yes	No
8:00	47	Yes	No
8:15	55	Yes	No
8:45	36	Yes	No
9:00	33	No	No
9:15	32	Yes	No
9:30	27	No	No
9:45	24	Yes	No
10:00	30	No	No
10:30	33	Yes	No
11:00	19	No	No
11:15	34	Yes	No
11:45	19	No	No

Table 3 Detailed analysis of local RHCF values and locations for HBU M5® sample 651E3D1

Orientation, o'clock	RHCF, %	ID Contact	OD Contact
12:00	86	Yes	No
12:30	43	No	Yes
1:00	32	Yes	No
1:30	57	Yes	No
1:45	43	No	Yes
2:00	44	No	No
2:15	69	No	No
2:30	79	No	Yes
2:45	46	No	No
3:00	29	No	Yes
3:15	41	No	No
3:30	29	No	No
3:45	45	No	Yes
4:00	26	No	No
4:15	41	No	No
4:45	41	No	No
5:00	48	No	No
5:30	46	No	No
5:45	38	No	No
6:00	54	Yes	No
6:30	44	No	No
6:45	57	No	No
7:00	32	No	No
7:30	43	No	No
7:45	33	No	No
8:00	63	No	No
8:15	50	Yes	No
8:45	23	No	No
9:00	40	No	No
9:15	63	No	Yes
9:30	50	No	No
10:00	73	Yes	No
10:45	78	No	Yes
11:00	29	No	Yes
11:15	63	No	No
11:45	33	Yes	No

3.2 Re-evaluation of Cladding RCT Ductility

Load-displacement curves were re-evaluated by using the unloading slope given by Eq. 2. Figures 11 and 12 show revised ductility vs. RCT temperature curves for M5® and ZIRLO™, respectively. The re-evaluated offset strains did not change the DBTT values previously established.

The hoop stresses shown in Figs. 11 and 12 are the maximum values at 400°C. From a mechanistic viewpoint, the hoop stress at the initiation of hydride precipitation, especially radial hydride precipitation, is more fundamental. Table 4 summarizes the HBU ZIRLO™ parameters relevant to determining the temperature (T_P) at which hydride precipitation would initiate and the corresponding hoop stress. The value of 65°C ΔT_{PD} (difference between the T_P and hydride dissolution temperature, T_D) used in Table 4 is based on the Kammenzind et al. data [13] shown in Fig. 1. Table 5 contains the same type of information for HBU M5®. The parameters T_D and T_P are determined for the average hydrogen content of the M5 samples, where the T_P (= T_D - ΔT_{PD}) values are based on the McMinn et al. data [14] for ΔT_{PD} in Fig. 1.

Table 4 Hoop stresses for HBU ZIRLO™ samples subjected to 1-cycle 400°C RHT.

Parameter	105B	105C	648C
C_H, wppm	535±50	530±115	350±80
p_i(23°C), MPa	4.65	5.22	6.60
σ_θ(400°C), MPa	80	89	112
T_P, °C	335	335	335
σ_θ(335°C), MPa	72	80	101

Table 5 Hoop stresses for HBU M5® samples subjected to 1-cycle 400°C RHT.

Parameter	651E3	651E5	645D
C_H, wppm	58±15	72±10	94±4
p_i(23°C), MPa	4.65	5.22	6.60
σ_θ(400°C), MPa	90	111	142
T_D, °C	288	306	330
T_P, °C	245	261	283
σ_θ(335°C), MPa	69	88	117

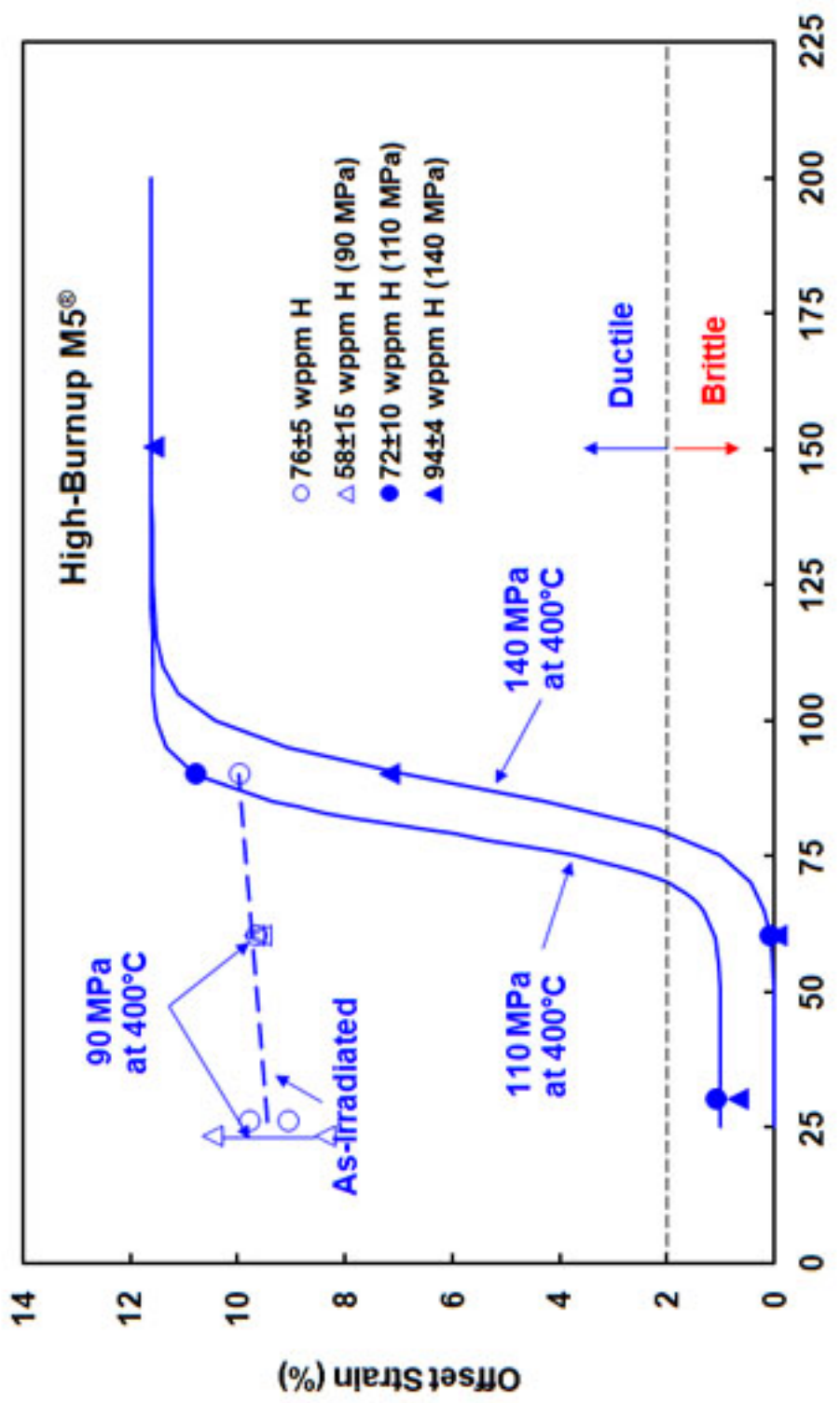

Figure 11: RCT offset strain vs. RCT temperature for HBU M5® following irradiation and following RHT at peak 400°C hoop stresses of 90 MPa, 110 MPa, and 140 MPa.

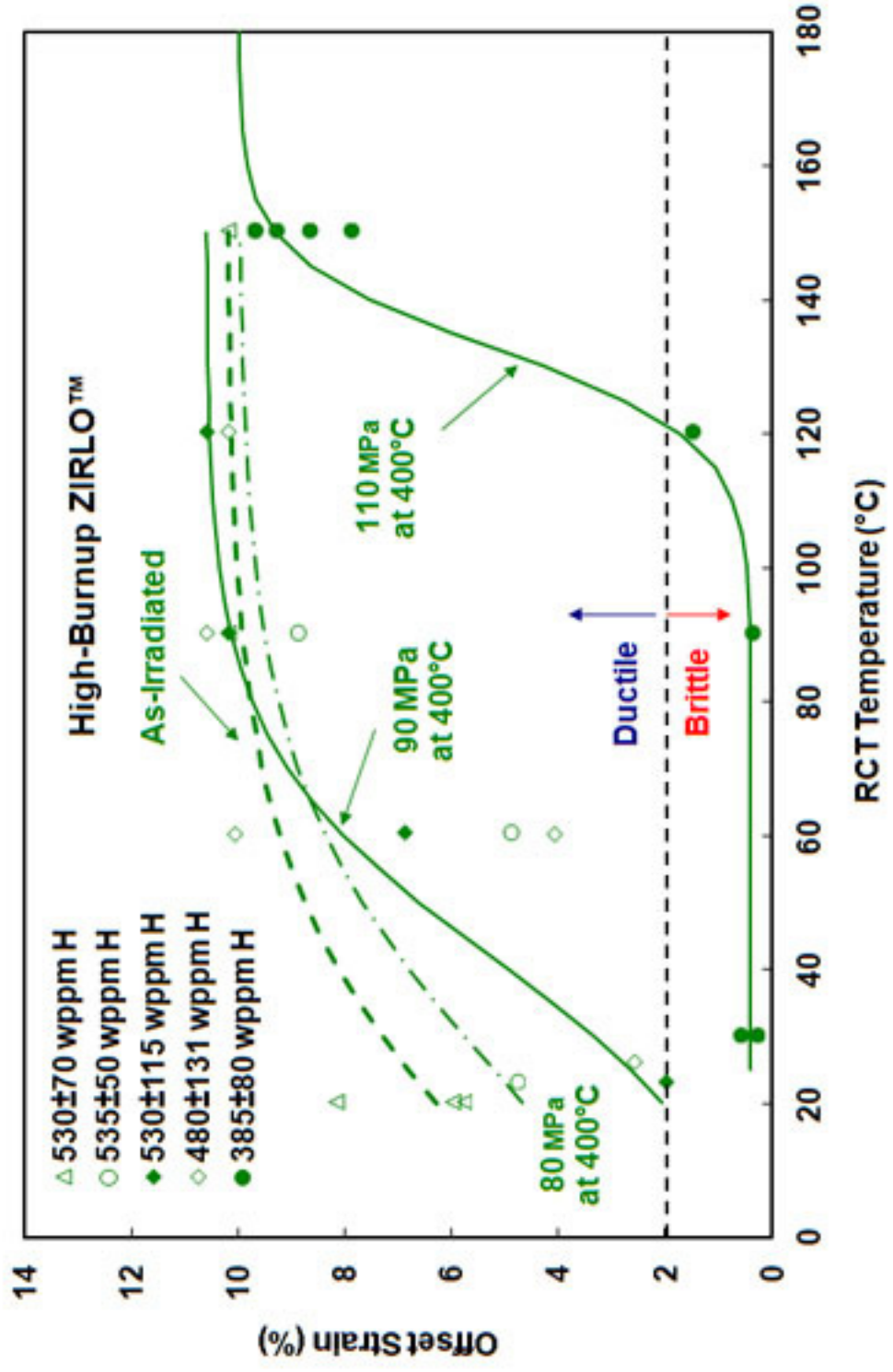

Figure 12: RCT offset strain vs. RCT temperature for HBU ZIRLO™ following irradiation and following RHT at peak 400°C hoop stresses of 80 MPa, 90 MPa, and 110 MPa.

4. RESULTS FROM MULTIPLE-CYCLE DRYING TESTS

4.1 Three-Cycle Drying Test at 400°C Peak RHT Temperature

This test serves as a baseline for the test results reported in Section 4.2 for three-cycle drying at 350°C. In shorthand notation, it is referred to as "3-cycle 400°C RHT." Some of the results presented in Ref. 10 are repeated here for the convenience of the reader. New results are also presented for RCT ductility.

Figure 13 shows the sectioning diagram for rodlet 105D, which was subjected to a 3-cycle 400°C RHT at a peak RHT hoop stress of 90 MPa. The average hydrogen content of the sample was 480±131 wppm, and the RHCF was 20±9%. The DBTT was 20°C. Figure 14 shows a micrograph of the location with the maximum RHCF (36%).

The RCT ductility values for rings 3, 4, 7, and 8 were corrected based on the unloading slope correlation given in Eqs. 2a and 2b. However, the load-displacement curve for ring 7 was re-evaluated to better determine the ductility at which >50% wall cracking may have occurred. Figure 15 shows the load-displacement curve for the HBU ZIRLO™ RCT sample (105D7) tested at 60°C. In Ref. 10, the precipitous load drop of 52% was used to determine a high corrected offset strain of 9.4%. However, during the loading phase, the ring achieved a peak load of only about 400 N, which is less than the expected 460 N based on a companion ring from rodlet 105C also tested at 60°C. Therefore some cracking, likely in the hydride rim, occurred prior to achieving peak load. This effect corresponds to about a 13% load drop, which is too small to result in a crack >50% of the wall thickness. The load remained relatively flat prior to the precipitous load drop at 407 N. This result is indicative of increased number of cracks and/or increased crack depth. Based on a re-analysis of this curve, a crack >50% of the wall might have occurred anywhere between corrected offset strains of 4.1% to 10.1% or within 7.1±3.0%. Figure 16 shows the re-evaluated ductility results for rodlet 105C rings (1 cycle) and rodlet 105D rings from the 3-cycle 400°C RHT test at the same peak hoop stress of 90 MPa. Clearly, the temperature cycling had no impact of the ductility vs. temperature and the DBTT.

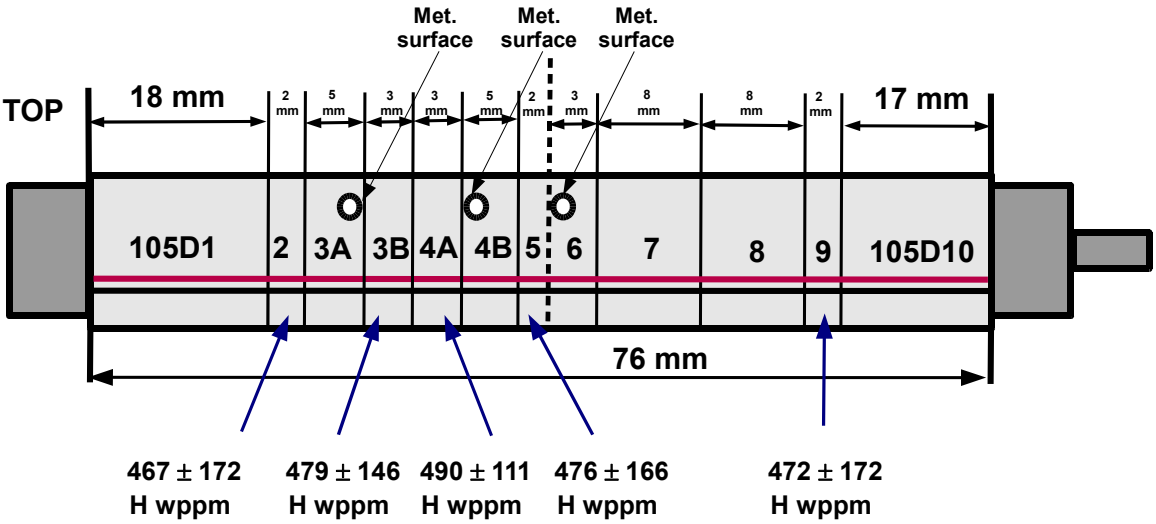

Figure 13: Sectioning diagram for HBU ZIRLO™ rodlet 105D subjected to 3-cycle 400°C RHT at peak hoop stress of 90 MPa.

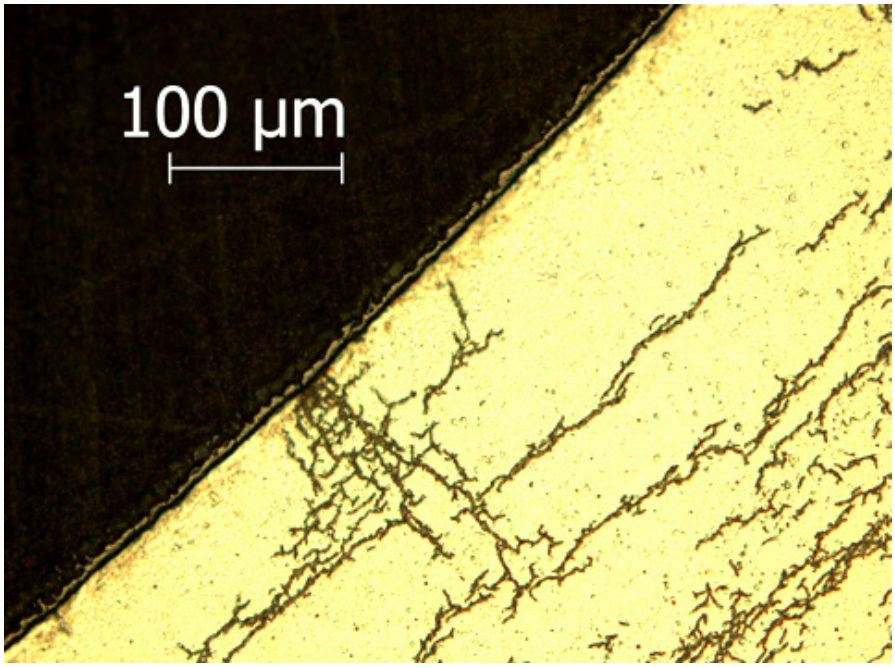

Figure 14: Peak RHCF value (36%) for HBU ZIRLO™ rodlet 105D subjected to 3-cycle 400°C RHT at peak hoop stress of 90 MPa.

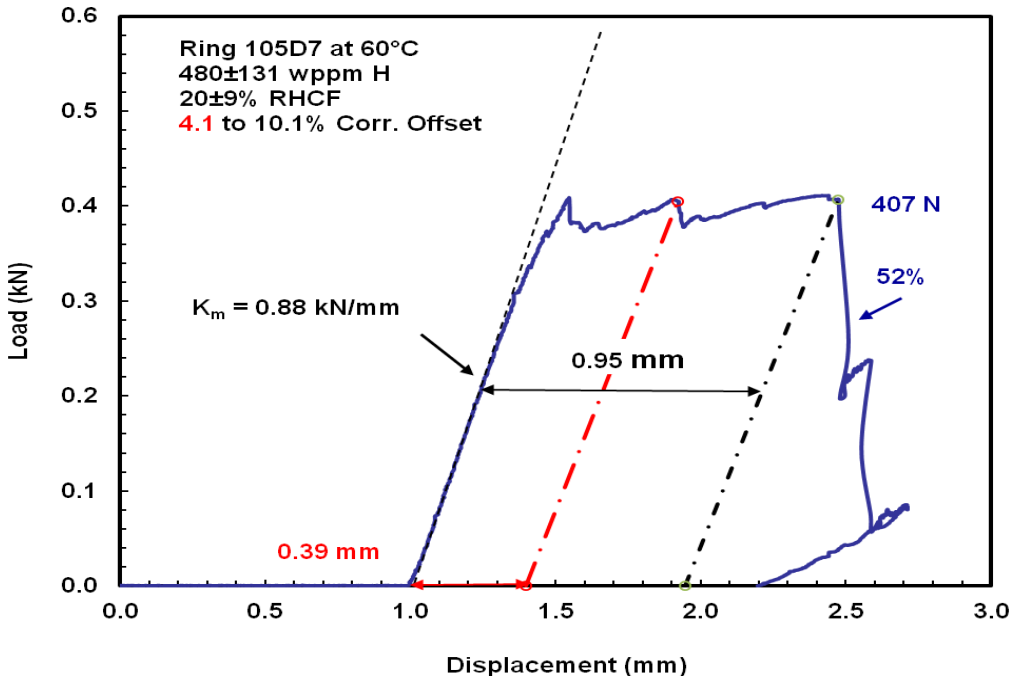

Figure 15: Load-displacement curve for RCT conducted at 60°C with sample from the HBU ZIRLO™ rodlet subjected to 3-cycle 400°C RHT at peak hoop stress of 90 MPa.

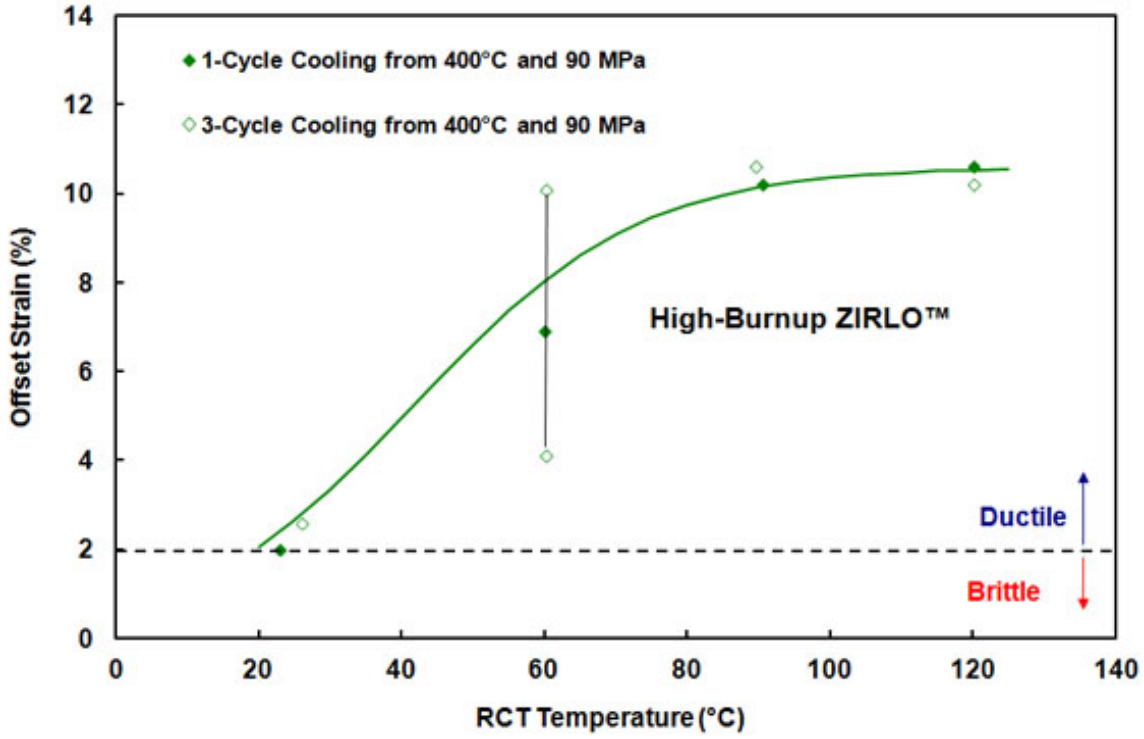

Figure 16: Ductility data and DBTT for HBU ZIRLO™ subjected to 1-cycle and 3-cycle 400°C RHT at peak hoop stress of 90 MPa.

4.2 Three-Cycle Drying Test at 350°C Peak RHT Temperature

The three-cycle peak temperature in the simulated drying/storage for HBU ZIRLO™ rodlet 105E was reduced to 350°C, the temperature drop per cycle was maintained at 100°C for comparison of results to those for rodlet 105D, and the RT internal pressure was increased to 5.97 MPa to give an intermediate RT internal pressure between those used in the 3-cycle 400°C RHT test at peak hoop stress of 90 MPa (see Section 4.1) and the 1-cycle 400°C RHT test at peak hoop stress of 110 MPa, for which the DBTT was 125°C. If rodlet 105E had been heated to 400°C, the hoop stress would have been about 100 MPa. At 350°C, the peak hoop stress is 92 MPa. The sectioning diagram for the 3-cycle 350°C RHT rodlet 105E is shown in Fig. 17.

Three hydrogen measurements were performed on sectioned rings 2, 5, and 9, as indicated in Fig. 17. Local values varied from 377 wppm to 838 wppm, with most of that variation occurring in the circumferential direction due to the variation in hydride rim thickness. The mass-averaged hydrogen content for rodlet 105E was 560±196 wppm, where the 196 wppm represents one standard deviation for the 12 measurements.

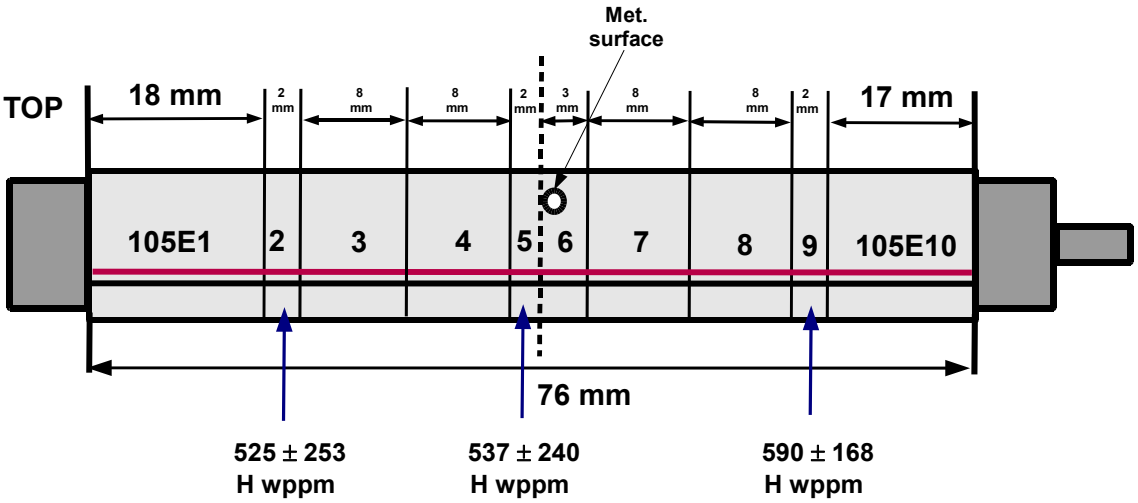

Figure 17: Sectioning diagram for HBU ZIRLO™ rodlet 105E subjected to 350°C RHT at peak hoop stress of 92 MPa with two intermediate cooling-heating cycles (ΔT = 100°C).

Extensive metallographic images of the etched cross section of ring 105E6 were taken to characterize the hydride morphology after 3-cycle simulated drying and storage at 350°C. Appendix A contains 34 images from this characterization, along with the corresponding RHCF values. In general, the effective lengths of the hydrides (18% to 53%) were much greater than expected. The average RHCF was 32±12%, which is the same value obtained for rodlet 648C following the 1-cycle 400°C RHT test at peak hoop stress of 110 MPa. The peak RHCF value was even higher (89%) if the absolute gap values of ≤5 μm were used to determine the continuous pathway for radial-circumferential hydrides. The partial cross section for this peak RHCF value was at the 7:30 o'clock orientation. Figures 18(a) and 18(b) show 100X and 200X images at this same location, respectively. The pathways P1 (50% RHCF) and P2 (89% RHCF) for the hydride in question are labeled in Fig. 18a.

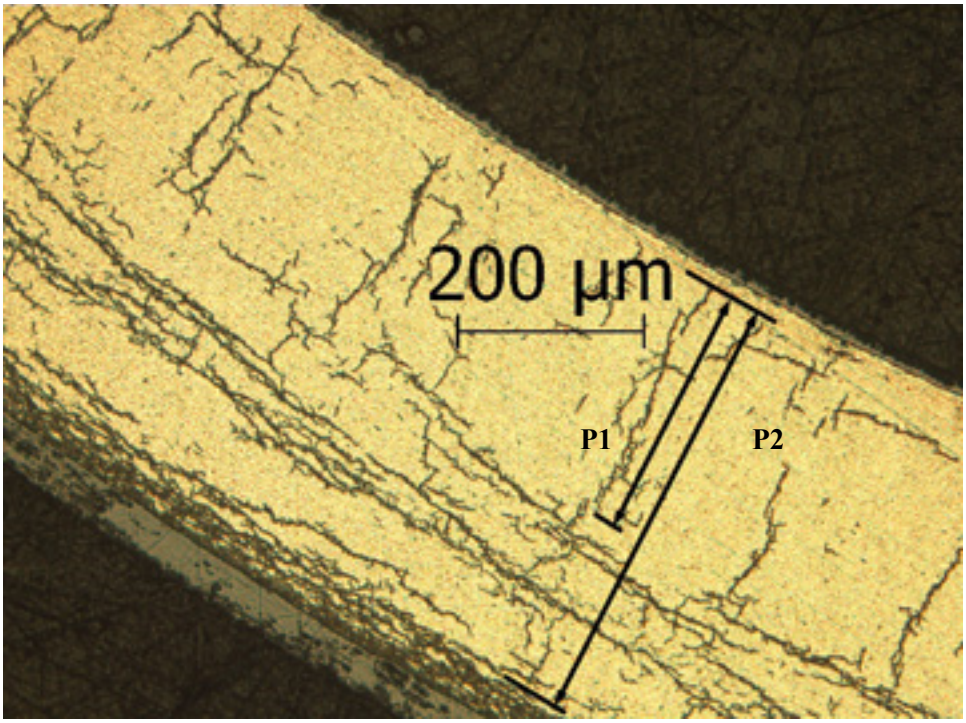

(a)

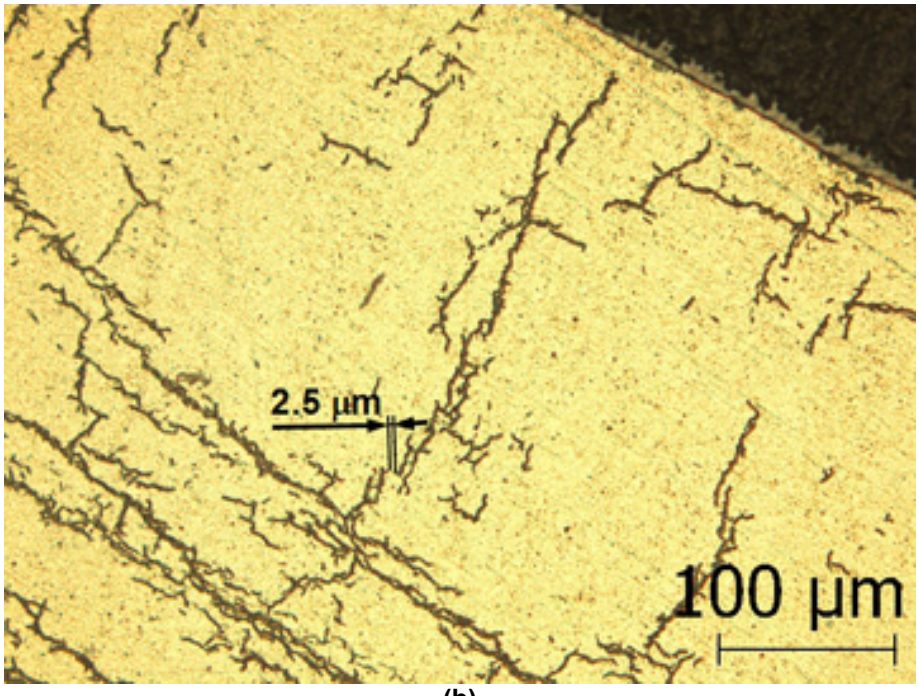

(b)

Figure 18: Metallographic images for HBU ZIRLO™ sample 105E6 at the 7:30 o'clock orientation from the 3-cycle 350°C rodlet: (a) 100X and (b) 200X.

Note that the apparent gap labeled as 2.5 µm in Fig. 18(b) appears to be in the range of 4 to 8 µm based on the 100X image shown in Fig. 18(a) and more clearly shown in Fig. A.21. Also, the gap is in

the circumferential direction, which is parallel to the global stress field. It would be difficult for the radial crack to propagate across a gap in the circumferential direction. As is standard for determining cladding dimensions, the cladding outer diameter was measured before and after RHT using a micrometer. Metallographic examination of the as-polished (i.e., not etched) 105E6 cross section was used to determine the oxide layer thickness (at 200X magnification) and cladding metal wall thickness (at 100X magnification). These data were used to determine the geometrical parameters of interest listed in Table 6 for the 3-cycle 350°C test of the HBU ZIRLO™ rodlet 105E and the 3-cycle 400°C test of rodlet 105D at peak hoop stress of 92 MPa and 90 MPa, respectively.

Table 6 Post-RHT characterization results for HBU ZIRLO™: 3-cycle 350°C rodlet (105E) subjected to 92 MPa and 3-cycle 400°C rodlet (105D) subjected to 90 MPa prior to cooling at 5°C/h.

Parameter	Rodlet 105E 350°C RHT 3-Cycle Cooling	Rodlet 105D 400°C RHT 3-Cycle Cooling
Outer Diameter (D_o), mm	9.53	9.53
Oxide Layer Thickness (h_{ox}), µm	48	40
Metal Outer Diameter (D_{mo}), mm	9.43	9.45
Metal Wall Thickness (h_m), mm	0.56	0.56
Metal Inner Diameter (D_{mi}), mm	8.31	8.33
Hydrogen Content (C_H), wppm	560±196	480±131
RT Internal Pressure (p_i), MPa	5.97	5.28
Dissolved Hydrogen at T_{max} (C_{HD}), wppm	126	206
Precipitation Temperature (T_P), °C	282	335
Maximum Hoop Stress (σ_θ), MPa	92	88
Hoop Stress (σ_θ) at T_P, MPa	83	80
Radial-Hydride Continuity Factor (RHCF), %	32±12	20±9
Ductile-to-Brittle Transition Temp. (DBTT), °C	≈120	20

The hoop stresses at which new hydrides can precipitate are very similar for rodlets 105E (83 MPa) and 105D (80 MPa). As no radial hydrides are present in the as-irradiated cladding or at the peak RHT temperature, they must precipitate as new hydrides at the indicated temperatures of 282°C for rodlet 105E and 335°C for rodlet 105D. Given that the hoop stress for 105E is only marginally higher at initiation of precipitation than that for 105D, it is surprising that the extent of radial hydride precipitation is so much greater for rodlet 105E. This finding may be due to subtleties associated with differences in the effects of temperature cycling for the two rodlets. The Kammenzind et al. correlations (Fig. 1) were used to determine ΔT_{PD} = 65°C (117°F) – the allowable cladding temperature variations during drying cycles in ISG-11, Rev. 3. However, it needs to be emphasized that the results in Fig. 1 apply to cases in which all the hydrogen is dissolved at the peak drying temperature. Dissolution of hydrogen during heating and holding at a steady temperature is very rapid, as is hydrogen diffusion, so the equilibrium solubility limit is reached relatively quickly at the target hold temperature. Precipitation of hydrides, on the other hand, is complicated as it involves nucleation and growth and is seldom in equilibrium during vacuum drying. A simple explanation is that it would take more energy to precipitate new hydrides because the lower density of the hydrides results in a volume expansion that strains the matrix metal. That may explain why a

supersaturated solution is often needed to initiate precipitation. The C_{HP} vs. T curve in Fig. 1 represents the dissolved hydrogen needed to initiate precipitation. With incremental cooling below T_P, additional hydrides precipitate and existing hydrides grow in length. Another subtle complication with hydride precipitation is that if hydrides are present at the peak hold temperature, some hydrogen will precipitate during the 65°C temperature drop that occurs during cooling because it takes less energy to grow an existing hydride than it does to precipitate a new hydride. As the temperature continues to decrease below T_P, there is a competition between adding to the length of existing hydrides and precipitation of new hydrides.

In applying the results in Fig. 1, the following sequence is assumed to occur. For all HBU ZIRLO™ samples tested, the hydride morphology is essentially the same: very dense hydride rim whose thickness depends on the total hydrogen content and ≈140-wppm C_H below the hydride rim, as measured in the inner two-thirds of the cladding radius [9, 10]. Most of the hydrogen below the rim of as-irradiated HBU ZIRLO™ test samples is located in a band of circumferential hydrides at the cladding mid-radius. During heating to 400°C, it is likely that all the hydrogen below the hydride rim goes into solution (140 wppm), and the remaining 66 wppm of dissolved hydrogen comes from the hydride rim. This is based on the assumption that isolated hydrides dissolve more easily than the dense hydrides in the rim.

During heating to 350°C, enough hydrogen is below the rim to dissolve 126 wppm, and some hydrides likely remain below the cladding rim (at least 14 wppm). During cooling from 400°C to 300°C, some hydrogen will precipitate as new radial and circumferential hydrides, and a small amount of hydrogen may precipitate onto the existing hydride rim. Upon heating back to 400°C, essentially the same hydride morphology should be reproduced, with all the hydrogen below the hydride rim going into solution. If this were to be the case, then subsequent temperature cycles would not add to the number or lengths of radial hydrides. However, the situation is different for the 105E rodlet, which was heated to only 350°C. During cooling from 350°C to 285°C, some hydrogen will precipitate onto existing circumferential hydrides, and new hydrides would precipitate during cooling from 285°C to 250°C. At this point in the cycling, the extent of radial hydride precipitation should be similar for rodlets 105E and 105D. However, during re-heating to 350°C, dissolution of circumferential hydrides could be greater than dissolution of radial hydrides, such that some radial hydrides could remain after the second heating cycle. If this were the case, then the number and extent of radial hydrides could grow with each temperature cycle.

Experiments have been performed with pre-hydrided, non-irradiated Zry-4 under the thermal cycling conditions used for rodlet RHT temperatures [15]. However, these were performed at a higher, constant stress level, (160 MPa vs. 90 MPa for rodlet 105D). For samples with 130 wppm C_H (below the solubility limit), the most significant increase in radial hydrides occurred during the first heating cycle with a modest increase through the 4th cycle and essentially no increase from cycle 4 to cycle 12. However, the 250-wppm C_H case resulted in a much higher radial hydride fraction, which increased with each cycle from about 60% after the 1st cycle to 80% after the 2nd cycle to about 90% after the 4th cycle. Although it is difficult to compare the Argonne results to those of Chu et al. [15] because of differences in materials, hydride distributions, and stress histories, the above explanation is supported by the results in Ref. 15.

Page intentionally blank

5. DISCUSSION AND SUMMARY

Effects of Multiple Drying Cycles on DBTT

The 400°C results for HBU ZIRLO™ indicated no effects of multiple drying cycles on the extent of radial hydride precipitation and the resulting DBTT. This conclusion could be reached because results from companion one-cycle and three-cycle tests were available to allow a direct comparison. These tests were conducted at peak RHT conditions of 400°C and 90-MPa hoop stress. The multiple-cycle drying test was conducted with a temperature drop of 100°C per cycle for the three drying cycles. Both the radial hydride continuity factor (20% RHCF) and the DBTT (20°C) were consistently low for these tests.

The three-cycle test was repeated for a maximum RHT temperature of 350°C, the same 100°C temperature drop per cycle, and a higher as-fabricated RT pressure. The important stress to compare for the three-cycle tests at 350°C and 400°C is the stress at which precipitation of new hydrides (radial and circumferential) would initiate: 83 MPa for the 350°C test and 80 MPa for the 400°C test. Although these stress levels are close, the 350°C test resulted in considerably longer radial hydrides (32% RHCF). Based on previous single-cycle test results with 32% RHCF, the DBTT for the 350°C test is estimated to be about 120°C. Possible reasons for the surprising increase in RHCF for this test are discussed in Section 4. As these reasons are very subtle, it is important to conduct another test with only one cycle at the same peak RHT temperature and hoop stress. Results of such a test would more definitively determine the effects of temperature cycling from 250°C to 350°C.

In addition to conducting tests with HBU ZIRLO™ at 350°C, at least one test with HBU M5® should be conducted at peak RHT temperature of 350°C. The database for HBU M5® is sparse for the peak RHT temperature of 400°C. Also, due to the low hydrogen content, it does not matter if additional testing is conducted at 400°C or 350°C because all the hydrogen in M5® is in solution at both of these temperatures. The issue to be resolved is the relative effects of decreasing RHT stress and decreasing C_H on the DBTT. Previous results indicated

- 80°C DBTT for peak RHT stress of 140 MPa and C_H of 94 wppm,
- 70°C DBTT for peak RHT stress of 110 MPa and C_H of 72 wppm, and
- <20°C DBTT for peak RHT stress of 90 MPa and C_H of 58 wppm.

At least one additional test is needed at an intermediate stress level (equivalent to 100 MPa at 400°C) and about 90-wppm C_H to distinguish the effects of hoop stress from hydrogen content in affecting the extent of radial hydride precipitation and the resulting DBTT.

Radial Hydride Metric(s)

In the context of the Argonne work, a meaningful metric or set of metrics for radial hydrides is one that correlates well with ductility and DBTT. The RHCF used throughout this work correlated well with the DBTT for HBU ZIRLO™ and Zry-4 with >300 wppm hydrogen. For HBU ZIRLO™, the DBTT decreased from 185°C to 125°C to 20°C as the RHCF decreased from 65% to 32% to 20%. However, these RHCT values do not translate to low-C_H HBU M5® with <20°C DBTT for 37% RHCF. Several metrics were evaluated and compared in Section 3. The two most promising metrics were the RHCF and the RHLD (total length of radial hydrides per unit surface area) if these metrics are weighted by location across the cladding wall to reflect the observation that radial hydrides within the inner third of the cladding wall are the most damaging, radial hydrides within the middle third of the cladding

wall are benign, and radial hydrides within the outer third of the cladding wall are moderately damaging with respect to crack initiation. This assessment is based on the distribution of RCT hoop bending stress across the cladding wall and around the circumference. In particular, radial hydrides that emanate from the cladding inner or outer surface have the most significant impact on crack initiation and subsequent propagation.

Future Work

Cladding hydride reorientation and embrittlement are areas that have been recommended in a recent DOE report [16] for additional R&D within the next 3 years. According to the scope of work planned for FY2015, one of the high priority activities is to establish the materials properties of cladding, especially for HBU cladding, and to supply models with the data necessary to determine how fuel rods will behave under normal, off-normal, and accident conditions, during both extended storage and transportation. Another FY2015 high-priority activity is to support the industry demonstration [17], which involves studies of fuel transfer options. The Argonne work next year will continue to focus on ring compression testing of HBU PWR cladding alloys subjected to peak drying-storage temperatures of 350°C to evaluate hydride re-precipitation at lower temperatures. This effort is based on thermal results for the demonstration analyses that indicate HBU PWR cladding alloys in the dry storage systems may operate at temperatures lower than the 400°C limit in ISG-11, Rev. 3.

REFERENCES

[1] K.J. Geelhood, W.G. Lusher, and C.E. Beyer, *PNNL Stress/Strain Correlation for Zircaloy*, Pacific Northwest National Laboratory Report PNNL-17700, July 2008.

[2] Nuclear Regulatory Commission, Interim Staff Guidance (ISG)-11, Revision 3, "Cladding Considerations for the Transportation and Storage of Spent Fuel," November 2003. [ML033230335 at http://www.nrc.gov/reading-rm/adams.html]

[3] Nuclear Regulatory Commission, "NRC Public Meeting to Obtain Stakeholder Feedback on Enhancements to the Licensing and Inspection Programs for Spent Fuel Storage and Transportation under 10 CFR Parts 71 and 72," August 16–17, 2012, Rockville, MD. [http://www.nrc.gov/public-involve/conference-symposia/2012-sfst-lic-process-conf.html]

[4] M.C. Billone, T.A. Burtseva, and Y. Yan, *Ductile-to-Brittle Transition Temperature for High-Burnup Zircaloy-4 and ZIRLO™ Cladding Alloys Exposed to Simulated Drying-Storage Conditions*, Argonne National Laboratory Report ANL-13/13, NRC ADAMS ML12181A238 (Sept. 2012).

[5] M.C. Billone, T.A. Burtseva, and R.E. Einziger, "Ductile-to-Brittle Transition Temperature for High-Burnup Cladding Alloys Exposed to Simulated Drying-Storage Conditions," J. Nucl. Mater. *433*, 431–448 (2013).

[6] M.C. Billone, T.A. Burtseva, J.P. Dobrzynski, D.P. McGann, K. Byrne, Z. Han, and Y.Y. Liu, *Phase I Ring Compression Testing of High-Burnup Cladding*, FCRD-USED-2012-000039, Dec. 31, 2011.

[7] M.C. Billone, T.A. Burtseva, and Y.Y. Liu, *Baseline Studies for Ring Compression Testing of High-Burnup Fuel Cladding*, Argonne National Laboratory Report ANL-12/58, FCRD-USED-2013-000040, Nov. 23, 2012.

[8] M.C. Billone, T.A. Burtseva, and Y.Y. Liu, "Effects of Drying and Storage on High-Burnup Cladding Ductility," Proc. IHLRWMC, Albuquerque, NM, April 28−May 2, 2013, Paper 6973, 1106–1113 (2013).

[9] M.C. Billone, T.A. Burtseva, and Y.Y. Liu, "Baseline Properties and DBTT of High-Burnup PWR Cladding Alloys," Proc. PATRAM 2013, San Francisco, CA, August 18–23, 2013 (2013).

[10] M.C. Billone, T.A. Burtseva, Z. Han, and Y.Y. Liu, *Embrittlement and DBTT of High-Burnup PWR Fuel Cladding Alloys*, Argonne National Laboratory Report ANL-13/16, FCRD-UFD-2013-000401, Sept. 30, 2013.

[11] M. Aomi, T. Baba, T. Miyashita, K. Kaminura, T. Yasuda, Y. Shinohara, and T. Takeda, "Evaluation of Hydride Reorientation and Mechanical Properties for High-Burnup Fuel-Cladding Tubes in Interim Dry Storage," J. ASTM Intl., JAI101262 (2008). [www.astm.org]

[12] J.J. Kearns, "Terminal Solubility and Partitioning of Hydrogen in the Alpha Phase of Zirconium, Zircaloy-2 and Zircaloy-2," J. Nucl. Mater. *22*, 292-303 (1967).

[13] B.F. Kammenzind, D.G. Franklin, H.R. Peters, and W.J. Duffin, "Hydrogen Pickup and Redistribution in Alpha-Annealed Zircaloy-4," *Zirconium in the Nuclear Industry: 11th Intl. Symp.*, ASTM STP 1295, E.R. Bradley and G.P. Sabol, Eds., ASTM, pp. 338-370 (1996).

[14] A. McMinn, E.C. Darby, and J.S. Schofield, "The Terminal Solid Solubility of Hydrogen in Zirconium Alloys, *Zirconium in the Nuclear Industry: 12th Intl. Symp.*, ASTM STP 1354, G.P. Sabol and G.D. Moan, Eds., ASTM, pp. 173-195 (2000).

[15] H.C. Chu, S.K. Wu, and R.C. Kuo, "Hydride Reorientation in Zircaloy-4 Cladding," J. Nucl. Mater. *373*, 319–327 (2008).

[16] C.T. Stockman, B.D. Hansen, S.C. Marschman, H.A. Alsaed and K.B. Sorenson, *Used Fuel Extended Storage and Transportation Research and Development Review and Plan*, FCRD-UFD-2014-000050, August 9, 2014.

[17] Electric Power Research Institute, *High Burnup Dry Storage Cask Research and Development Project: Final Test Plan*, Contract No. DE-NE-0000593, Rev. 0, February 27, 2014.

APPENDIX A METALLOGRAPHIC IMAGES OF ZIRLO™ CROSS SECTION FROM THREE-CYCLE 350°C TEST OF SAMPLE 105E6

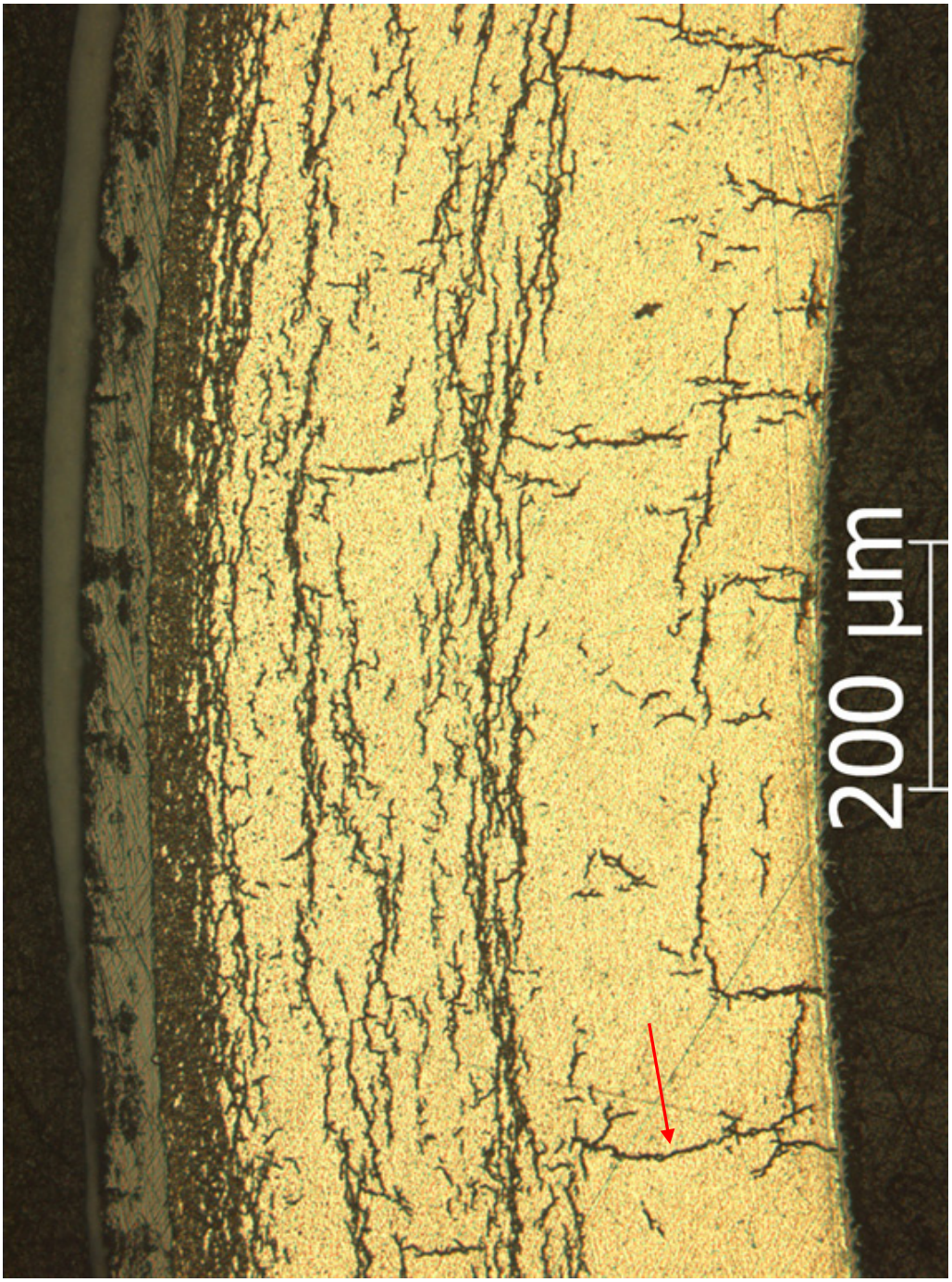

Figure A.1: Image (100X) of ZIRLO™ sample 105E6 at 12:00 o'clock orientation from 3-cycle 350°C rodlet. RHCF = 36%.

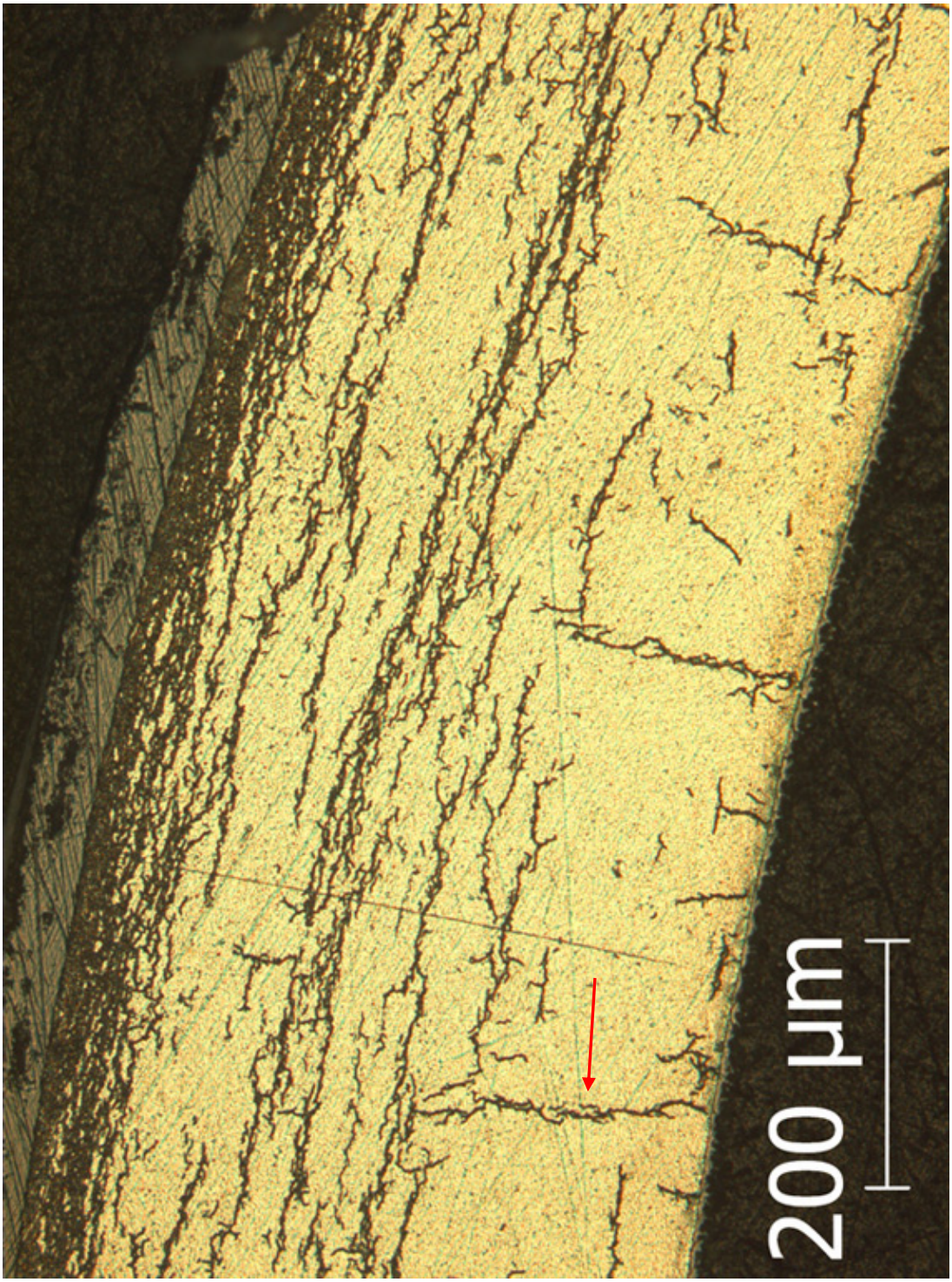

Figure A.2: Image (100X) of ZIRLO™ sample 105E6 at 12:30 o'clock orientation from 3-cycle 350°C rodlet. RHCF = 46%.

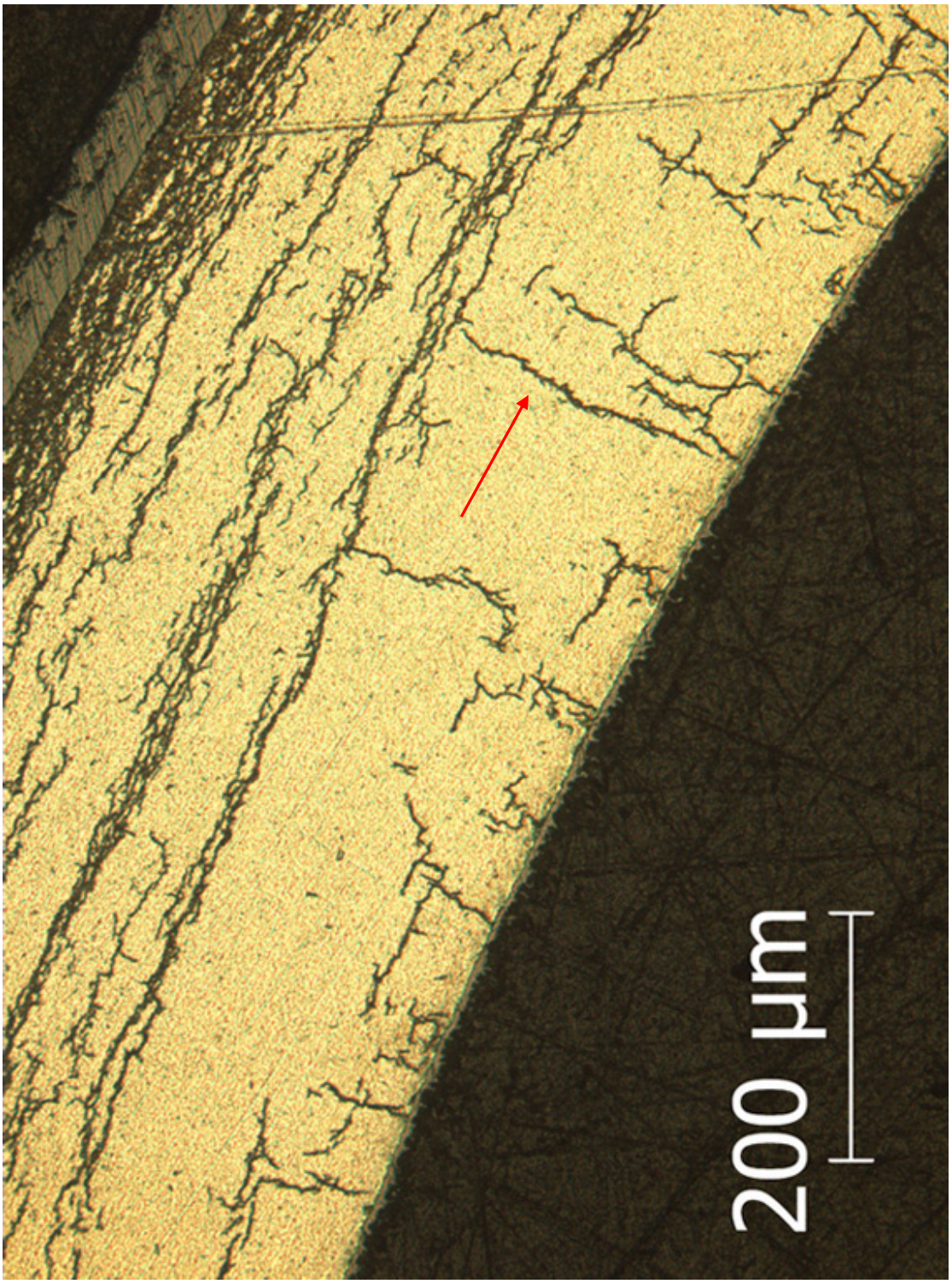

Figure A.3: Image (100X) of ZIRLO™ sample 105E6 at 1:00 o'clock orientation from 3-cycle 350°C rodlet. RHCF = 42%.

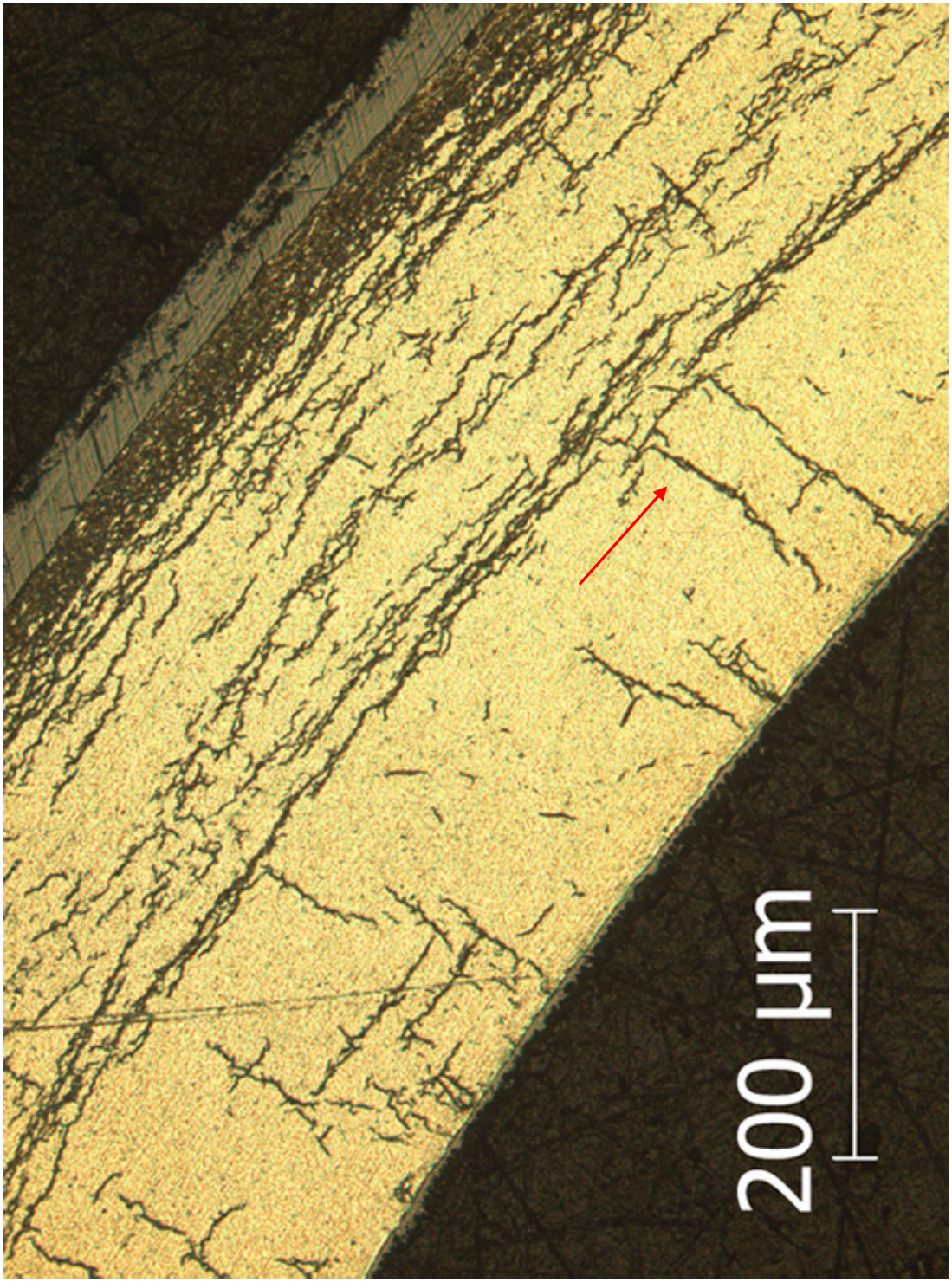

Figure A.4 Image (100X) of ZIRLO™ sample 105E6 at 1:30 o'clock orientation from 3-cycle 350°C rodlet. RHCF = 40%.

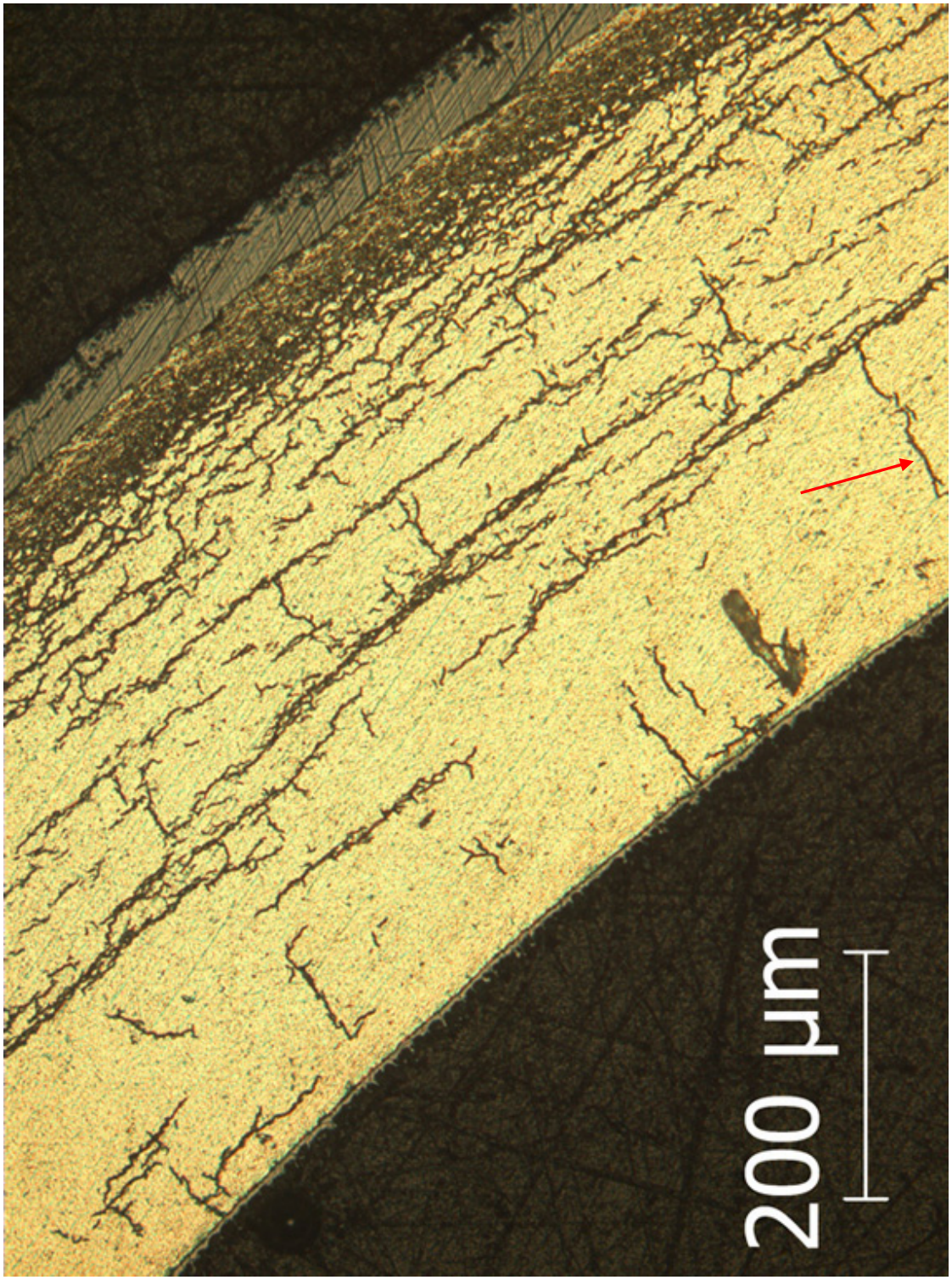

Figure A.5: Image (100X) of ZIRLO™ sample 105E6 at 2:00 o'clock orientation from 3-cycle 350°C rodlet. RHCF = 16%.

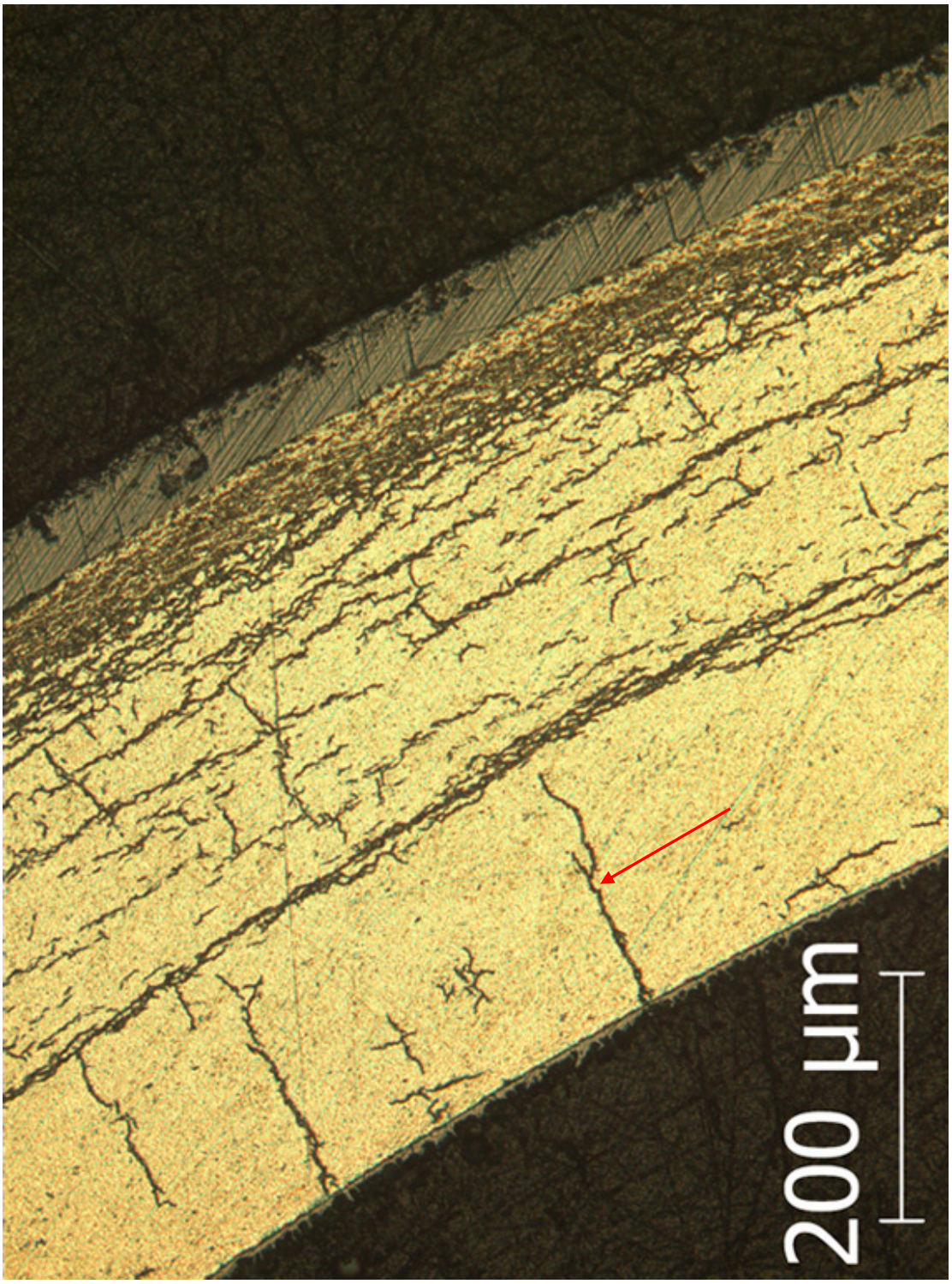

Figure A.6: Image (100X) of ZIRLO™ sample 105E6 at 2:15 o'clock orientation from 3-cycle 350°C rodlet. RHCF = 38%.

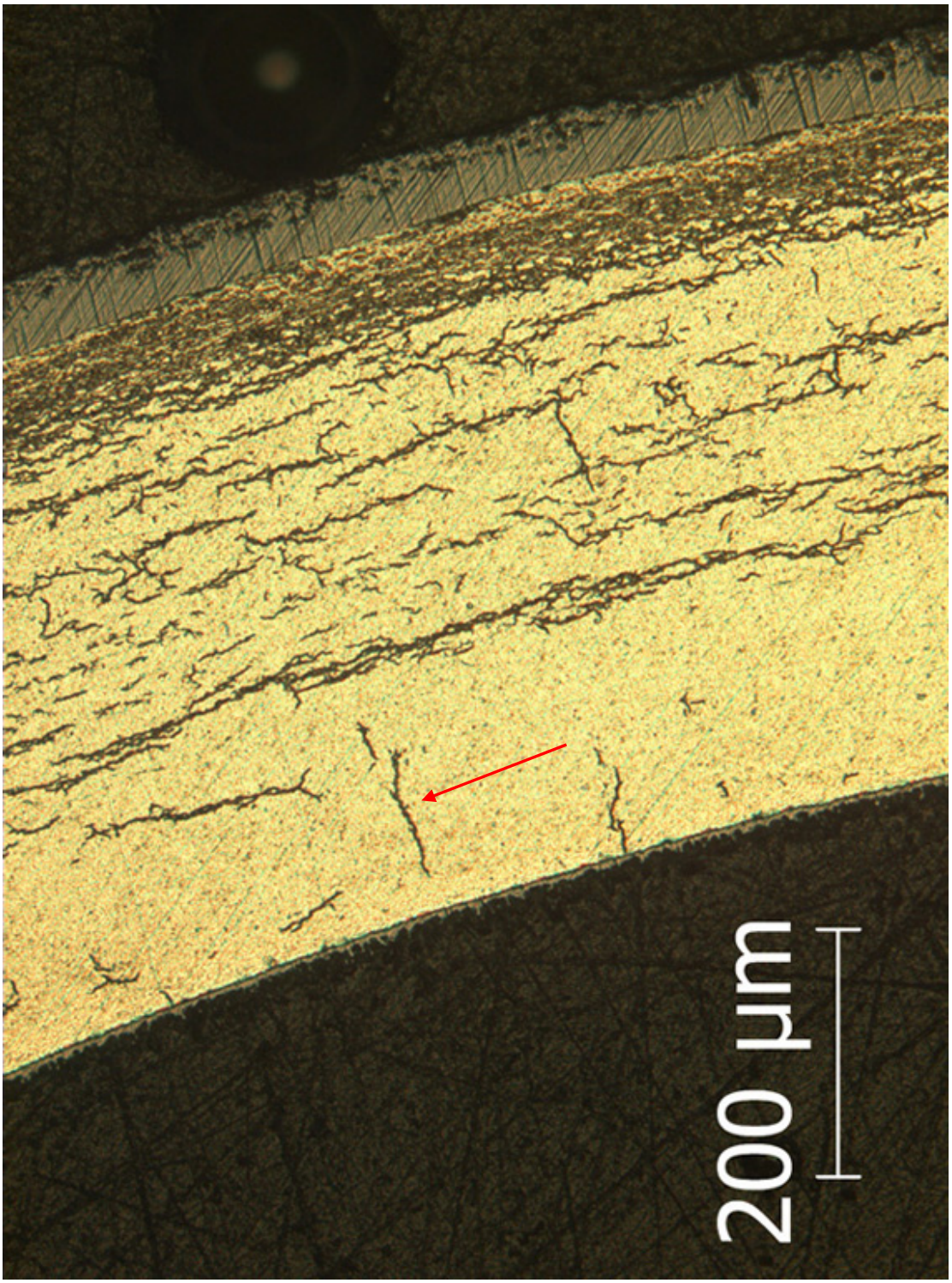

Figure A.7: Image (100X) of ZIRLO™ sample 105E6 at 2:30 o'clock orientation from 3-cycle 350°C rodlet. RHCF = 19%.

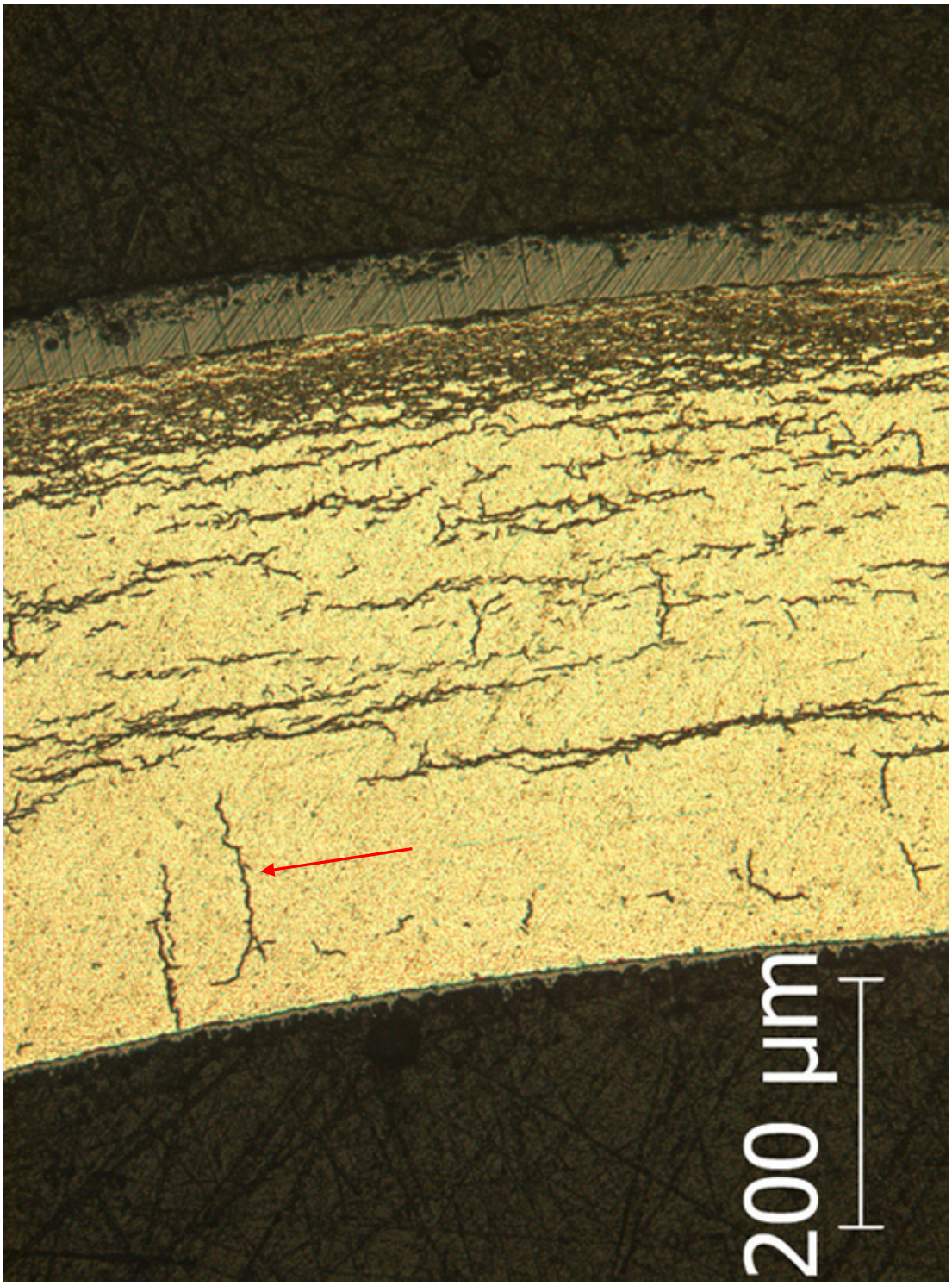

Figure A.8: Image (100X) of ZIRLO™ sample 105E6 at 2:45 o'clock orientation from 3-cycle 350°C rodlet. RHCF = 28%.

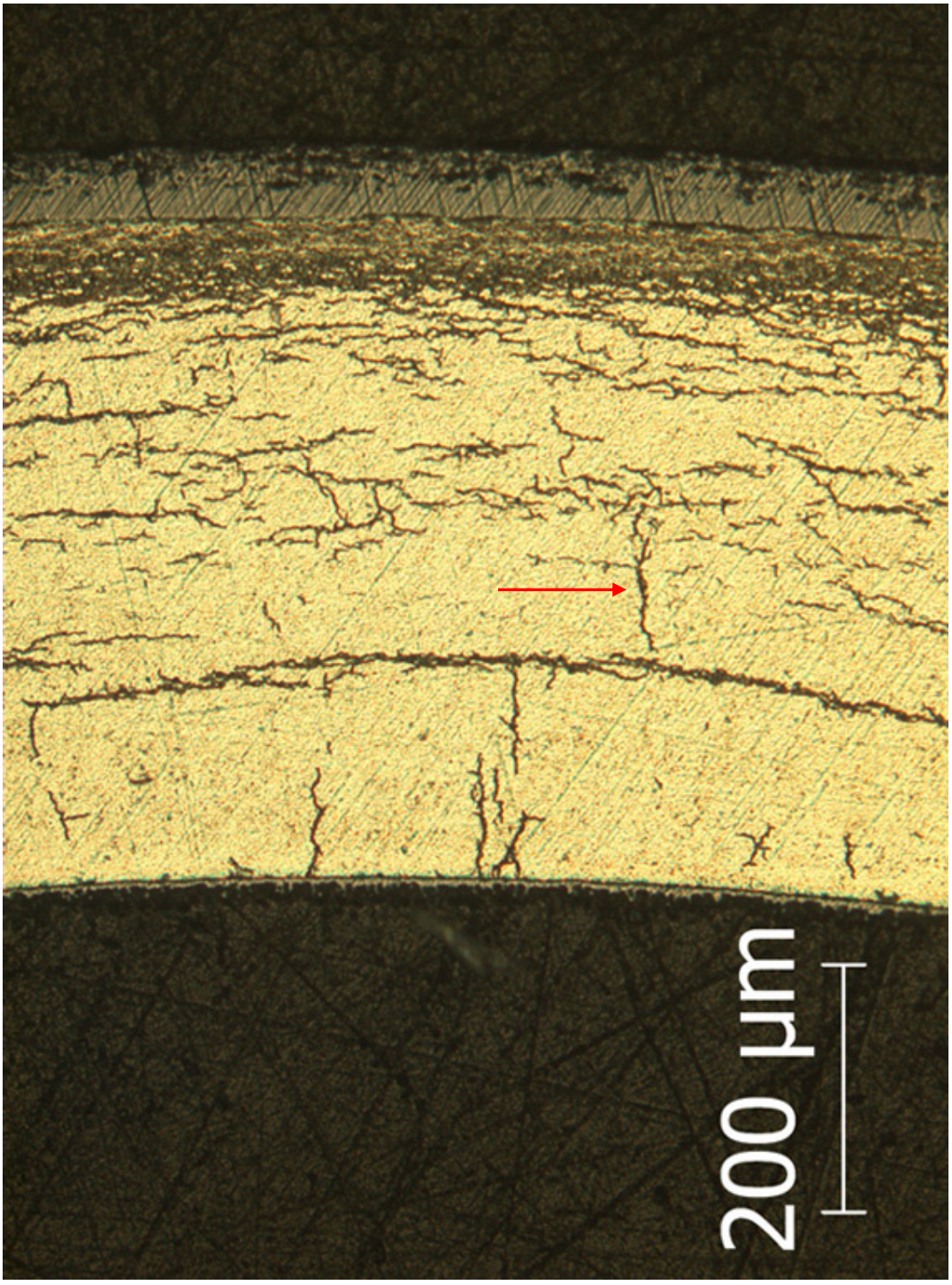

Figure A.9: Image (100X) of ZIRLO™ sample 105E6 at 3:00 o'clock orientation from 3-cycle 350°C rodlet. RHCF = 22%.

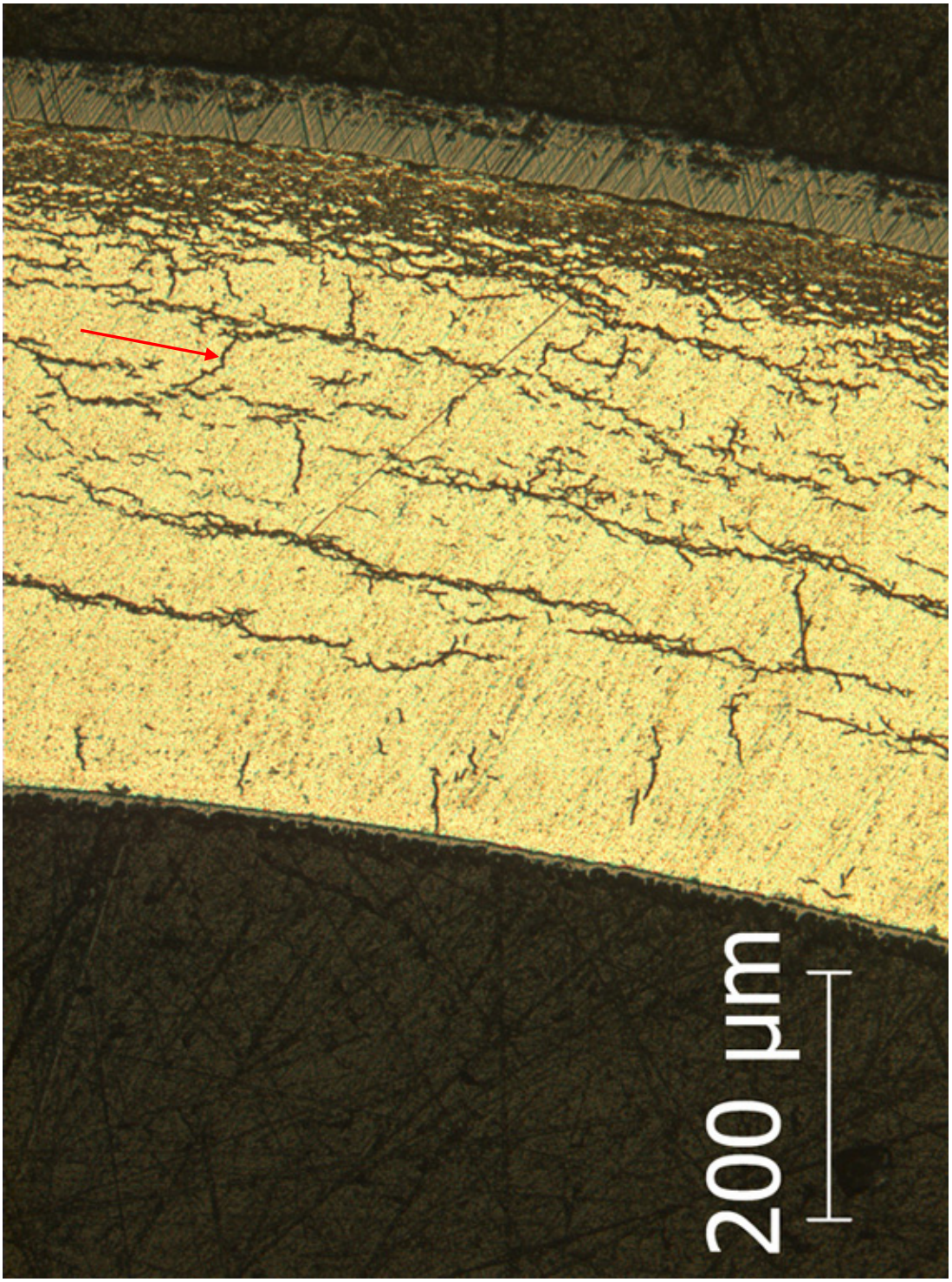

Figure A.10: Image (100X) of ZIRLO™ sample 105E6 at 3:15 o'clock orientation from 3-cycle 350°C rodlet. RHCF = 20%.

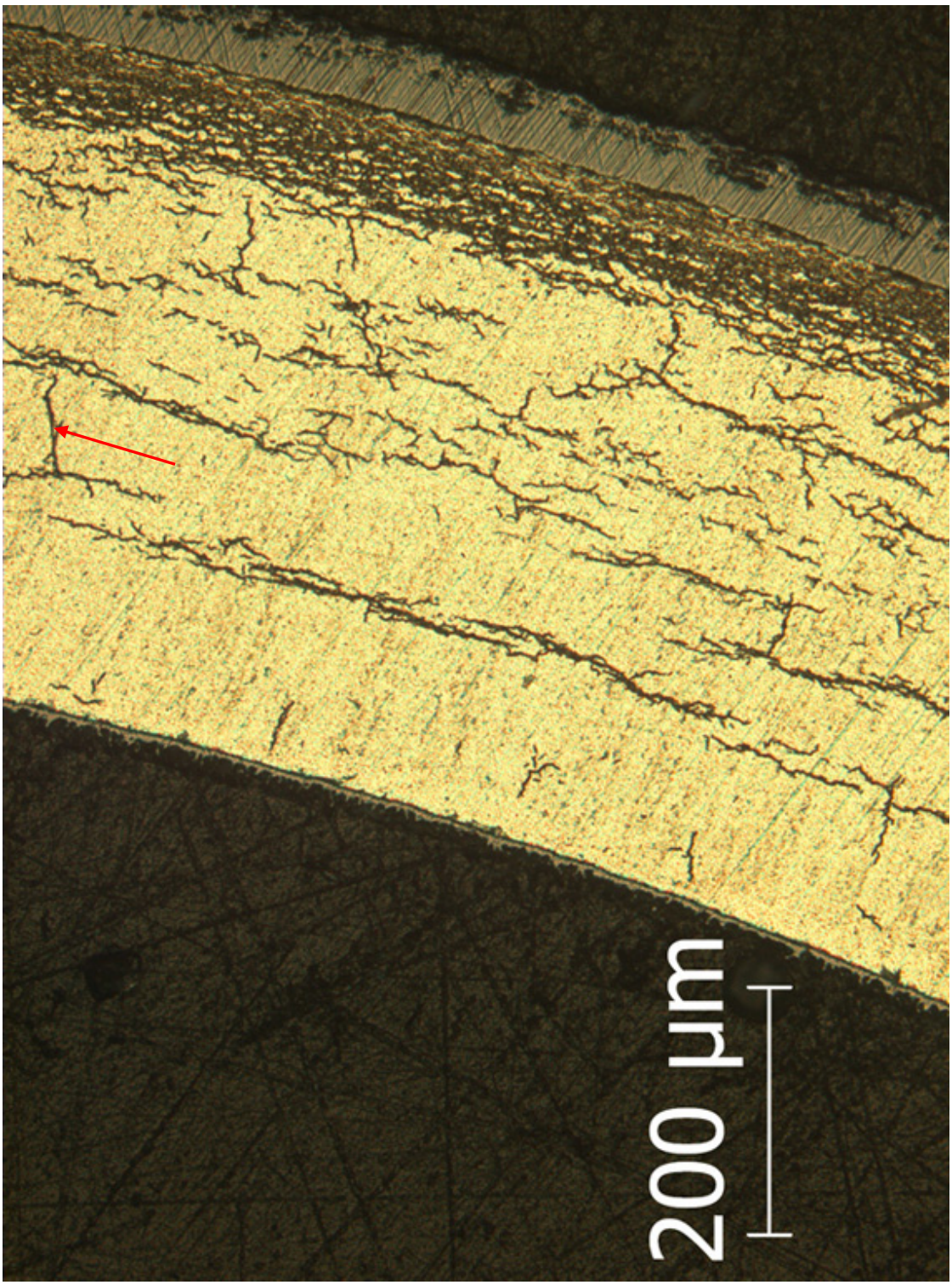

Figure A.11: Image (100X) of ZIRLO™ sample 105E6 at 3:30 o'clock orientation from 3-cycle 350°C rodlet. RHCF = 15%.

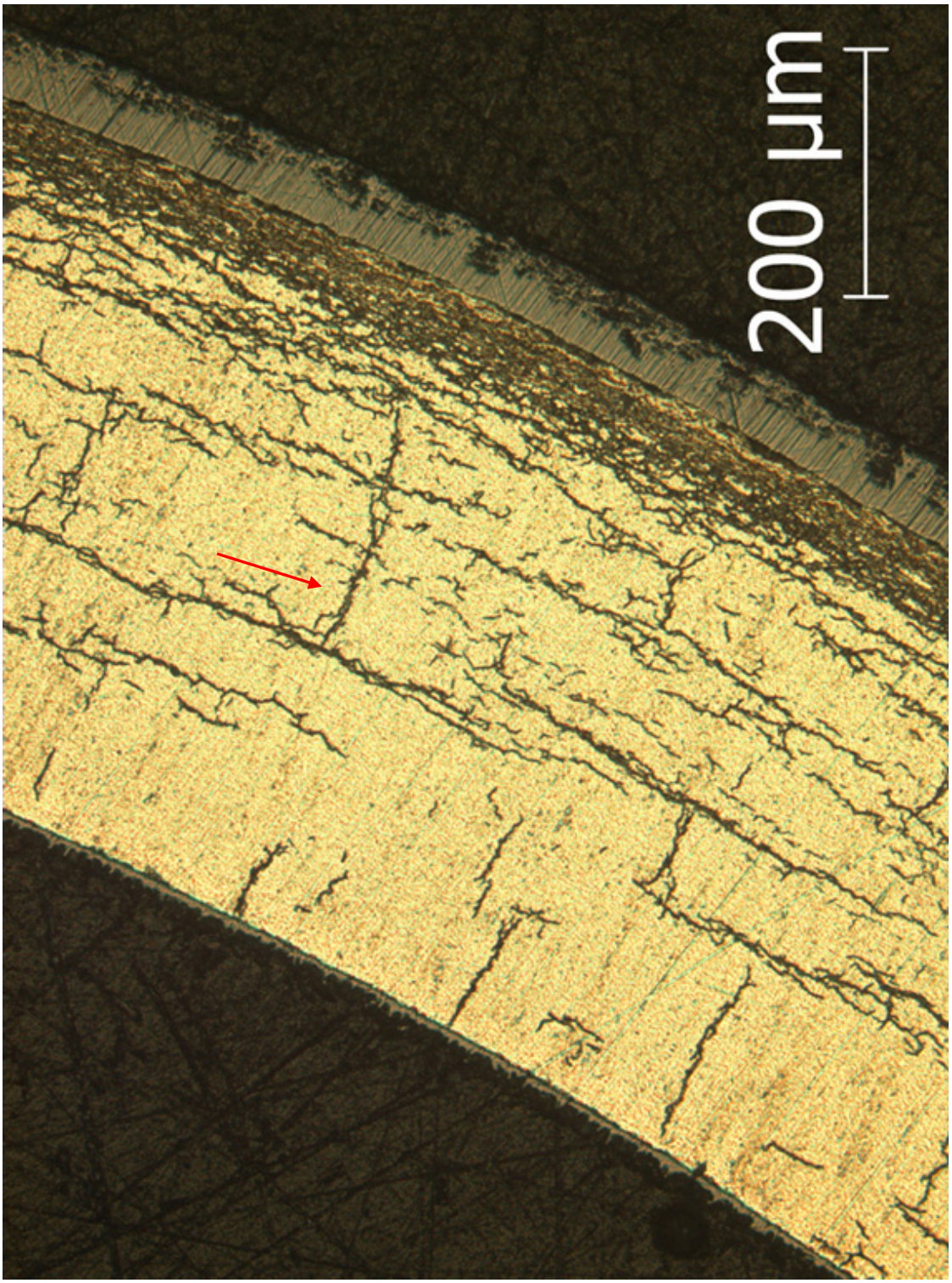

Figure A.12: Image (100X) of ZIRLO™ sample 105E6 at 3:45 o'clock orientation from 3-cycle 350°C rodlet. RHCF = 39%.

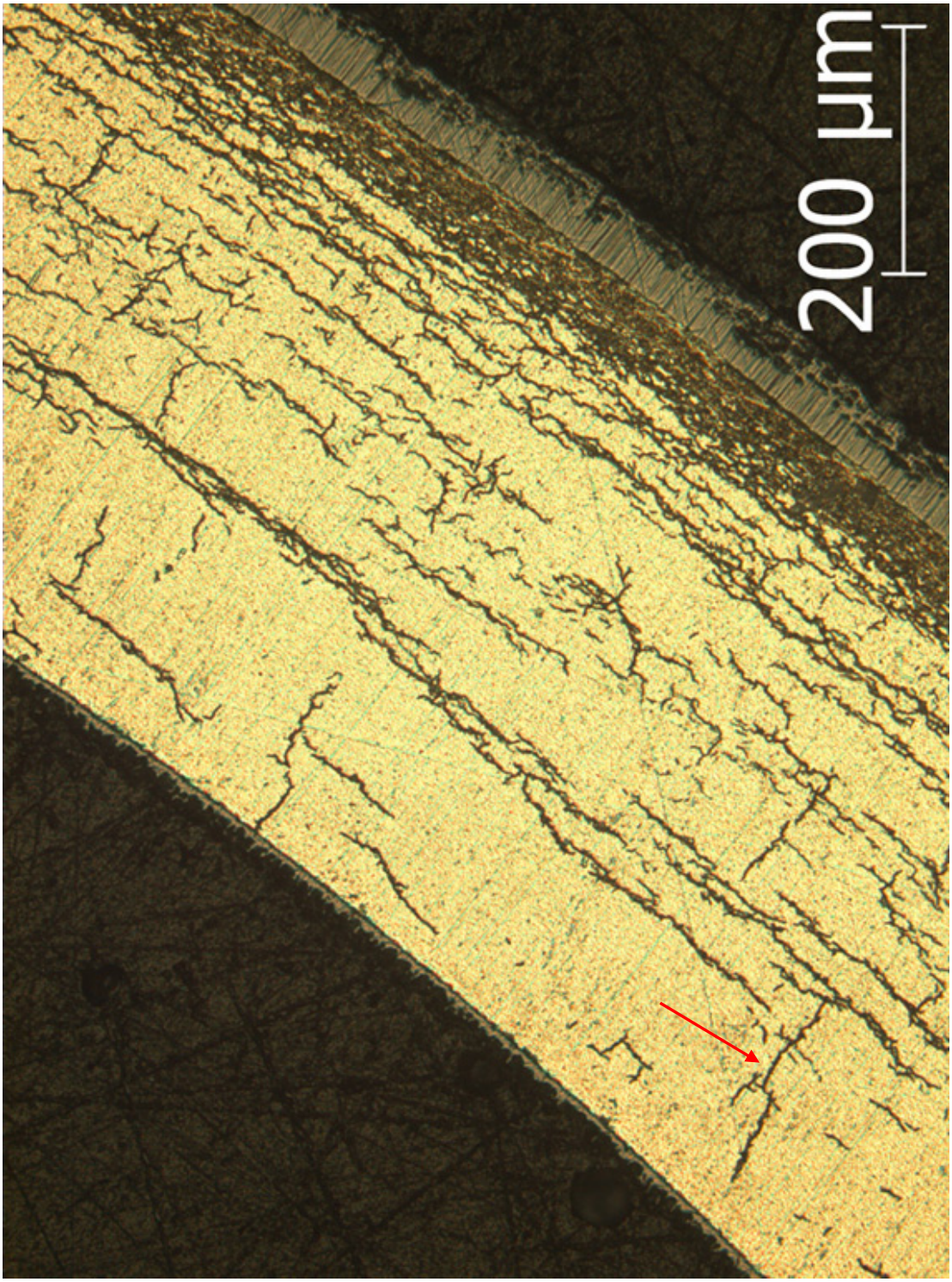

Figure A.13: Image (100X) of ZIRLO™ sample 105E6 at 4:00 o'clock orientation from 3-cycle 350°C rodlet. RHCF = 34%.

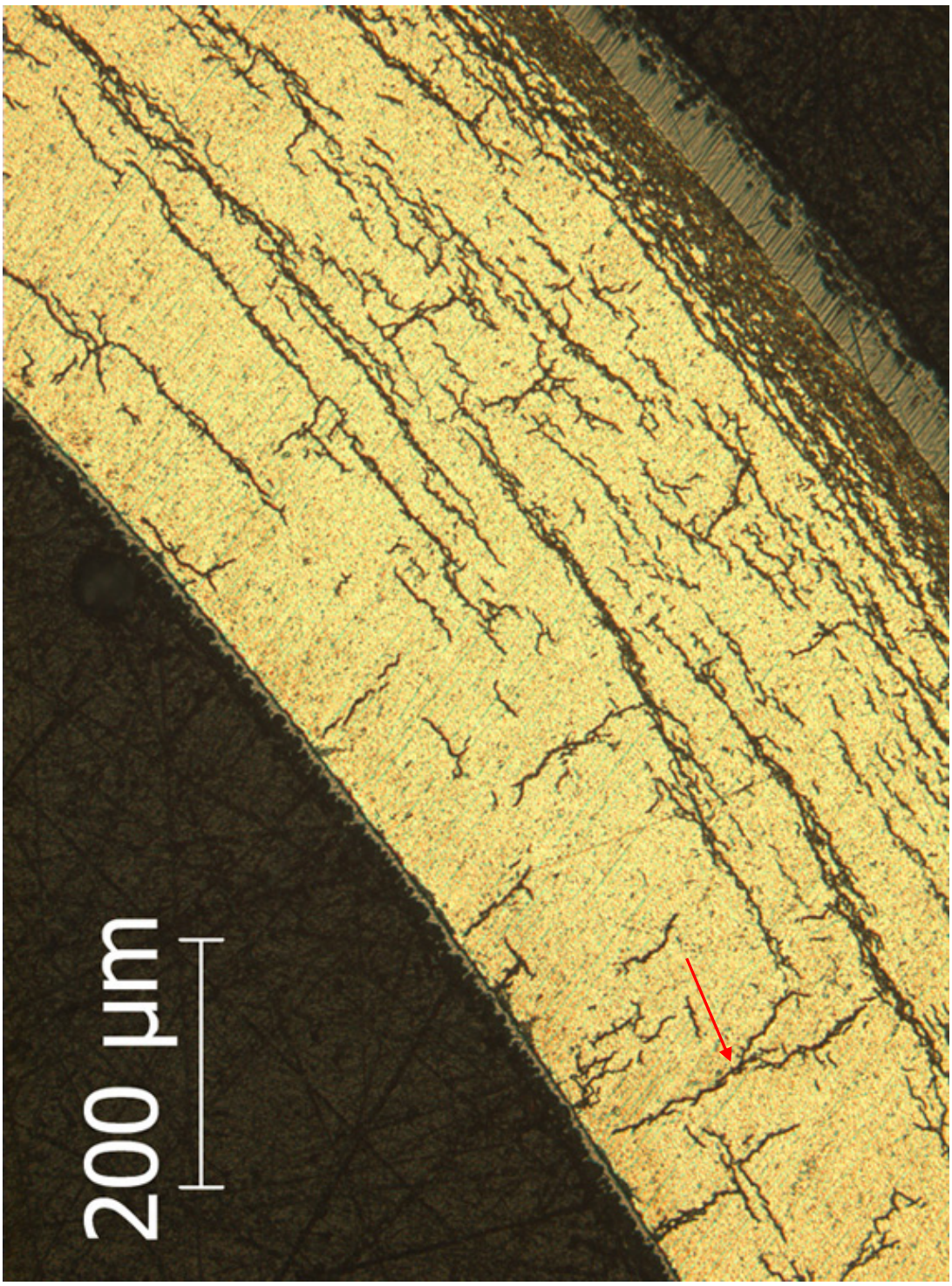

Figure A.14: Image (100X) of ZIRLO™ sample 105E6 at 4:30 o'clock orientation from 3-cycle 350°C rodlet. RHCF = 53%.

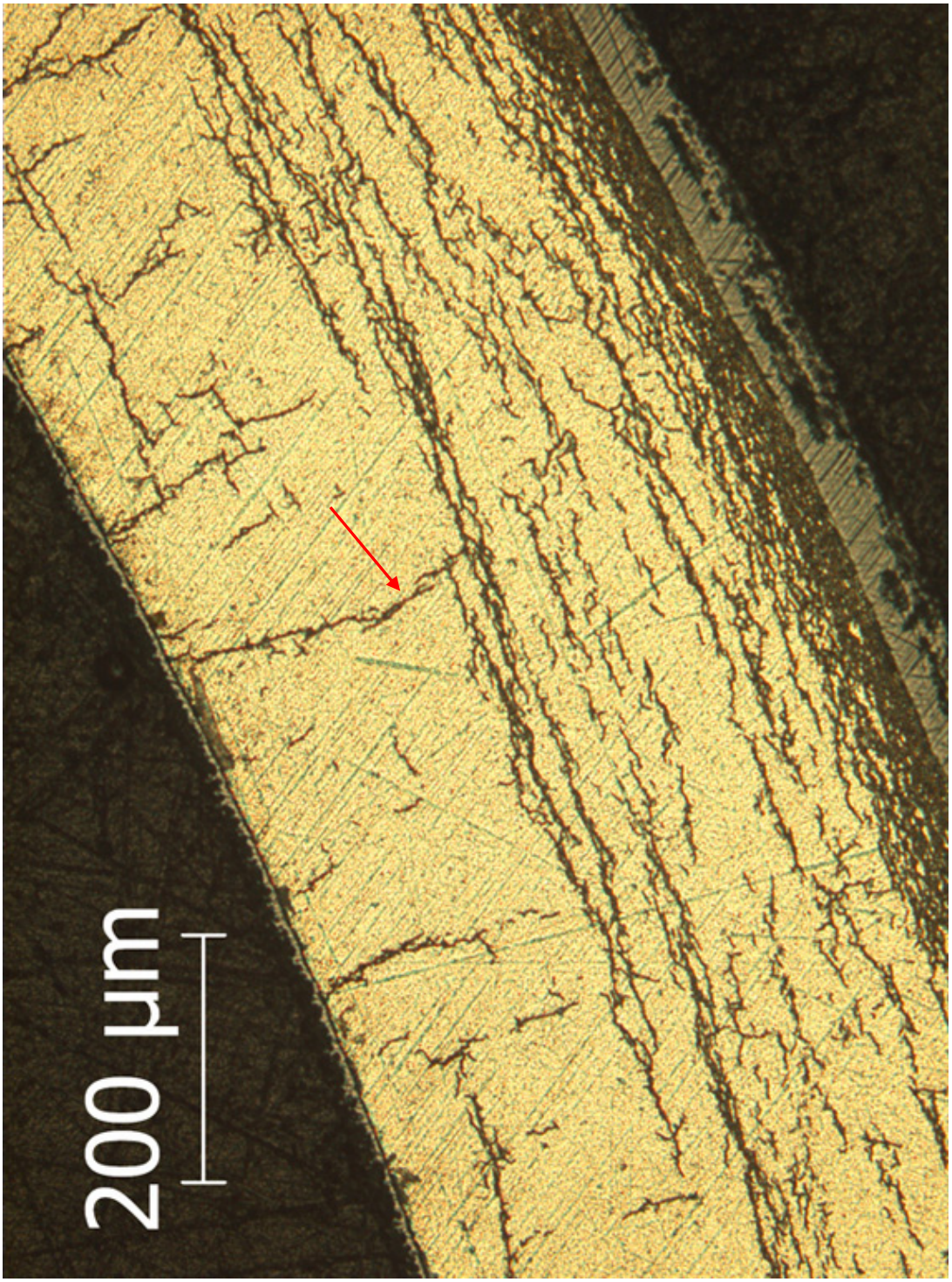

Figure A.15: Image (100X) of ZIRLO™ sample 105E6 at 5:00 o'clock orientation from 3-cycle 350°C rodlet. RHCF = 55%.

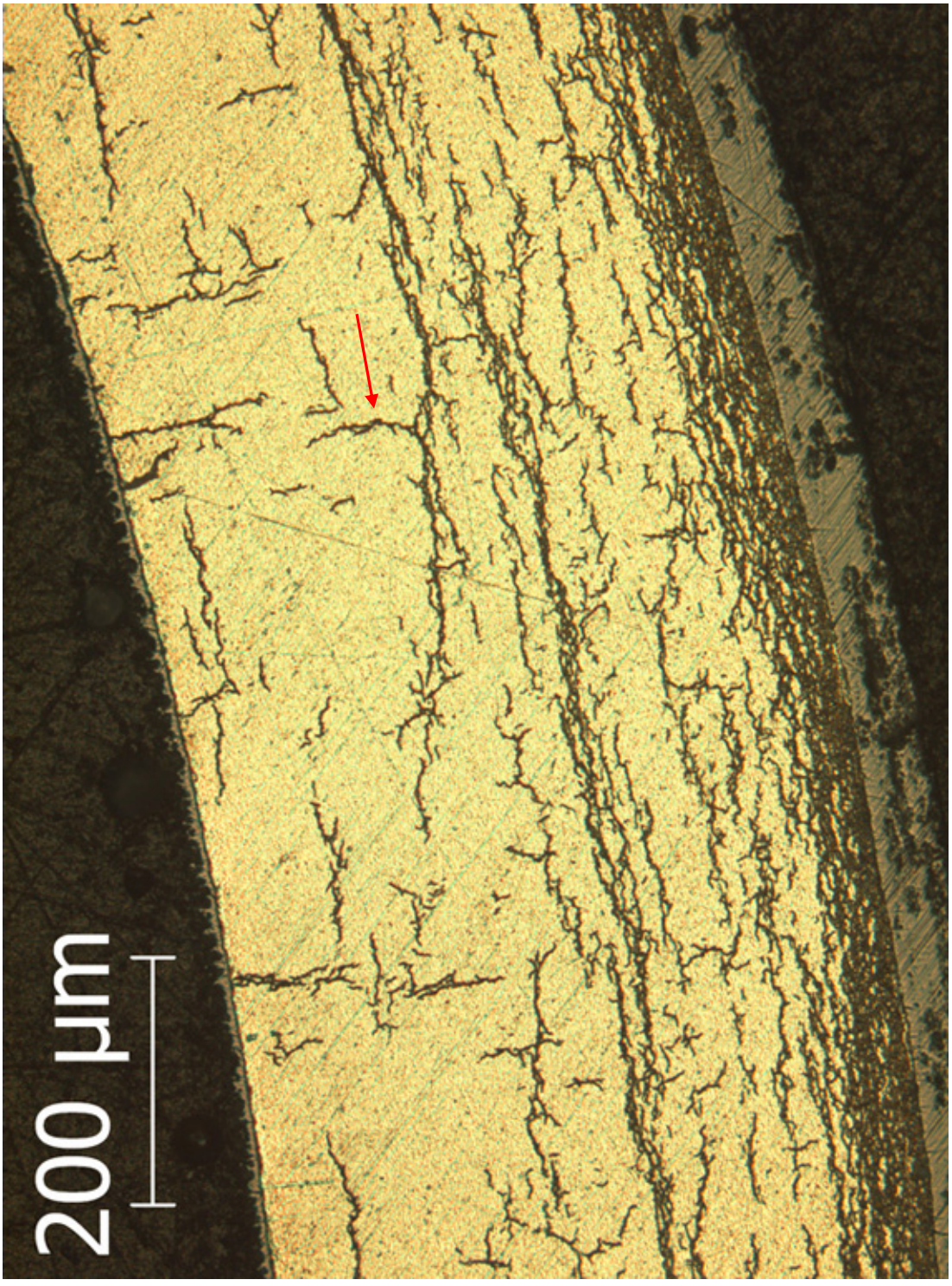

Figure A.16: Image (100X) of ZIRLO™ sample 105E6 at 5:30 o'clock orientation from 3-cycle 350°C rodlet. RHCF = 30%.

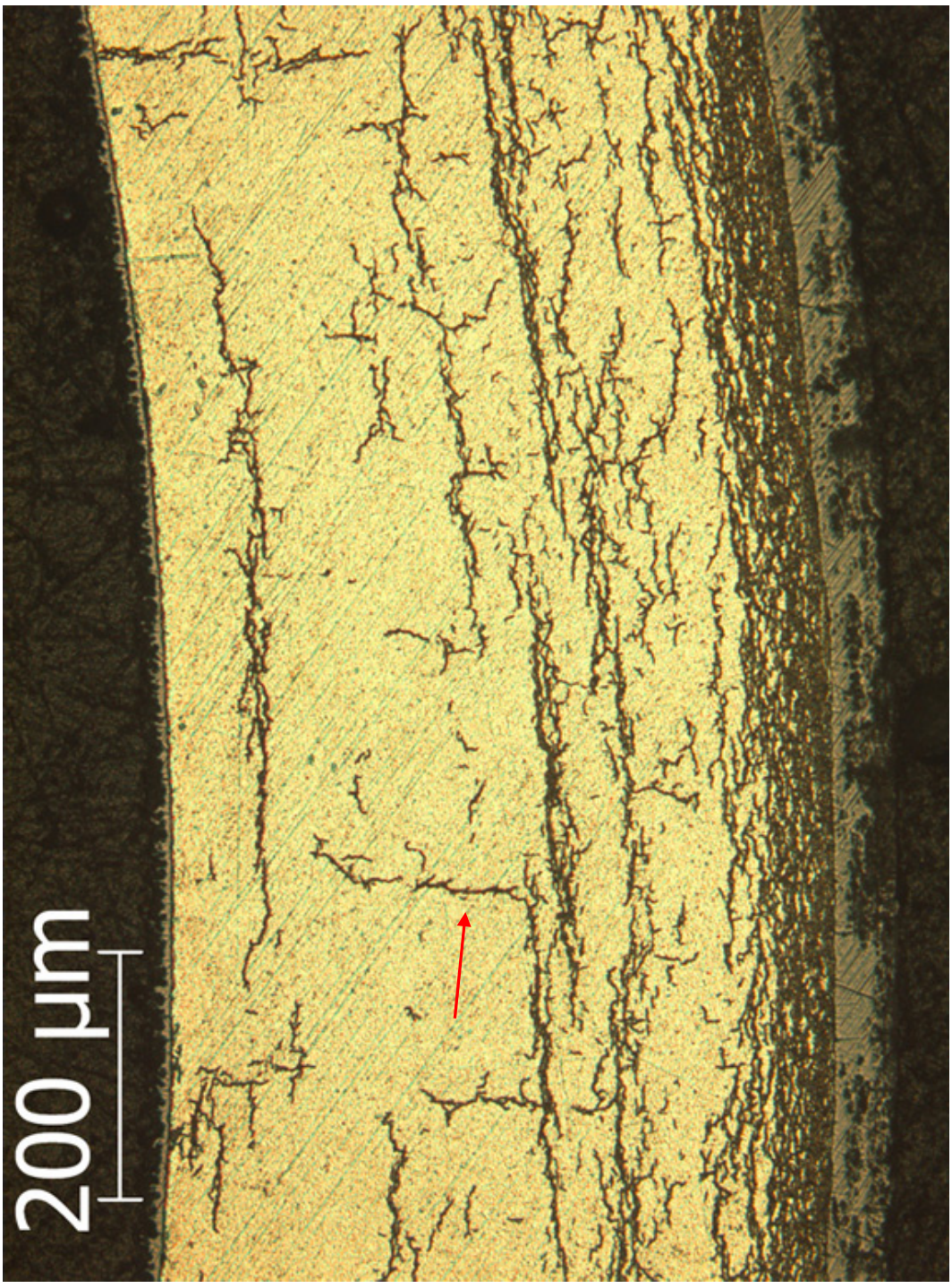

Figure A.17: Image (100X) of ZIRLO™ sample 105E6 at 6:00 o'clock orientation from 3-cycle 350°C rodlet. RHCF = 23%.

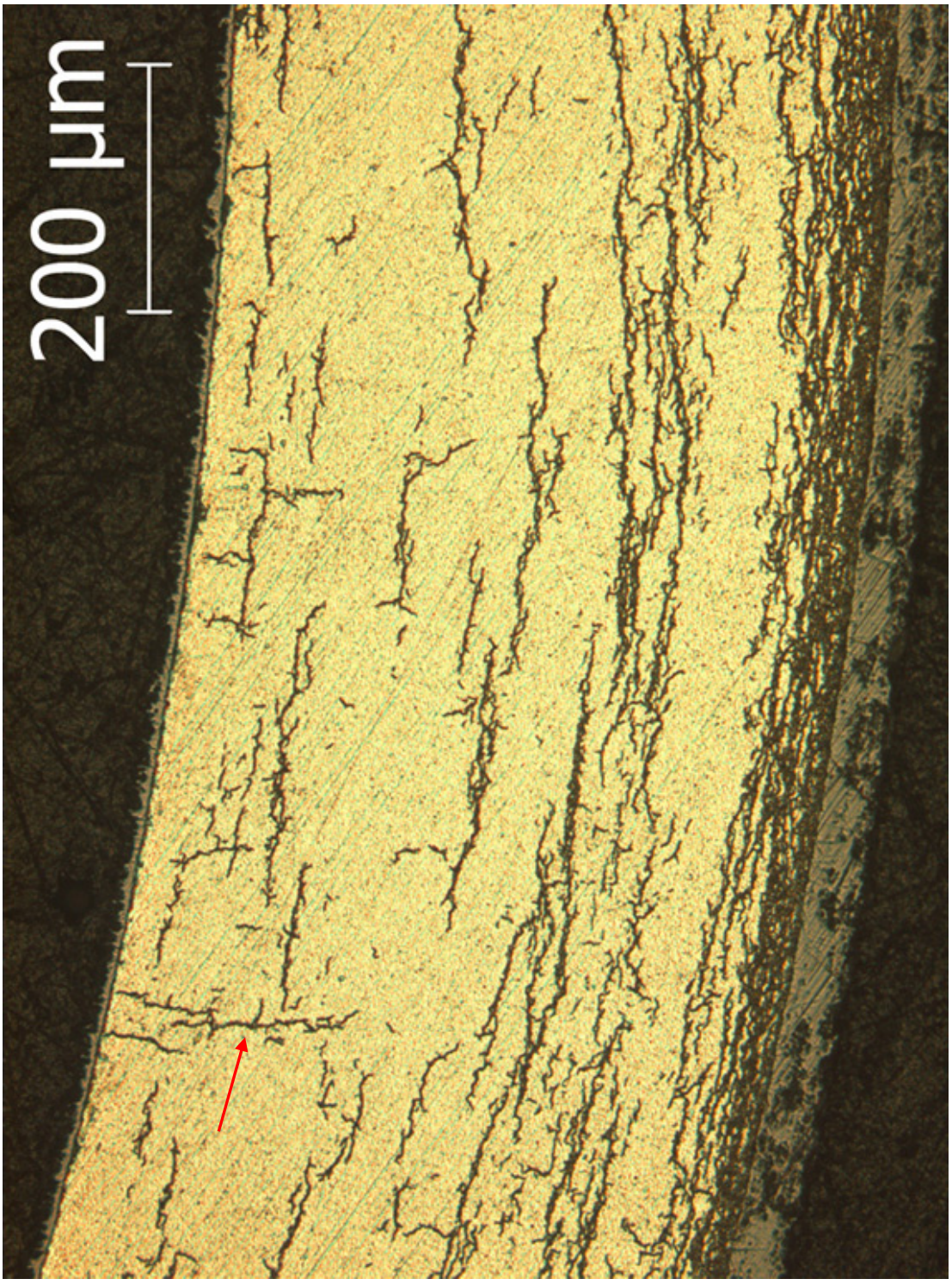

Figure A.18: Image (100X) of ZIRLO™ sample 105E6 at 6:30 o'clock orientation from 3-cycle 350°C rodlet. RHCF = 36%.

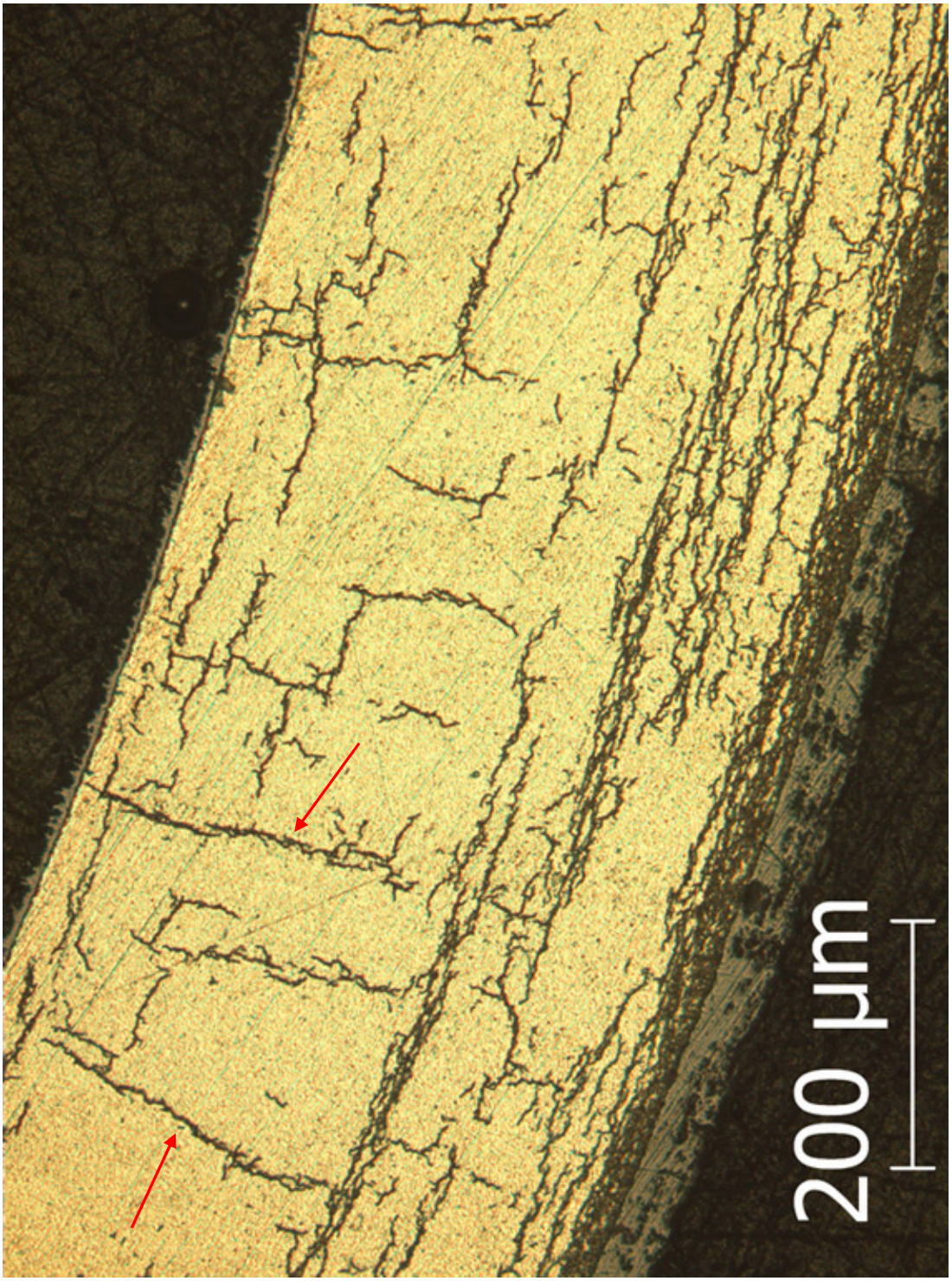

Figure A.19: Image (100X) of ZIRLO™ sample 105E6 at 7:00 o'clock orientation from 3-cycle 350°C rodlet. RHCF = 53%.

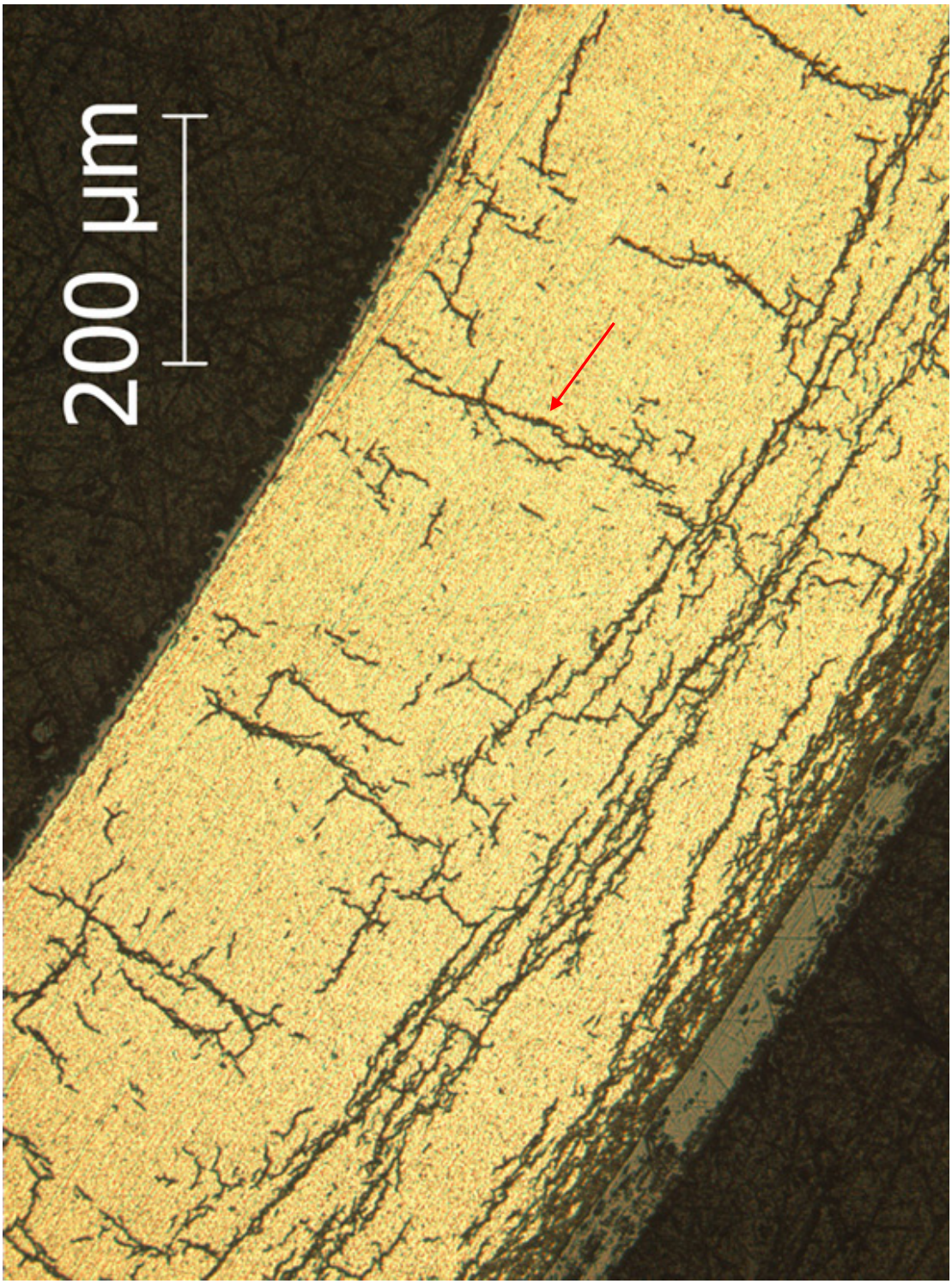

Figure A.20: Image (100X) of ZIRLO™ sample 105E6 at 7:30 o'clock orientation from 3-cycle 350°C rodlet. RHCF = 50%.

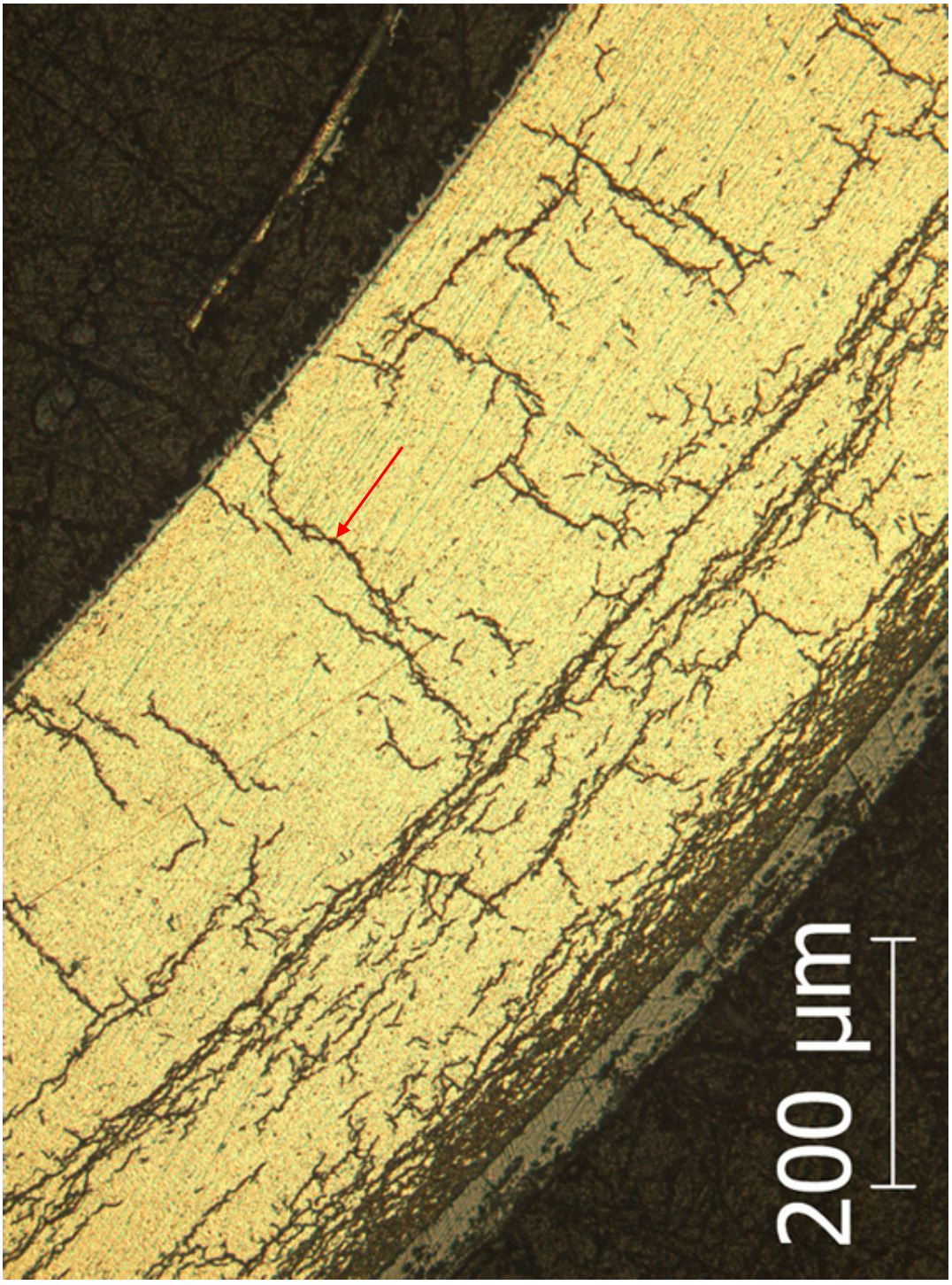

Figure A.21: Image (100X) of ZIRLO™ sample 105E6 at 7:45 o'clock orientation from 3-cycle 350°C rodlet. RHCF = 51%.

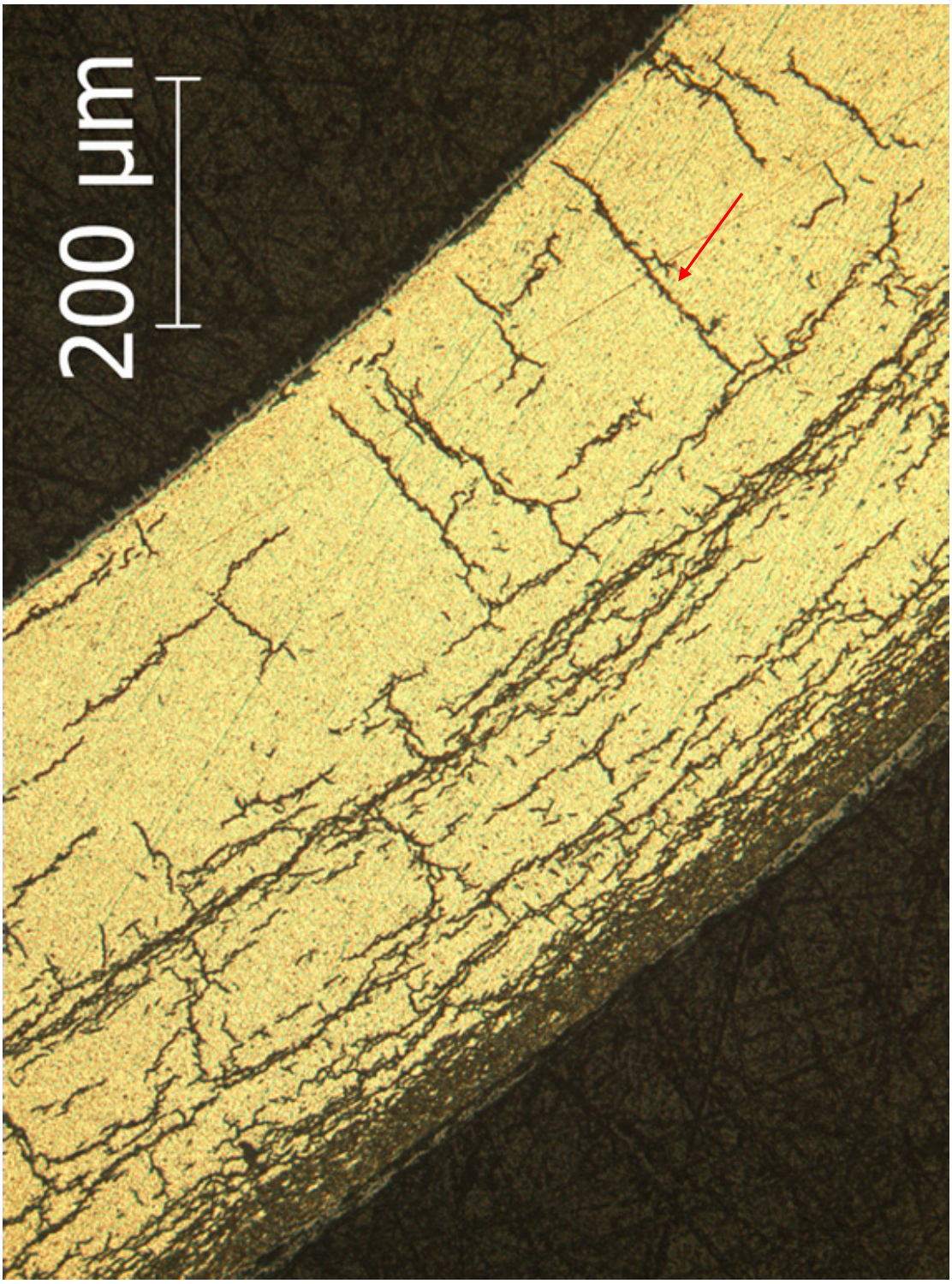

Figure A.22: Image (100X) of ZIRLO™ sample 105E6 at 8:00 o'clock orientation from 3-cycle 350°C rodlet. RHCF = 45%.

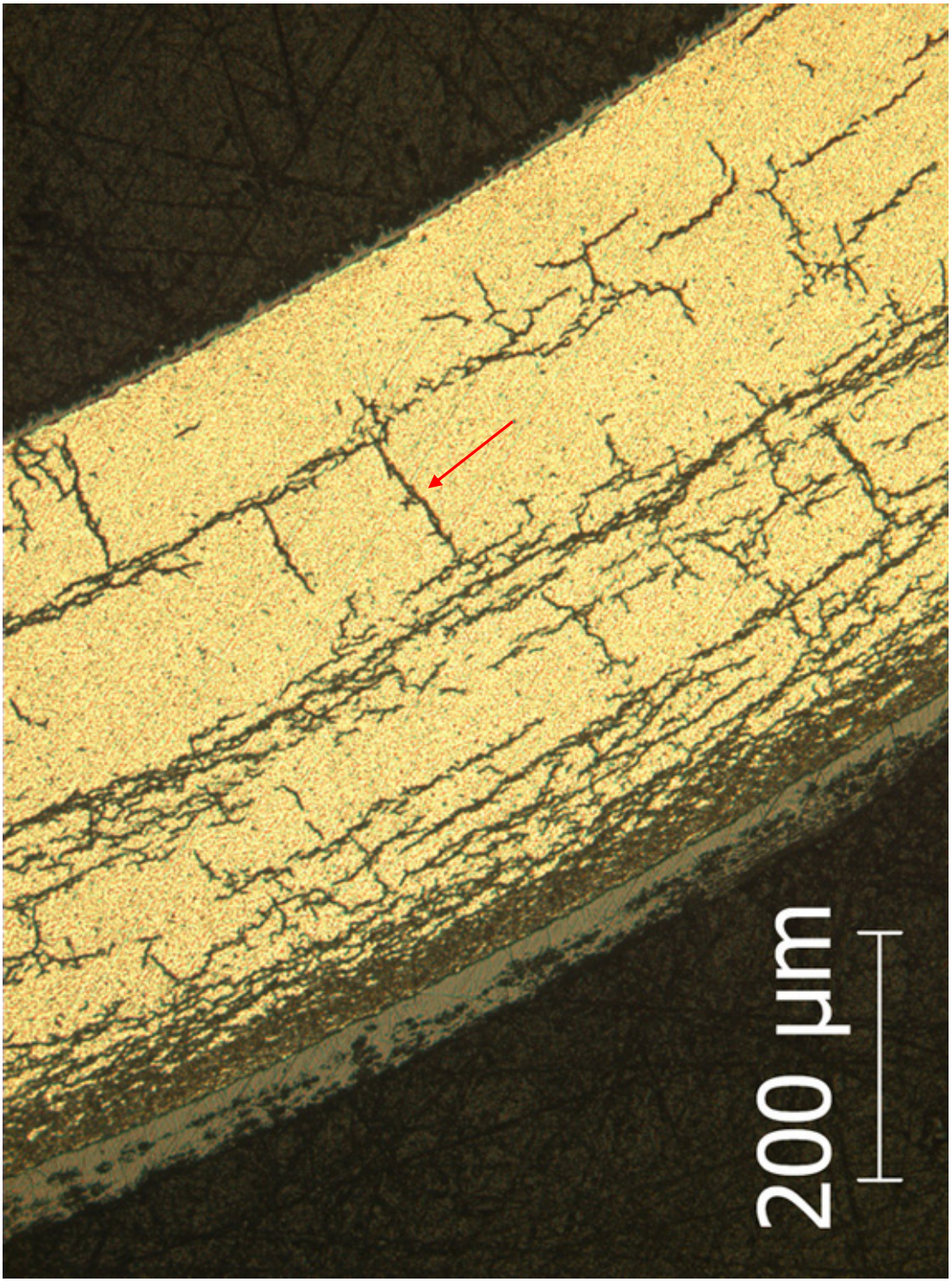

Figure A.23: Image (100X) of ZIRLO™ sample 105E6 at 8:15 o'clock orientation from 3-cycle 350°C rodlet. RHCF = 32%.

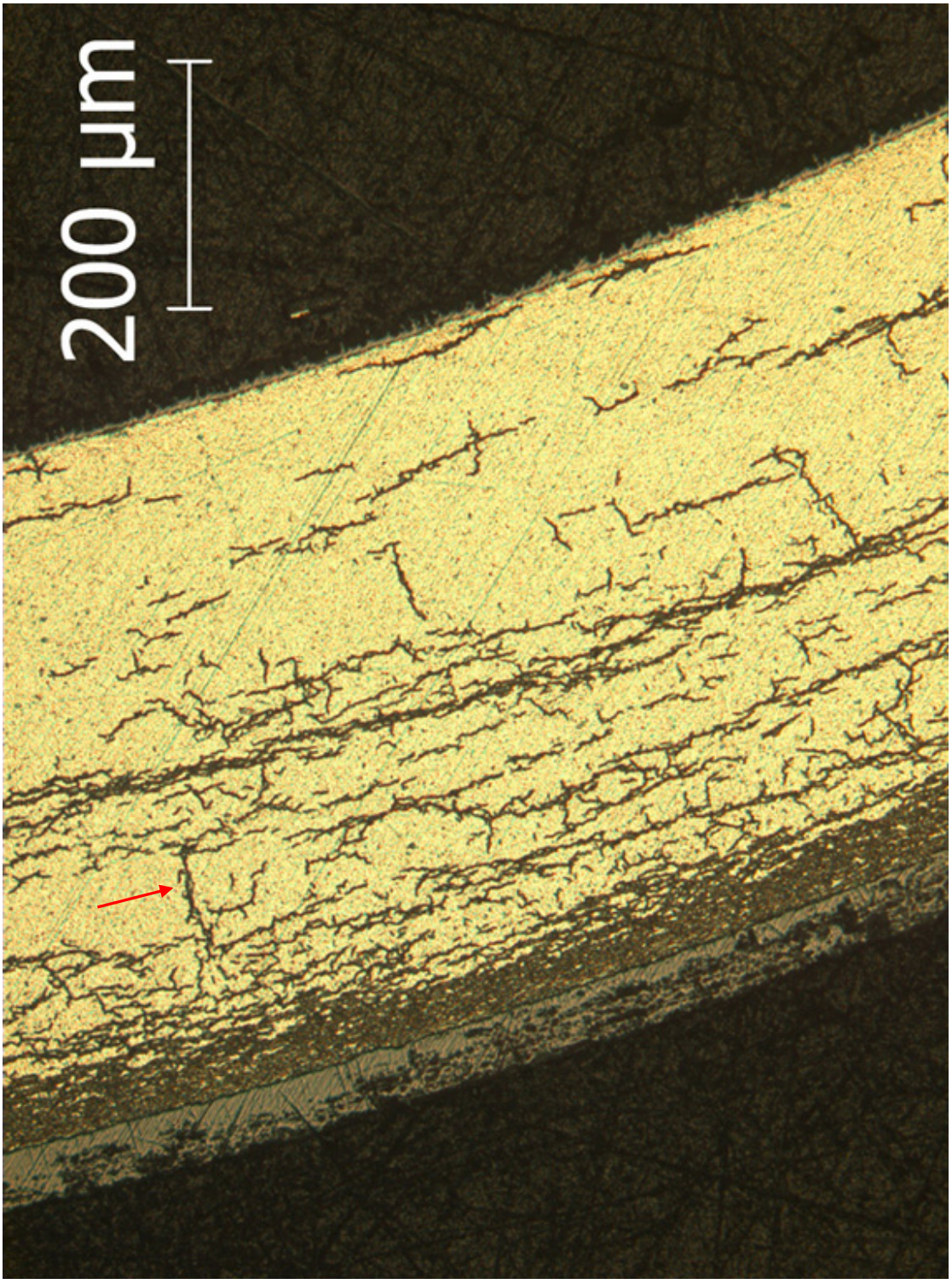

Figure A.24 Image (100X) of ZIRLO™ sample 105E6 at 8:30 o'clock orientation from 3-cycle 350°C rodlet. RHCF = 26%.

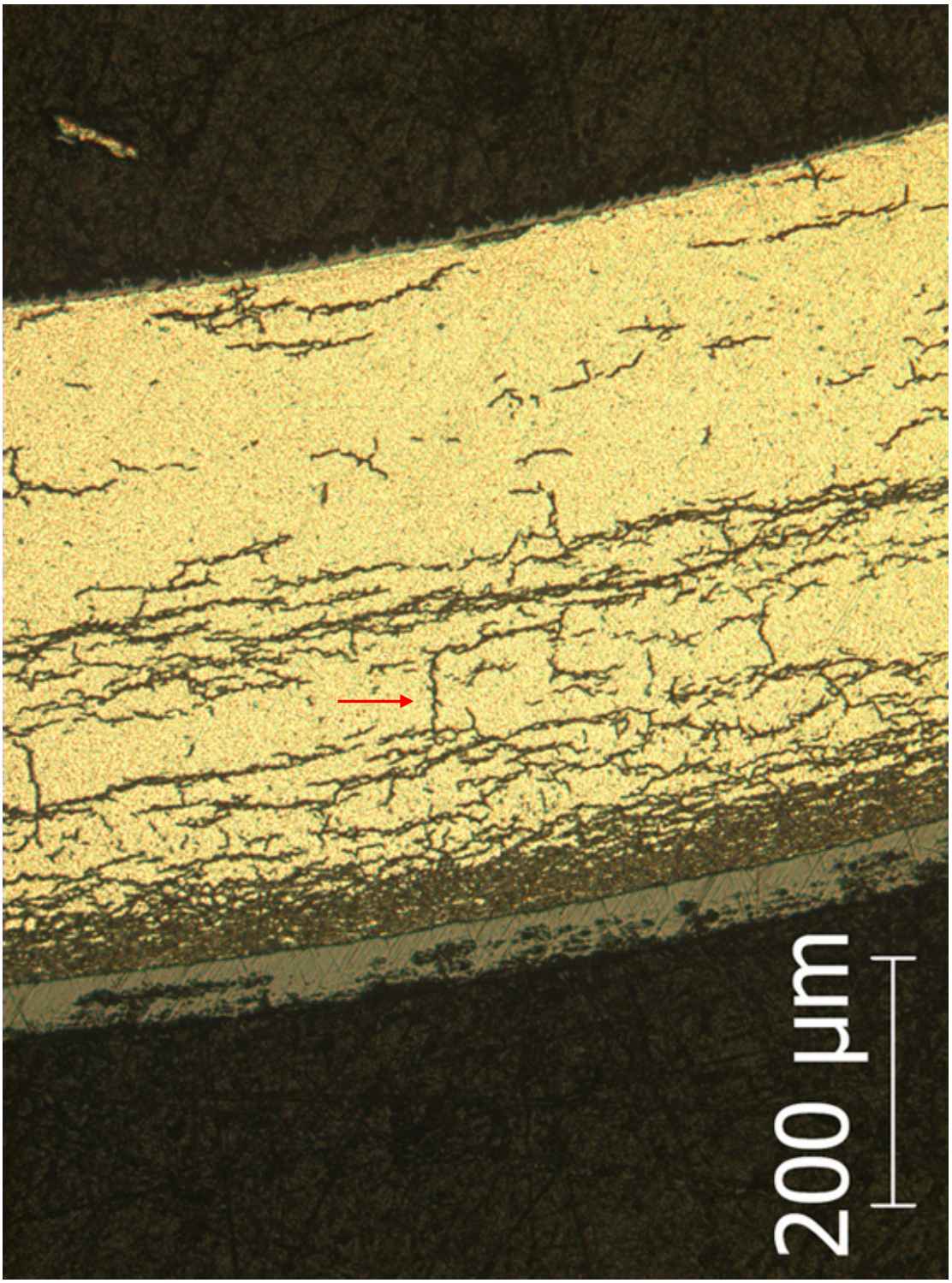

Figure A.25: Image (100X) of ZIRLO™ sample 105E6 at 8:45 o'clock orientation from 3-cycle 350°C rodlet. RHCF = 25%.

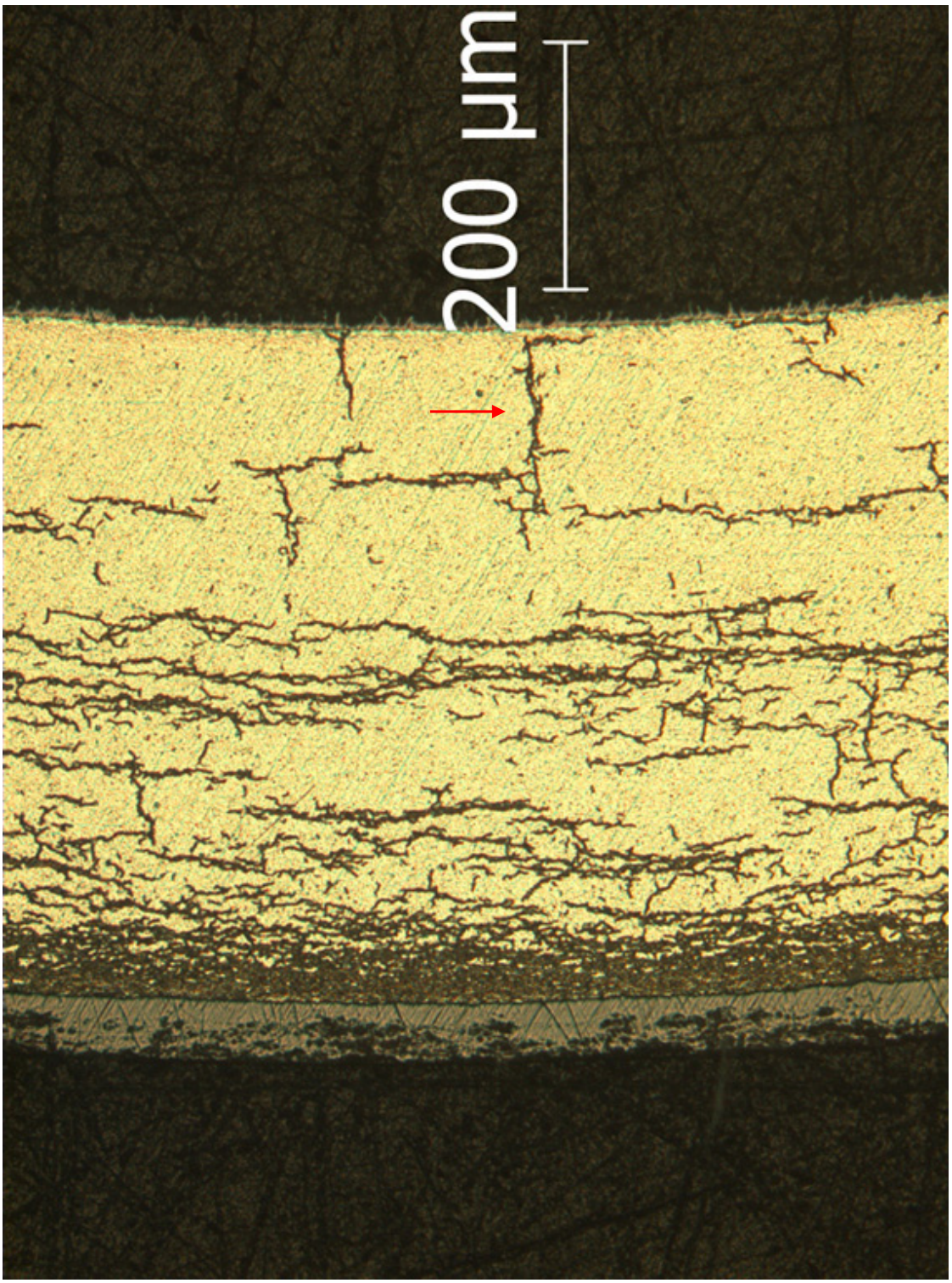

Figure A.26: Image (100X) of ZIRLO™ sample 105E6 at 9:00 o'clock orientation from 3-cycle 350°C rodlet. RHCF = 31%.

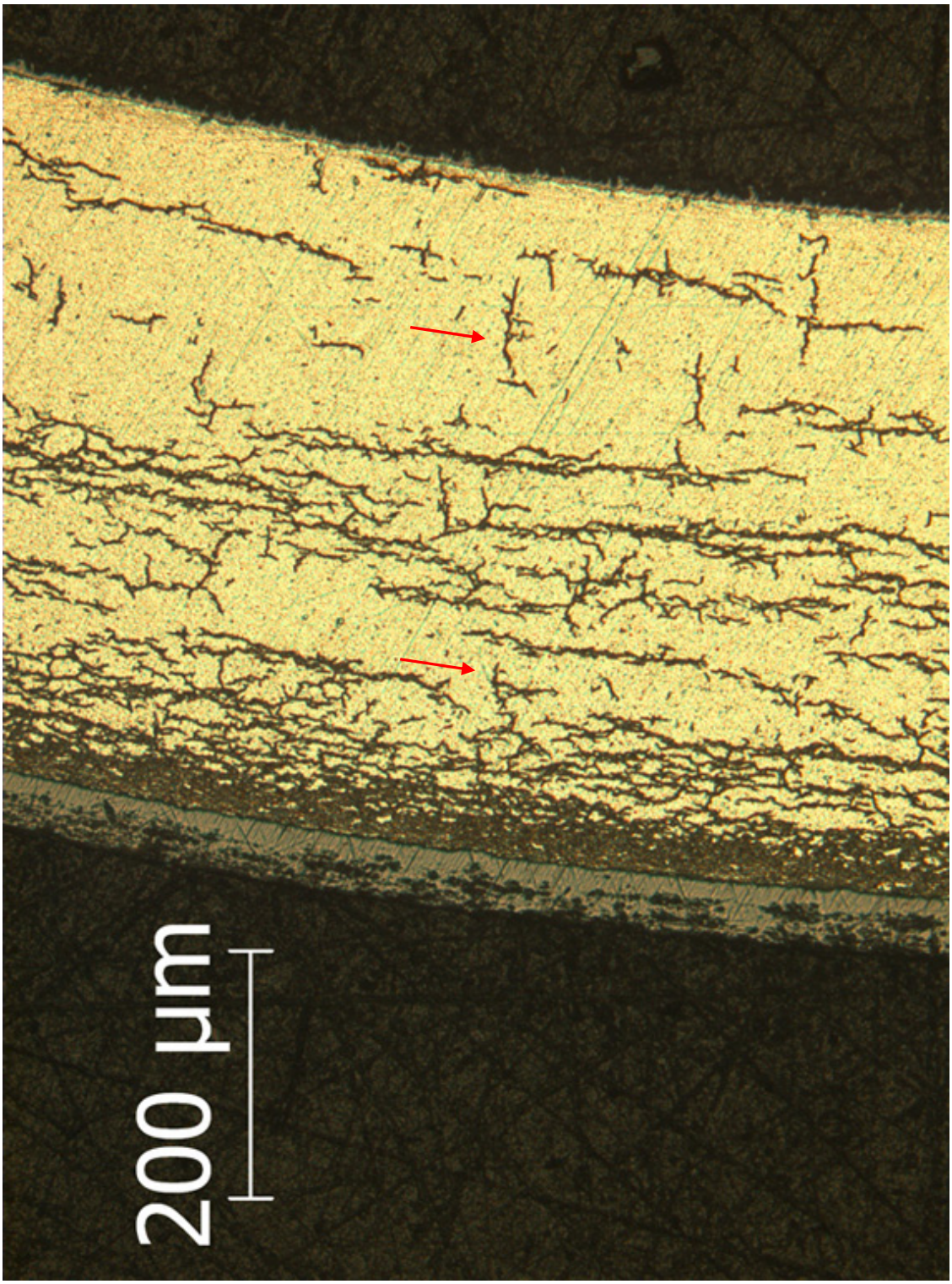

Figure A.27: Image (100X) of ZIRLO™ sample 105E6 at 9:15 o'clock orientation from 3-cycle 350°C rodlet. RHCF = 17%.

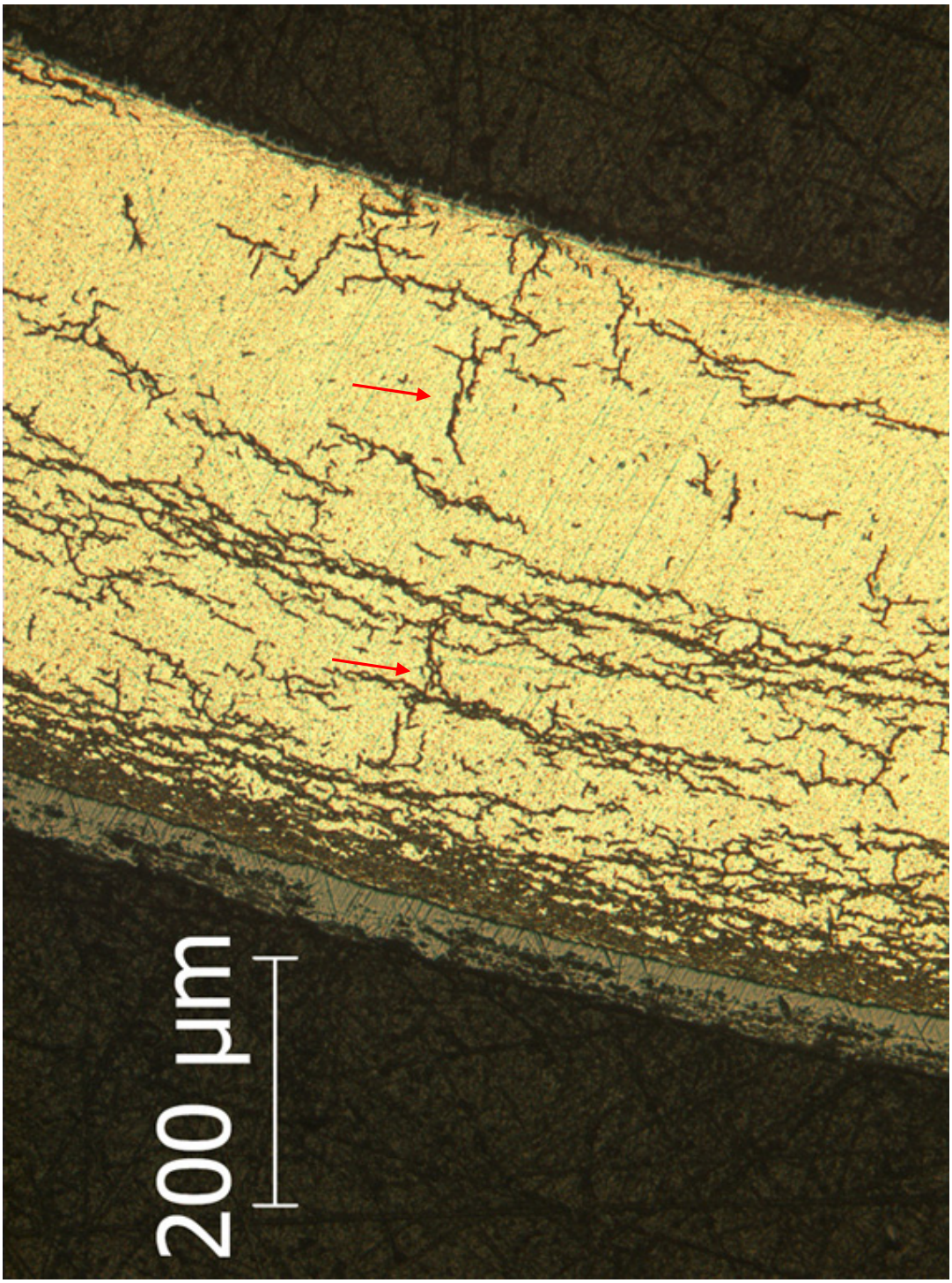

Figure A.28: Image (100X) of ZIRLO™ sample 105E6 at 9:30 o'clock orientation from 3-cycle 350°C rodlet. RHCF = 21%.

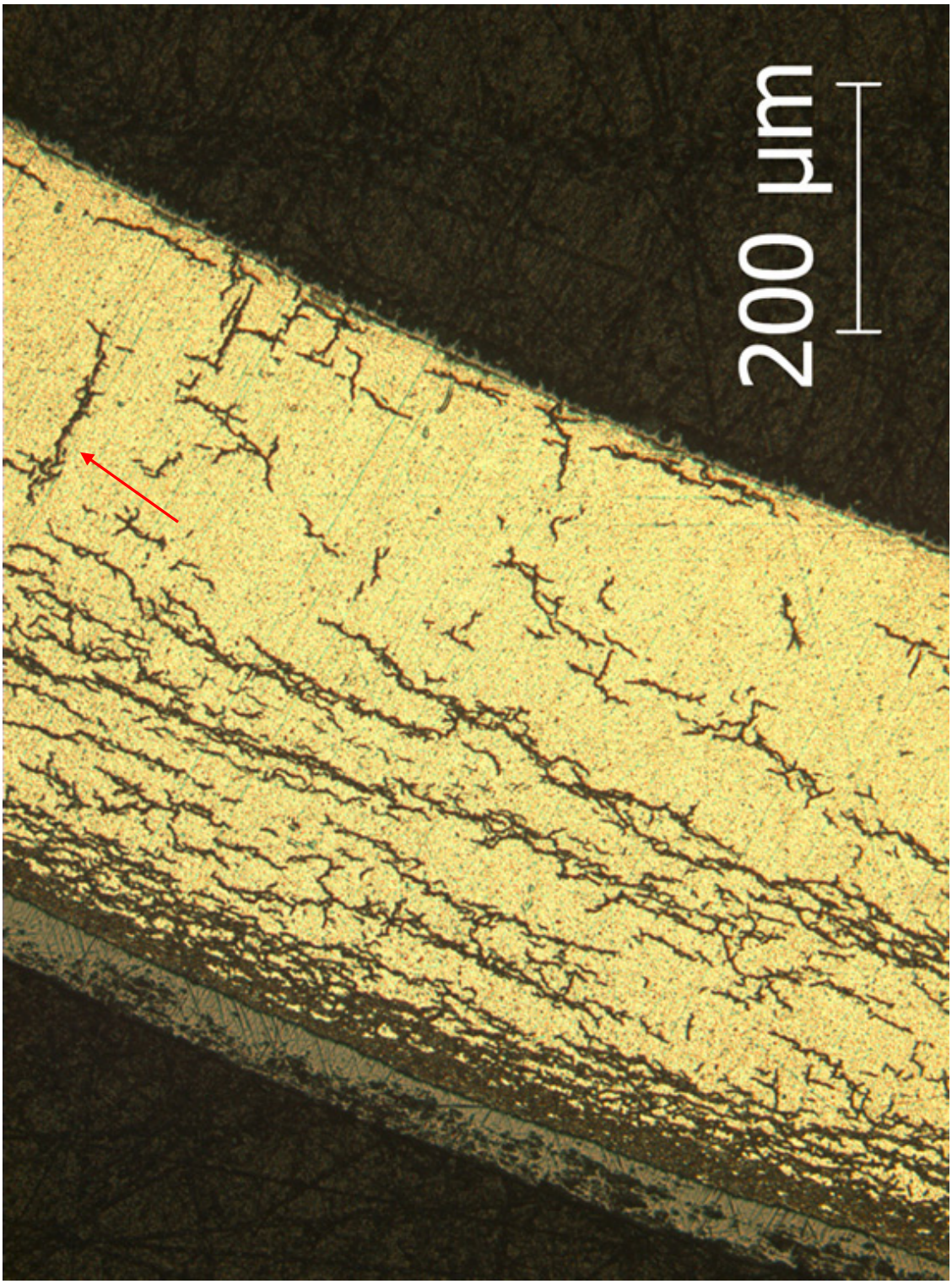

Figure A.29: Image (100X) of ZIRLO™ sample 105E6 at 9:45 o'clock orientation from 3-cycle 350°C rodlet. RHCF = 27%.

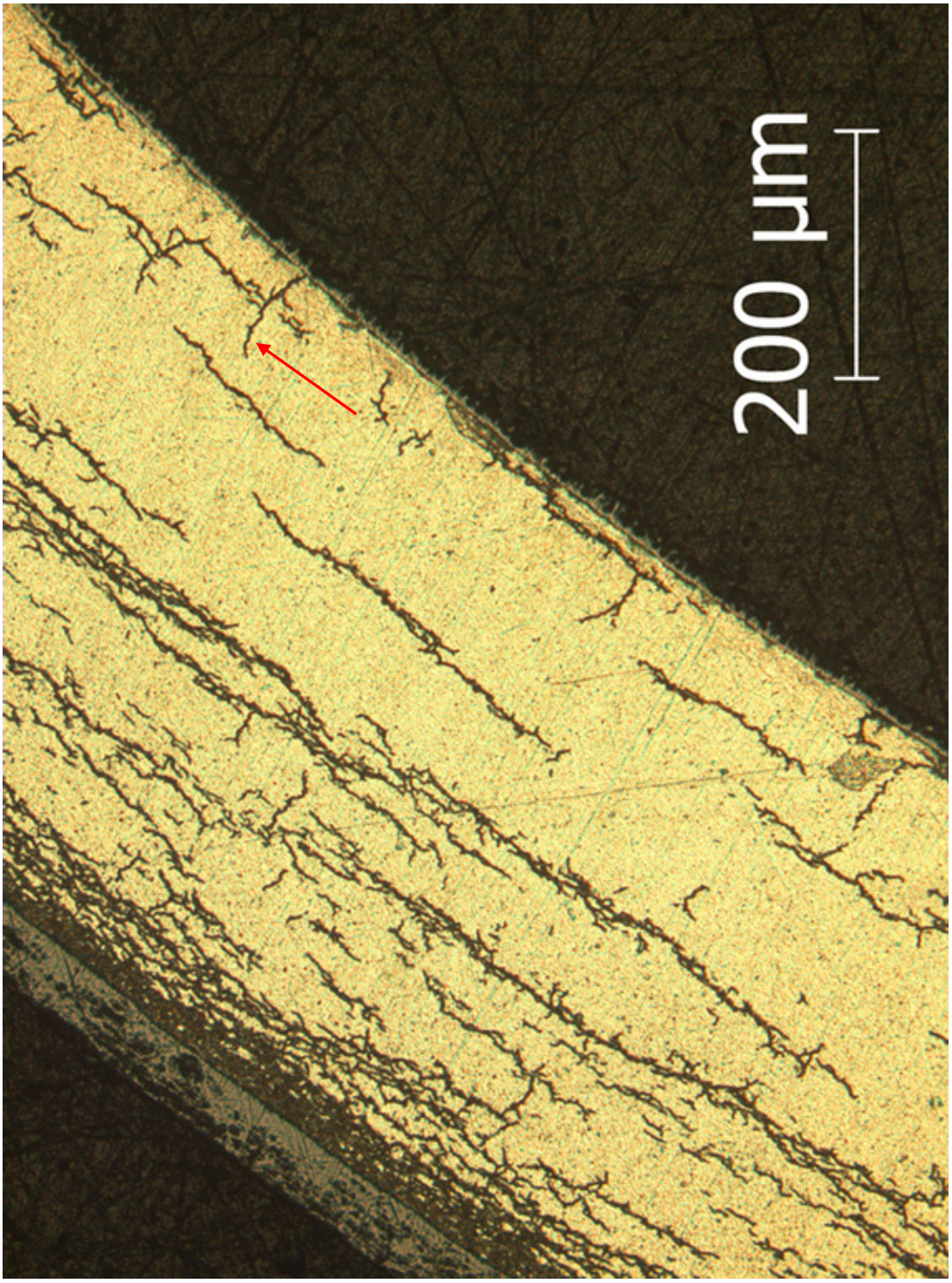

Figure A.30: Image (100X) of ZIRLO™ sample 105E6 at 10:00 o'clock orientation from 3-cycle 350°C rodlet. RHCF = 16%.

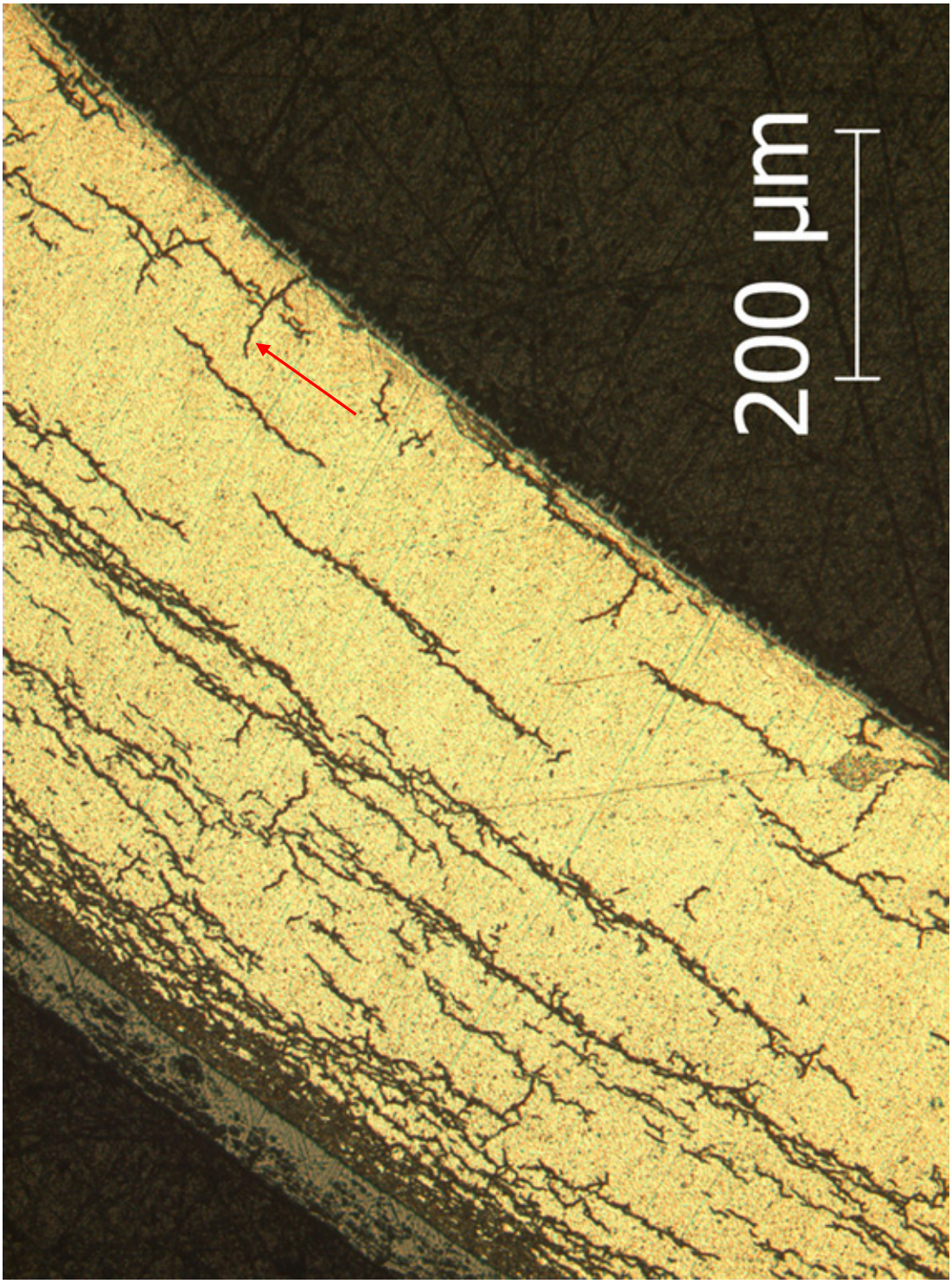

Figure A.31: Image (100X) of ZIRLO™ sample 105E6 at 10:30 o'clock orientation from 3-cycle 350°C rodlet. RHCF = 18%.

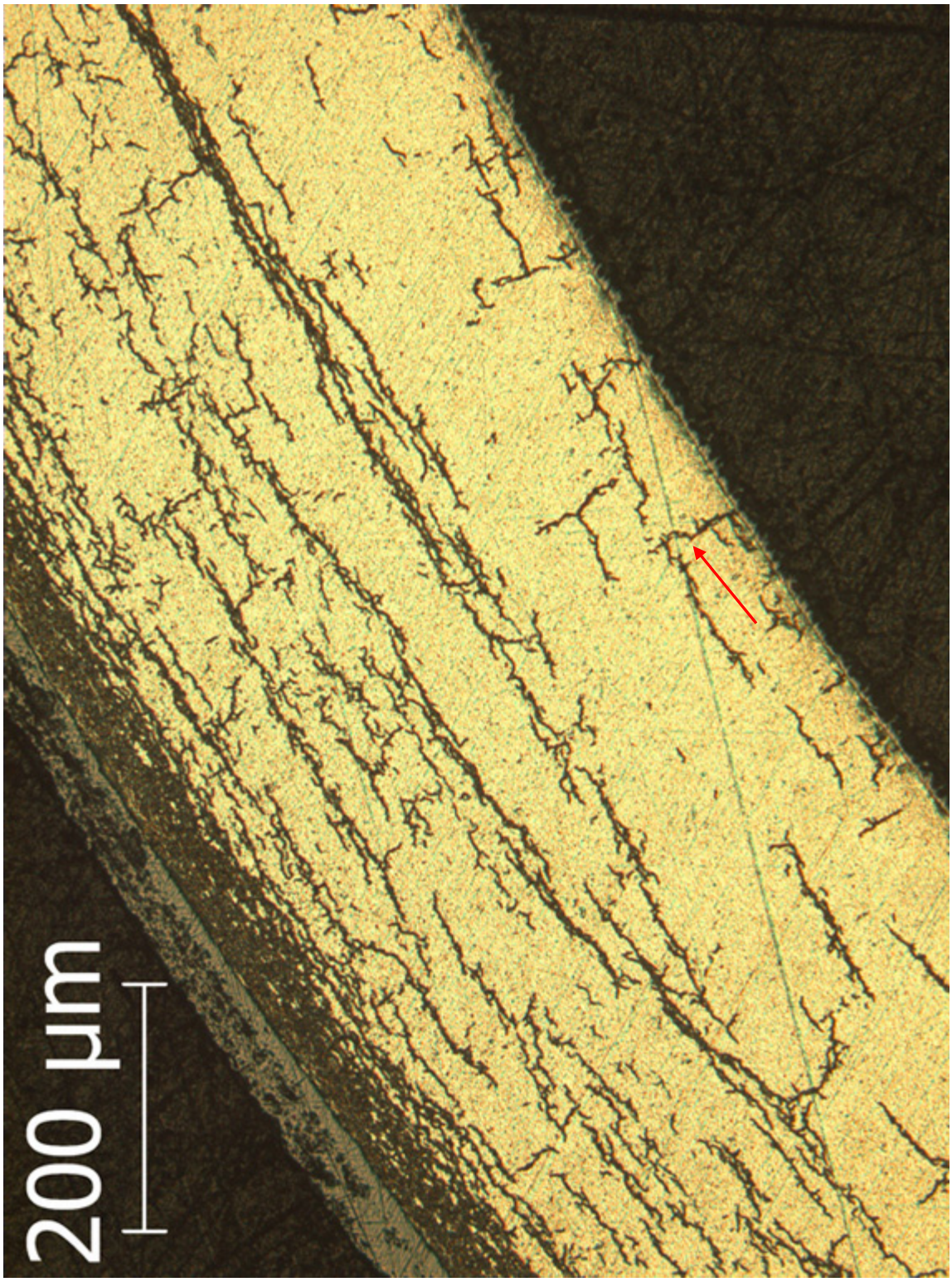

Figure A.32: Image (100X) of ZIRLO™ sample 105E6 at 11:00 o'clock orientation from 3-cycle 350°C rodlet. RHCF = 18%.

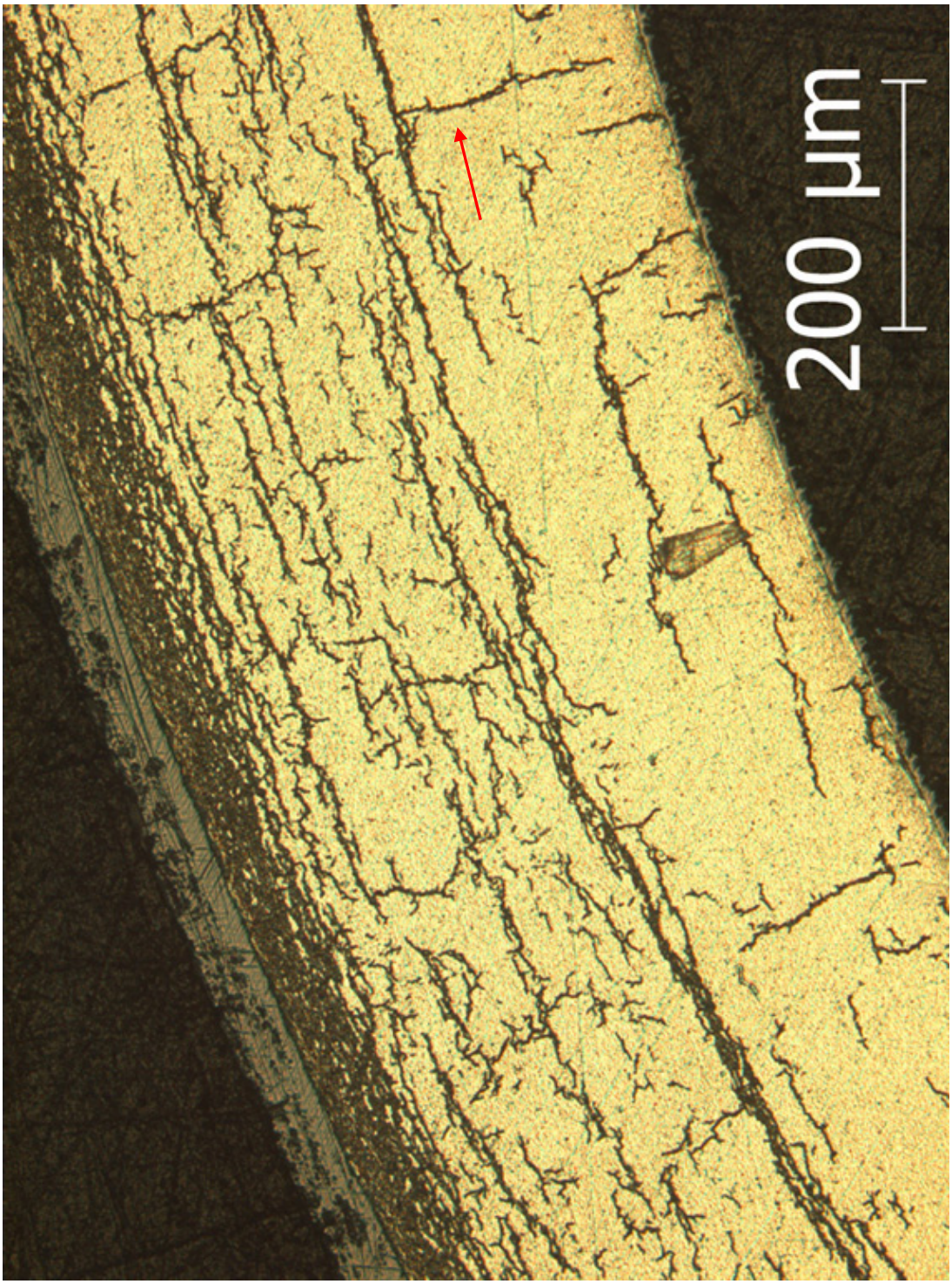

Figure A.33: Image (100X) of ZIRLO™ sample 105E6 at 11:30 o'clock orientation from 3-cycle 350°C rodlet. RHCF = 34%.

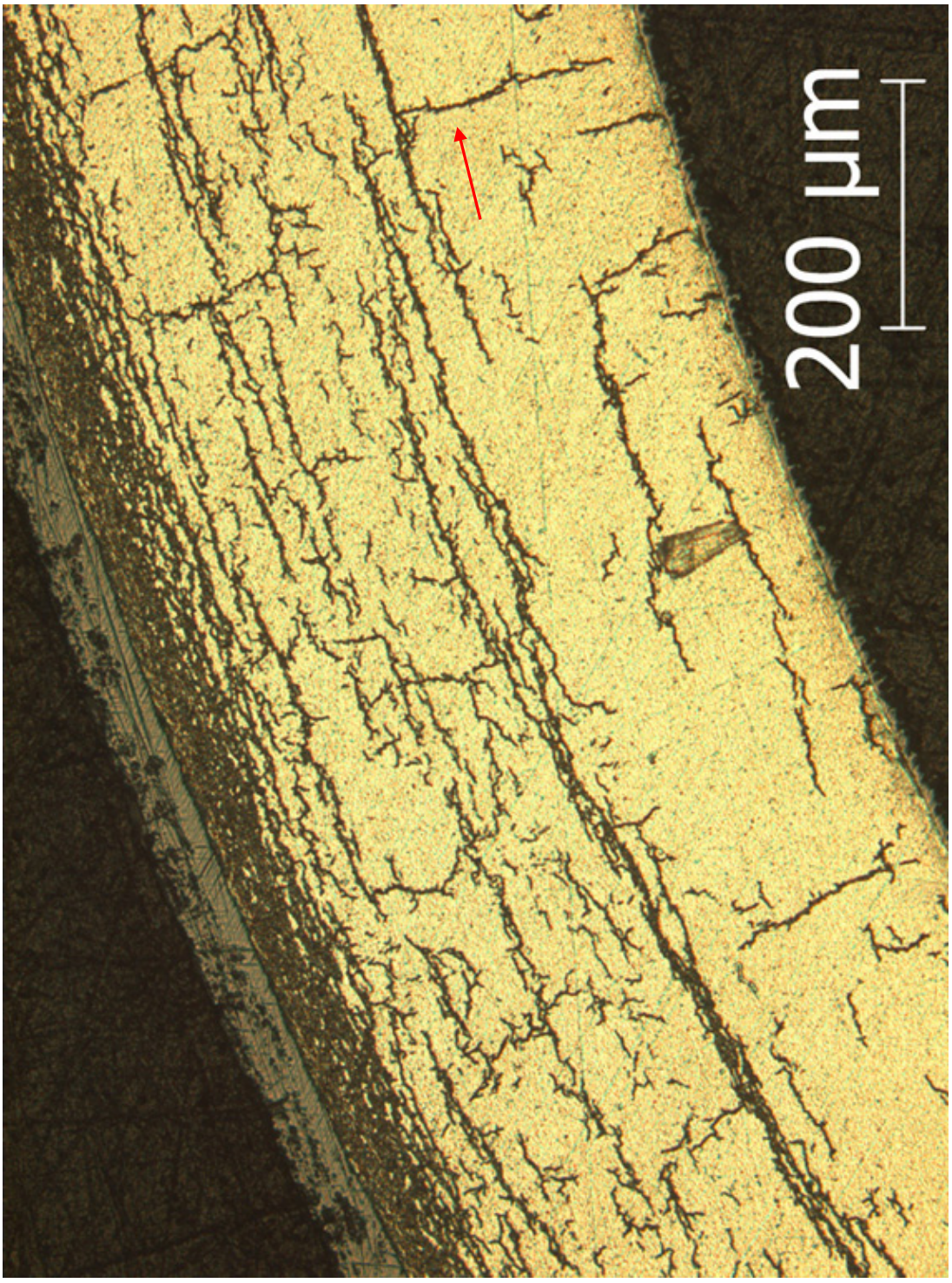

Figure A.34: Image (100X) of ZIRLO™ sample 105E6 at 11:45 o'clock orientation from 3-cycle 350°C rodlet. RHCF = 38%.

Appendix E
FCT Document Cover Sheet

Name/Title of Deliverable/Milestone	*Effects of Multiple Drying Cycles on High-Burnup PWR Cladding Alloy, FCRD-UFD-2014-000052/M2*
Work Package Title and Number	ST Experiments - ANL
Work Package WBS Number	FT-14AN080501
Responsible Work Package Manager	Yung Liu (Name/Signature)

Date Submitted 09/26/2014

Quality Rigor Level for Deliverable/Milestone	☐ QRL-3	☒ QRL-2	☐ QRL-1 ☐ Nuclear Data	☐ N/A*

This deliverable was prepared in accordance with Argonne National Laboratory
(Participant/National Laboratory Name)

QA program which meets the requirements of
☒ DOE Order 414.1 ☐ NQA-1-2000

This Deliverable was subjected to:

☒ Technical Review

Technical Review (TR)

Review Documentation Provided

☐ Signed TR Report or,
☐ Signed TR Concurrence Sheet or,
☒ Signature of TR Reviewer(s) below

Name and Signature of Reviewers

Dr. Hanchung Tsai, Argonne National Laboratory

☒ Peer Review

Peer Review (PR)

Review Documentation Provided

☐ Signed PR Report or,
☐ Signed PR Concurrence Sheet or,
☐ Signature of PR Reviewer(s) below

Dr. Jorge Monroe-Rammsy, DOE/NE-53
Dr. Brady Hansen, PNNL
Comments documented in e-mails

*Note: In some cases there may be a milestone where an item is being fabricated, maintenance is being performed on a facility, or a document is being issued through a formal document control process where it specifically calls out a formal review of the document. In these cases, documentation (e.g., inspection report, maintenance request, work planning package documentation or the documented review of the issued document through the document control process) of the completion of the activity along with the Document Cover Sheet is sufficient to demonstrate achieving the milestone. QRL for such milestones may be also be marked N/A in the work package provided the work package clearly specifies the requirement to use the Document Cover Sheet and provide supporting documentation.